5-6-2014

Rapid Prototyping Tools for Power Electronic Converters

Amruta V. Kulkarni
University of Connecticut - Storrs, amruta.kulkarni@uconn.edu

Rapid Prototyping Tools for Power Electronic Converters

Ms. Amruta Vasant Kulkarni

B.E., University of Pune 2008

A Thesis

Submitted in Partial Fulfillment of the

Requirements for the Degree of

Master of Science

At the

University of Connecticut

2014

APPROVAL PAGE

Master of Science Thesis

Rapid Prototyping Tools for Power Electronic Converters

Presented by

Amruta V. Kulkarni, B.E.

Major Advisor_____

Dr. Ali Bazzi - University of Connecticut

Associate Advisor_____

Dr. Krishna R. Pattipati - University of Connecticut

Associate Advisor_____

Dr. Sung Yeul Park - University of Connecticut

University of Connecticut

2014

ACKNOWLEDGEMENTS

I take this opportunity to express my profound gratitude and deep regards to my advisor Prof. Ali Bazzi for his exemplary guidance, mentoring and constant encouragement throughout the course of this thesis. The help and guidance given by him from time to time was instrumental in making my research a success. I would also like to express a deep sense of gratitude to Dr. Krishna Pattipati and Dr. Sung Yeul Park for their cordial support, valuable information and guidance, which has helped me in completing this task well through various stages. I am obliged to my colleagues in the Advanced Power Electronics and Electric Drives Lab (APEDL) lab for the constant and extremely valuable help provided by them. I am grateful for their cooperation during the period of my research through numerous problem solving and idea-sharing exercises. I thank my parents Mrs. Madhuri Kulkarni and Mr. Vasant Kulkarni for preparing me to succeed in all walks of life and my husband Mr. Hrushikesh Gandhi for standing by me through this entire endeavor. Lastly, all my friends and family members deserve a big thanks for their constant encouragement without which this day would not be possible.

TABLE OF CONTENTS

LIST OF TABLES

LIST OF FIGURES

ABSTRACT

In recent years, demand for utilization of power electronic converters in industrial, commercial and household applications has increased significantly. It is critical for engineers to design these converters in a short duration. Considering the time constraints on engineers it's not surprising that rapid prototyping tools have become very popular in the industry. Through rapid prototyping, users can estimate power loss and cost which are essential to design decisions. The research presented here treats main power electronic components of a converter as building blocks that can be arranged to obtain various topologies to facilitate rapid prototyping. In order to get system-level power loss and cost models, two processes are implemented. The first process automatically provides minimum power loss or cost estimates and identifies components for specific applications and ratings; the second process estimates power losses and costs of each component of interest as well as the whole system. Power loss models are analytical and include effects of parasitic elements and non-idealities. Cost models for each building block are derived based on an extensive market survey. Three examples are used to illustrate the proposed research - boost and buck converters in continuous conduction mode (CCM) and flyback converter in discontinuous conduction mode (DCM). Optimization of component selection is based on the minimum possible cumulative power loss in these components or minimum cumulative cost of components. These techniques help engineers to select the best components for their applications and aid researchers in prototyping different converters for several applications. The proposed cost and loss estimates are shown to be over 92% accurate when compared to measured losses and real cost data. This research presents derivations of the proposed models, detailed experimental measurements and demonstration of a friendly user interface that integrates all the models.

CHAPTER 1: INTRODUCTION

Power electronics literature and patent records over many years show radical developments and modifications in power electronic converters. In the early 1960's, basic converters such as boost, buck and flyback converters were developed by utilizing semiconductor devices [1]. As progress in the performance, efficiency and structure of semiconductors increased, basic converters were modified for different applications and requirements. For instance, DC-DC converters were developed for automobile applications [1, 2], high frequency DC-DC switching converters [3, 4] or switched mode power supplies [5, 6] began to be used in battery chargers, home appliances, hybrid electric vehicles, and many other applications. Also, resonant switching converters [7, 8] were observed as an efficient solution for lighting applications, smart grids, renewable energy systems and power supplies [9]. Thus, today power electronic converters are in high demand in many areas of electrical and electronics technology.

The diversity of applications, power ratings, and energy levels of power electronic converters require different converter topologies and ratings with numerous component options and combinations. The design of high efficiency, cost effective and reliable power converters in a short time is a challenging task for any power electronics engineer. A designer has to review a vast amount of existing literature, datasheets and web-based information in order to select a single component. Thus, researchers find it beneficial to work on developing tools which can help select appropriate components for new converter designs so that they can achieve minimum power loss and/or minimum cost for their application.

Over the past few decades, several power loss and cost estimation models or methods have been developed for power converters. When designers first start to design a converter, they have to start with the ratings and from an application point of view. Thus, it has become a critical

issue to develop rapid prototyping tools or methods on the basis of the specifications. The power loss models developed in the existing literature do not always consider most non-idealities and parasitic elements. Furthermore, printed circuit board (PCB) and gate drive losses are not observed along with component power losses in some existing power loss rapid prototyping tools. From a cost perspective, even though cost is a major driving factor for the power electronics industry, research literature shows limited cost models. Moreover, user-friendly rapid prototyping tools, which can accurately estimate the cost and power loss of a component as well as the whole system in a short time, are not present in the literature. The techniques and methodologies which are observed in the literature are described in detail in Chapter 2.

Rapid prototyping tools based on power loss and cost models are expected to reduce engineering time and enhance product cost and quality in electronic manufacturing in many applications such as DC-DC converters, inverters, LED drivers, smart grid systems.

Rapid prototyping tools for DC-DC converters are of main interest here due to the converters' simplicity, wide range of their applications and since the methodology for developing models is of main interest here. The main goal of this research is thus to achieve rapid prototyping capability through a systematic methodology to estimate and minimize power losses and cost of DC-DC converters. Generalized power loss equations for fundamental power electronic components are composed from existing literature and then reformulated in terms of input and output requirements, switching frequencies and duty ratio to obtain a simple and uniform approach in power loss estimation tools for different converters. To validate these tools, boost and buck converters in continuous conduction mode (CCM) and flyback converter in discontinuous conduction mode (DCM) are implemented since they are widely applicable and popular among power electronic converters. It is important to note that methodology developed

in this research can be extended for other converters, inverters as well as other electronic development applications. On the other hand, cost models are based on an extensive market survey of component costs. A database for all applicable components is used to model costs of these components using their major ratings and values, e.g. cost of a capacitor is modeled as dependent on capacitance and voltage rating. The power loss and cost models are then integrated into the rapid prototyping tools developed using a MATLAB Graphical User Interface (GUI). The power loss and cost model presented here are only for power electronic components. However, connectors' power loss and cost models are not included. The rapid prototyping tools based on these models can use component-specific information, or can run in optimization mode which can perform converter component selection for power loss minimization or cost minimization. A major goal for these tools is to minimize the estimation error when comparing actual component cost and power loss values with the measured or real ones, and their main advantage is the ability to evaluate a large number of possible component combinations and achieve instantaneous cost and loss estimates. It is important to note that the models provided here can easily evolve over time and changes in technology and cost.

In addition to power loss and cost models, researchers and designers are very interested in the reliability estimation and prediction techniques. Several methods and models have been proposed to estimate the reliability of components and derive accelerated testing methods for power electronic systems. These methodologies are discussed in detail in Chapter 2, but as reliability is a broader topic for research, rapid prototyping methods proposed here are limited to the power loss and cost estimation techniques while rapid prototyping tools based on reliability and accelerated testing methods can be developed in the future research.

The thesis proceeds as follows. Chapter 2 discusses existing literature for power loss, cost and reliability models. This includes power loss estimation and reduction techniques for system level and component level power losses, cost, as well as reliability. It provides deep insight into the topic and helps to develop rapid prototyping tools and concludes with the discussion of limitations of existing literature. Chapter 3 describes the concept behind power loss models, procedures for rapid prototyping tools for power loss models in optimization mode and component-specific mode, derivations of power loss model equations for basic building block components, and reformulation of these equations for boost, buck and flyback converters. Chapter 4 presents cost estimation methodology in optimization mode and component-specific mode with cost surfaces based on a large database of basic building block components. Chapter 5 elaborates on the optimal selection of components using the rapid prototyping tools, in addition to component-specific cost and power loss models. Research conclusions are covered in Chapter 6, which also provides recommendations for future research efforts. The Appendix includes detailed results for case studies of component-specific and optimization modes for various converters and different operating points, along with experimental verification of the provided models and detailed derivation of mathematical expressions.

Related Publications

[1] A.V. Kulkarni, A. M. Bazzi, " Empirical Cost and Analytical Power Loss Models of DC-DC Inductors," *in Proceedings of Electrical Manufacturing & Coil Winding Association, Milwaukee, Wisconsin*, May 2013.

[2] A.V. Kulkarni, A. M. Bazzi, "A Building-Block Approach to Efficiency and Cost Models of Power Electronic Systems," *in Proceedings of the IEEE Applied Power Electronics Conference and Exposition , Dallas Forth worth, Texas*, March 2014.

CHAPTER 2: LITERATURE REVIEW

Contributions from existing literature help to develop the concepts upon which the power loss and cost models are built and to highlight the ways in which power loss and cost models developed here are different. An important take-away from this chapter is that while the vast literature reviewed here does not address non-idealities and parasitic elements frequently, the power loss model presented here does focus on these elements along with PCB and gate drive losses leading to more accurate power loss models. The cost models developed in this research are based on an extensive market survey. The most important aspect of this research is that the power loss and cost modeling methodologies developed here are such that they can evolve over time and changes in technology. Subsequent sections of this chapter address related work on power loss, cost, and reliability models, and rapid prototyping methods.

2.1 Power Loss Modeling

This section provides information about the existing power loss models for components and converters. This information helps uncover the problems associated with existing power loss estimation models and aids to develop more accurate models. This section also describes power loss estimation methods and their advantages and disadvantages. Section 2.1.1 reviews power loss models of power electronic components. Section 2.1.2 reviews system-level power loss estimation models, and Section 2.1.3 summarizes different power loss estimation methods.

2.1.1 Power Loss Models for Components

Several techniques have been implemented to find the power losses in power electronic component. Majority of the research has focused on selecting components for power electronic converters, e.g. [10]. Extensive research has been conducted for finding specific losses in

semiconductors and magnetic components. For example, in [11] a qualitative analysis is carried out on six non-isolated DC-DC topologies such as buck, boost, buck-boost, Ćuk, SEPIC, and Zeta to select components for these converters. This process is then verified with the help of conduction and switching losses in the MOSEFTs and IGBTs, but gate losses in IGBTs and MOSFETs are ignored in this research.

The conduction and switching losses estimation in MOSFETs and IGBTs in boost converter CCM are given in [11] as,

$$P_C = P_{CS} + P_{CD} = \frac{2}{D} \ . \tag{1}$$

where P_C is the MOSFET loss, P_{CS} is the MOSFET switching loss, P_{CD} is the MOSFET conduction loss and D is the duty ratio. A similar approach has been developed in [12] for the DC converters which are used in telecommunication applications. The conduction power loss in MOSFET and its Schottky barrier diode conduction losses are observed but switching losses within it are ignored. In order to estimate exact power loss of MOSFET or IGBTs the conduction, switching and gate drive losses must be considered.

The conduction and switching losses should both be considered while calculating the diode total power loss. In [13] conduction losses of flyback diodes are obtained using three simple tasks viz. estimation of maximum power loss consumption, nonlinear finite element analysis of diode losses and actual implementation of these analyses in the flyback converter experiment. This approach gives a deeper insight into diode conduction power loss estimation, but it fails to explain how to measure switching losses in the flyback converter diode. In [14], while calculating light load efficiency of a buck converter with diode emulation method, switching losses of MOSFET and its effect on the diode power loss were considered but effect of diode switching loss on the total system-level loss was ignored. The MOSFET switching loss in the

buck converter is given as,

$$P_{Switch\_ctrl(CCM)} = \frac{1}{2} V_{in} \times (I_o + \Delta i_{(CCM)}) \times t_{f\_ctrl} \times f_{sw} \quad . \tag{2}$$

where $P_{Switch\_ctrl(CCM)}$ is the switching losses of buck converter in CCM, f_{sw} is the switching frequency, V_{in} is the input voltage, t_{f_ctrl} is the MOSFET fall times, I_o is the output current and $\Delta i_{(CCM)}$ is the inductor current ripples in CCM. An inductor core loss estimation method has been proposed in [15] for PFC application. This method is based on the Steinmetz equation, but for high switching power converters this equation is modified as,

$$P_{CORE} = K_1 V_e \left[\left(\Delta B^m / (2T_{on})^n \right) T_{on} / T_S + \left(\Delta B^m / (2T_{on})^n \right) T_{off} / T_S \right] \tag{3}$$

where ΔB^m is the maximum peak flux density, T_{on} is the interval when MOSFET is ON, T_{off} is the interval when MOSFET is OFF, T_S is the MOSFET switching time, V_e is the effective core volume, K_1 is the inductor core material constant and n is transformation ratio. The above equation considers the effect of high switching frequency on the core loss and the B-H curve. However, [15] did not consider the winding copper loss and the skin effect on core losses which is usually observed at high frequencies. For higher switching frequencies, lower power loss is observed in the copper windings in [16]. In this research the copper windings are used with center-gapped, side-gapped and spacer configuration cores. Copper loss estimation tools are developed for the inductors with these cores, but a generalized copper loss model is not considered.

Power losses in capacitors are generally lower as compared to power losses in other components. The power loss within a capacitor is calculated by combination of the power losses in ESR and the parallel parasitic resistance across it. For instance, fault detection and power loss estimation formulae are given in [17] for various switching frequencies in a PFC circuit. The

total power loss in the capacitor is shown as,

$$P_{LOSS} = \sum_{k=1}^{N} ESR_{(k)} I_{(k)}^2 \tag{4}$$

where P_{LOSS} is the power loss in capacitor, *ESR* is the equivalent series resistance, *I* is the capacitor current and *k* is the of harmonic order of the capacitor current. Similar to the power electronic components, the power loss estimation tools for PCBs and gate drive circuits are also observed in the literature. The procedures for proximity loss and conduction loss in PCBs are discussed in [18] with the help of finite element analysis. The proximity losses are obtained in [18] as,

$$P_{proxu.l.,x} = \frac{2\pi}{\sigma} \phi_{prox,x}(w,h,de) H_{ox}^2 . \tag{5}$$

In this equation $P_{proxul,x}$ is the proximity losses of the PCB, $\phi_{prox,x}$ is the geometry dependences of the conduction losses in traces, *w* is the width of the trace, *h* is the height of the trace, H_{ax} is the external magnetic field generated, *de* is the skin depth and σ is the conductivity of conductor. To analyze the high frequency power loss in a PCB, the analogy of basic principles of electromagnetic wave propagation in periodic media has been used in [19].

Methods for estimation and reduction of gate drive circuit power losses are proposed in [20] with the help of switching frequency and MOSFET gate to source capacitance. However, power losses within the gate drive capacitances are ignored in it. In [21], analytical power loss model is developed for the MOSFET and its current source resonant gate driver but power losses within bootstrap capacitor circuit are ignored. The total power loss in the gate driver IC is,

$$P_{GDRV} = V_{DD}^2 C_g f_{sw} \tag{6}$$

where V_{DD} is the gate drive IC supply pin and C_g is the gate capacitance.

2.1.2 Power Loss Models for Power Electronic Converters

Detailed analysis of power losses in different converters is further described in this subsection along with topology-specific power loss models. For example, power losses within a boost converter caused by reverse recovery characteristics of the rectifier have been modeled for minimization in [22]. Some researchers have also worked on specific component losses in the converters such as MOSFET losses in a boost converter [23]. Total system-level power losses are also discussed in the literature, for example the total boost converter power loss and its component losses in [24]. The total boost converter power losses are given in [24] as,

$$P_{loss} = P_{cond} + P_{fixed} + W_{TOT} \times f_{sw} \quad , \tag{7}$$

where the boost converter power losses depend on the conduction losses in the MOSFET and diode (P_{cond}), fixed losses of other components (P_{fixed}), and dynamic losses (W_{TOT}) that vary with the switching frequency (f_{sw}).

Most of the research in converter power loss modeling is targeted towards power loss estimation and component selection procedure for the converters. For instance, a dynamic power loss (P_D) model based on transient loss (P_T), datasheet parameters (P_f) and parasitic elements of the components (P_r) is developed for the buck converter in [25]. It also provides component selection procedure for the buck converters, but PCB and gate drive circuit losses are ignored. Dynamic losses of each component in the converter are approximated as,

$$P_D = P_f + P_r + P_T \tag{8}$$

Also, a power loss calculation method for power MOSFETs in buck converters is given in [26].

Power loss reduction techniques are also provided in the literature. For example, power loss reduction techniques for active clamped flyback converter are shown in [27]. However, this method fails to explain power loss estimation techniques in flyback or active clamped flyback

circuits. Another example is [28], where with the help of the Dowell equation, a power loss model for flyback transformer windings considers skin and proximity losses. The primary and secondary winding power loss of flyback transformer at various harmonics is given as,

$$P_{wp} = P_{wpdc} F_{Rpn} \tag{9}$$

$$P_{ws} = P_{wsdc} F_{Rsn} . \tag{10}$$

F_{Rpn} and F_{Rsn} are derived from Fourier transforms which provide the power loss values at various harmonics, P_{wp} is the primary winding power loss, P_{wpdc} is the primary winding DC power loss, P_{ws} is the secondary winding power loss and P_{wsdc} is the secondary winding DC power loss.

Some research also offers power loss estimation methods for flyback converters in DCM but ignores snubber circuit power loss estimation as in [29] where power loss in primary and secondary switches, magnetic components, and gate drive circuits are presented but snubber circuit power losses are ignored.

2.1.3 Power Losses Calculation Methods

Several methods to measure system-level power losses have been presented in the literature. For example, references [30] and [31] provide electrical and calorimetric methods. Electrical methods utilize voltage and current measurements to estimate losses, while calorimetric methods utilize temperature measurements and temperature rise. Problems are observed in the measurement of individual component power losses with the help of both voltage and current measurements and calorimetric measurements [32]. Problems observed in the voltage and current measurements are related to bandwidth limitations, offset voltages of probes, and limitations of oscilloscope accuracy, while calorimetric measurements are time-consuming and difficult. To overcome these limitations, a temperature-based power loss measurement method has been proposed for estimating power losses in each component and the overall converter. In this

method, temperature profile of each component is obtained at desired operating point in a thermal equilibrium. A low voltage power is then fed to each component until the desired operating point is reached where a relationship is derived between the component power loss and corresponding temperature. This method is more accurate than both methods but it requires a large set up. Also, weather fluctuations and their effects on component temperature are not considered in [32].

Analysis of adaptive power loss estimation techniques are developed on the basis of serial and parallel resistances in [33]. Average on-state mathematical model is presented including parameters such as core hysteresis loss, eddy current loss, conduction ohmic loss and switching loss. Although this method gives power loss estimation of semiconductors in converters, it is unable to estimate power losses in the PCBs and gate drive circuits.

2.2 Cost Modeling

This section provides information about the existing cost models for components and converters. Along with cost estimation methods and the associated advantages and disadvantages. Section 2.2.1 explains cost model dedicated to power electronic components. Section 2.2.2 describes cost estimation models for different power electronic systems.

2.2.1 Cost Models for Components

Existing literature indicates significant research related to cost estimation of various power electronic components. Component cost is one of the most important parameters to be analyzed because its value changes with market trends

Some research has focused on the cost estimation and reduction techniques for system and components based on power loss measurement techniques. In [34] cost estimation is provided for capacitor-type and SCR-type magnetizer systems and their components. Cost model is provided

for the capacitors, transformers, semiconductor devices and magnetic fixture. The cost model for semiconductor devices such as SCR, MOSFET and IGBT is given in the system as,

$$Cost_{SCR} = P_{SCR} U_{SCR} \tag{11}$$

where $Cost_{SCR}$ is the SCR cost, P_{SCR} is the power loss in SCR and U_{SCR} is the unit cost of SCR ($/VA). However, generalized IGBT or MOSFET cost modeling equations for any application are not provided in this paper.

Another methodology that is observed in the literature is to reduce the cost of components based on energy consumption and energy storage volume. This technique is mostly observed for capacitors, e.g. [35], where energy-to-volume ratio (*EVR*) of electrolytic capacitors is given as,

$$EVR = \frac{0.5 \times C \times V_{rated}}{Volume} . \tag{12}$$

C is the capacitance value, V_{rated} is the rated voltage, *Volume* of the electrolytic capacitor. It is shown in [35] that cost is directly proportional to EVR of the capacitor and thus a cost reduction technique for electrolytic capacitors is presented. Similar methodology was implemented in [36] to estimate the cost of capacitor bank. Energy stored in each capacitor for capacitor discharge impulse magnetizer is obtained along with unit cost of the capacitor; however unit price estimation method for the capacitor is not presented in that paper. The capacitor bank cost estimates as,

$$Cost_{Capacitor} = E_{Capacitor} U_{Capacitor} \tag{13}$$

where $Cost_{Capacitor}$ is the capacitor cost, $E_{Capacitor}$ is the energy of the capacitor and $U_{Capacitor}$ is the unit price of capacitor. Inductor cost estimates are obtained using cost estimates of the core and magnet wire. In [37], core cost, core volume and switching frequency are related to each other. The core volume increases as per the switching frequency and cost of the core depends upon the core volume. In [38], magnet wire cost model is presented based on cost per unit mass (C_m) for

given unit length of wire (l), wire diameter (d), number of turns (n) and cost per unit length of wire (C_o),

$$Cost = \left(C_0 + C_m d^2 n\right) l \tag{14}$$

Also in [38], an inductor cost model is presented and depends on magnet wire, cost per weight of the core and weight of the wire. The inductor cost model is presented as,

$$\sum\nolimits_{lab,L} = \sigma_{lab,x} W_{wdg} + \sum\nolimits_{lab,x}^{fc} \tag{15}$$

σ_{lab} is the cost per weight of winding, W_{wdg} is the weight of winding material and $\sum_{lab,x}$ is the cost per weight of winding. Semiconductor cost models are not as common, but the majority of research in semiconductor cost modeling is related to microcontroller or IC cost estimation. For instance, [39] develops cost estimates of 3D IC at early design stages to reduce manufacturing time and cost expenditure. A similar approach is provided in [40] to obtain cost estimates of 3D IC while factoring in the effect of change in temperature on manufacturing cost. Generally, 3D IC design cost depends upon the wafer cost, bonding cost, packaging and cooling cost. Cost of the IC is obtained as,

$$Cost_{IC} = Cost_{Wafer} + Cost_{bondingmaterial} + Cost_{packaging} + Cost_{cooling} \tag{16}$$

where $Cost_{IC}$ is the IC cost, $Cost_{wafer}$ is the wafer material cost, $Cost_{bondingmaterial}$ is the bonding material cost, $Cost_{packaging}$ is the packaging cost and $Cost_{cooling}$ is the cooling material cost. Cost parameters in the above equation depend on the material used and manufacturing techniques. Although this method can predict IC costs with high accuracy, the parameters of this cost equation are not easily available in the datasheet or manual. Thus, this technique is useful for manufacturers but not so much for distributors or end users.

2.2.2 System Cost Models

Cost estimation and reduction techniques are also utilized to predict system level cost. For example, [41] and [42] present cost models of a battery, inverter, converter, and other subsystems on the basis of power ratings of these sub-systems. In [41] cost models for battery, driving motor, inverter, controllers and overall system level costs are obtained. These cost estimates are assumed to be dependent on energy consumed in the system and the unit price of the component. For example, the driving motor cost (C_M) is presented as,

$$C_M = P_M U_M + C_{cc}\,. \tag{17}$$

where P_M is the power loss in the motor, U_M is the unit price of the motor and C_{cc} is the control circuit cost. Models presented in [42] assess the cost of a PV power generation system based on the ratings and internal component specifications. This cost model includes initial cost of the system installation and cost of each component in the system but the changes in cost parameters as per the market trends are not considered. Another example is [43] where costs of the series PV string (C_{PV}), microcontroller (C_{sysMC}) and micro inverter PV systems cost ($Cinv$) are modeled. The cost estimation for micro-converters is given as,

$$C_{sysMC} = nC_{PV} + n\left(C_{dcdc} + \sum_{j\in x} C_{s,j} + C_{\mu,x}\right) + C_{inv} + \sum_{k\in x} C_{s,\mathrm{k}} + C_{\mu,\psi} \tag{18}$$

The cost per watt is obtained in [44] as,

$$C_{pW} = \frac{C_{sysMC}}{P_{sys}}\,. \tag{19}$$

where C_s is the set of sensor cost, C_μ is the microcontroller cost, $C_{\mu,\psi}$ is the set of microcontroller sensor cost , C_{dcdc} is the DC-DC converter cost, C_{pW} is the cost per watt, $C^{cPV}{}_{cell}$ is the cost of per PV cell and P_{sys} is the system power loss.

According to [44] the cost boundaries of PV panels are dependent upon life cycle costing, PV rating, inflation, discounts, number of replacements, and maximum number of replacements. Reference [45] presents an algorithm for a PV system cost (*PV cost*) estimation Simulink model for the cost estimation tool, and simulation results where the system cost is approximated as,

$$System\ \cos t = (PV \cos t + Battery\ \cos t) \times BOS\ factor + Labor\ \cos t \tag{20}$$

While the method in [45] addresses the system installation cost (*Labor cost*), the component cost is not presented. Battery cost, balance of system factor (*BOS*) is also considered.

Some of the existing reaserch provides cost estimates to other electrical systems from which lessons can be learned. Examples include nonlinear optimization of interconnected power systems cost [46], life-cycle cost modeling of transmission lines [47], manufacturing processes [48], and others. Most of these efforts are at a power system scale and not power electronics scale. For example, [48] assesses manufacturing cost of a product by obtaining design, manufacturing and maintenance costs and the time required to perform specific operations on machines. With these two parameters, cost based on machine operation can be obtained as,

$$C_{ij} = M_h T_{ij} + S_h \ , \tag{21}$$

where C_{ij} is the cost for each operation, M_h is the unit cost of machining h , T_{ij} is the temperature of machine at the operation and S_h is the setup cost for machine h but other cost parameters such as fault cost and packaging cost are not analyzed in this research.

Reference [49] shows a combined reliability and cost model for power switching devices such as MOSFET and IGBT. First, the component reliability is estimated based on its total power loss within the semiconductor device and then the cost is calculated based on reliability. In this paper, the reliability and cost relation is developed based on the junction temperature and the number of power switching devices *Tj(N,t)* and it is given as,

$$T_j(N,t) = T_C + \int_0^t \left[\frac{d}{dz} P_{loss/N}(N,z) \right] \times Z_{th}(N,t-z)dz \tag{22}$$

where T_C is the case temperature, $P_{loss/N}$ is the power losses in semiconductor devices and Z_{th} is the thermal impedance.

Note that interest in this research is to have cost models of electronic components at the component level to achieve system-level cost models. Manufacturing processes and large-scale system cost models are beyond the scope of this research.

2.3 Reliability Modeling

Literature shows that significant work has been conducted in all aspects of reliability, failure rate analysis, and diagnosis considering failures observed in components and across overall system. There are several stages of failures in the components which are described by the bath tub curve shown in Figure 1 [50]. Failure stages of the components are classified as infant mortality, field failures or random failures and wear out. However, failure analysis in the infant mortality and wear out region has not been included frequently enough in the literature [51, 52].

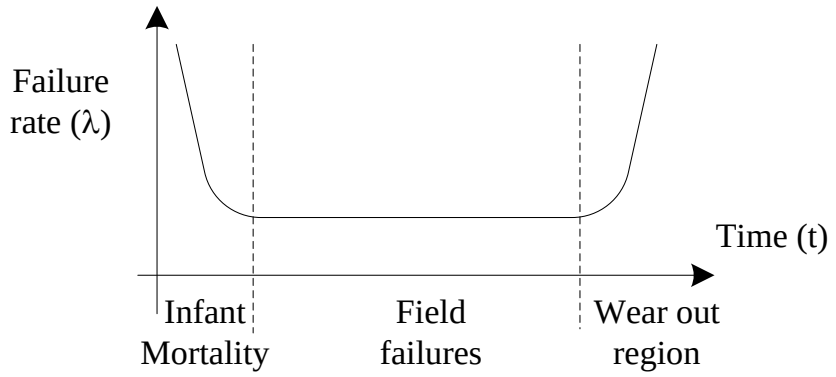

Figure 1 Bath tub curve

This subsection provides information about the existing reliability models for components and power electronic systems and seeks to highlight the problems associated with existing

estimation models in order to help develop more efficient models. This section also describes reliability modeling methods, their advantages as well as disadvantages. Section 2.3.1 explains reliability models for power electronic components and systems, while Section 2.3.2 summarizes different reliability estimation methods.

2.3.1 Reliability Models for Power Electronic Components and Converters

Reliability estimation techniques for MOSFETs, diodes, capacitors, inductors and transformers, controller ICs, and overall converters are discussed in this section. A very useful but conservative component-level reliability modeling resource is the military handbook MIL-HDBK-217F [53]. As per MIL-HDBK-217F, a MOSFET failure rate is obtained as,

$$\lambda_M = \lambda_b \pi_T \pi_A \pi_Q \pi_E \tag{23}$$

MOSFET reliability can be obtained as,

$$R_{MOSFET}(t) = e^{-\sum \lambda_M t} \tag{24}$$

In these equations λ_M is the failure rate of MOSFET, λ_b is the base rate of each component from [53], π_A is the device application stress factor, π_Q is the quality factor, π_E is the environmental stress factor, π_T is the temperature factor and R_{MOSFET} is the reliability of the MOSFET. In [54], an accelerated stress test is developed to analyze field failures of the power MOSFETs used in power supplies. Several accelerated tests are also performed on diodes to estimate their in-circuit reliability. In [55] the wire bonding scheme of SiC-diodes is observed at high temperatures with the help of a surge current test and power cycling test. [56] provides a reliability prediction model for signal diodes, MOSFETs, and metal oxide varistor. The diode is tested with different high temperature cycles and its reliability is obtained. The total multiplier (M) for extrapolation from accelerated testing is given as,

$$M = M_T M_V M_M \tag{25}$$

where M_M is the multiplying factor, M_V is the voltage time multiplier and M_T is the time temperature factor. From this multiplier diode reliability is obtained as,

$$\lambda = e^{(A+B)/MT} \tag{26}$$

Failure rate of component (λ) is obtained from empirically developed constants (*A*, *B*) and total multiplier. In [57], IGBT module reliability is evaluated in wind power converter using various methods. This reliability approach is implemented on interleaved boost and buck converters. The reason for using boost and buck converters is the simplicity in the circuit and system design and high conversion efficiency as compared to the other topologies [58]. Overall, significant research in semiconductor reliability is focused on LEDs and SiC diodes, but generalized reliability estimation model for power diodes is not included.

Research has also been carried out to estimate the reliability of capacitors. Existing literature shows that there are several accelerated testing methods applicable to multilayer capacitors. Different reliability methods are presented for the chip capacitor mounted on a hybrid IC in [59]. In this research deterioration of the dielectric was observed at high-temperature and under high-voltage condition. Some reliability models for capacitors are developed for dedicated applications such as [60] where a reliability model for capacitors is developed for power factor correction circuits within power supplies. The performance of a capacitor degrades with variations in the harmonic voltage and current ($\psi(S)$) so the capacitor goes through different high voltage and temperature cycles. The capacitor failure rate (λ_C) is obtained as,

$$\lambda_C = \frac{1}{\psi(S)} = \frac{1}{F_s^{-1}(P)} \tag{27}$$

where $F_S(P)$ is the probability of conditional distribution. Generalized capacitor reliability models are still lacking in the literature.

The reliability models for inductors and transformers are presented and discussed in [59-61]. To estimate the life span of PCB mounted inductors and capacitors, temperature cycling and humidity bias life cycles are carried out in [60]. The inductor reliability is calculated in [61] and a model for that is given in [53] as,

$$\lambda_I = \lambda_b \pi_C \pi_Q \pi_E \tag{28}$$

where λ_I is the failure rate of inductor and π_C is the capacitor stress factor. Although the failures in transformers at converter and inverter levels are not frequently observed in experiments, transformer reliability and its life span estimations can be found in some literature [62, 63].

From a system-level or converter-level perspective, reliability models are more common and utilize conservative sources such as [53]. In [64], the reliability of a boost converter has been analyzed to avoid periodic replacement of components and high maintenance cost. Each component failure rates, Mean Time To Failure (MTTF) and Mean Time Between Failure (MTBF) are also obtained. The converter failure rate is obtained in [64] as,

$$\lambda_{system}(t) = \lambda_{sw}(t) + \lambda_{Cap}(t) + \lambda_{Diode}(t) + \lambda_{Inductor}(t)\,. \tag{29}$$

where λ_{system} is the failure rate of system, λ_{sw} is the failure rate of switching element, λ_{Cap} is the failure rate of capacitor, λ_{diode} is the failure rate of diode and $\lambda_{Inductor}$ is the failure rate of inductors. A similar approach has been shown in [65] for a 250 W multiphase boost converter for PV applications. This paper also follows equation (29) for failure rate estimation of boost converter. In these two papers [64, 65] the component level variation is not observed and its impact on the system level reliability is also not presented.

Some of the research is based on specific system reliability analysis and its degradation due to the effect of other parameters in the system. For instance, [66] studies the effect of nuclear radiation and ionization on power electronic converters. Generally DC-DC converters are used to supply power to various systems in a nuclear power plant. These experiments are carried out with the help of a simulation that includes gamma radiation effects to predict the life span of a buck converter. The buck converter failure rate is obtained in [66] as,

$$\lambda_{system} = {}^{N_f}\!/_{t \times No} \tag{30}$$

where λ_{system} is the failure rate of system, N_f is the number of component failures at time t , No is the number of components. The impact of ionization, high temperature and radiation on buck converter MOSFET is also observed in [67]. Component parasitic element performance is also checked for different temperature and radiation values. Flyback converter reliability is addressed in [68] for zero-voltage-switching (ZVS) flyback converters. In [69], a simulation model is developed for flyback converters used in heavy load applications and in order to improve their reliability for various temperature ranges, an atomic circuit block has been developed. In [70], electro-thermal and thermo-mechanical accelerated testing methods are implemented on a power inverter for the photovoltaic AC modules with the help of the rain flow cycle counting approach.

Thus, overall system reliability estimation methods are widely observed in the literature but generalized system-level reliability estimation methods for any converter type need to be developed.

2.3.2 Reliability Modeling and Rapid Prototyping Methods

In this section reliability modeling methods available in the literature are discussed. Majority of the research is mainly focused on failure rate analysis and reliability modeling methods. A useful reference for definitions of the Mean Time To Failure, Mean Time Between Failures,

failure rate, and reliability is MIL-HDBK-338B [71]. For example, failure rate of power electronic components is analyzed with the help of MIL-HDBK-217F in [72] and in [73] where the Weibull failure rate analysis method is used to determine failure rate in automotive components. Monte–Carlo method is broadly used to determine system failure analysis and diagnosis, for instance in [74] where the reliability of a light sensor system is analyzed. In [74] a multistage automotive assembly process is considered as a case study to validate the reliability model. Failure Mode and Effect Analysis (FMEA) method is also frequently used to perform root cause analysis and failures of components as can be seen in [75] where solar module and power electronic converter failures are analyzed using FMEA. Other probabilistic methods have also been proposed. For example, the probability of occurrence of each fault sequence in an induction motor drive is studied using a Markov reliability modeling approach in [76].In this paper FMEA, Monte–Carlo method and Markov models are used to analyze faults in different controllers, sensors and power electronic systems. Reliability modeling methods with the help of fault tree analysis are also observed in the existing literature. This tool is especially useful to evaluate safety and risk analysis aspect of system. For example in [77] the reliability of cores, windings, brushing and tank of the HVDC transformers is obtained using fault tree analysis. Other research such as [78] has focused on six-sigma methods mainly because the failure rate of some components or circuits is assumed to be normally distributed. In [78] specific designs for reliability practices are prepared for the designers to understand the relationship between selected components and predicted system failure rates.

Literature on power electronics reliability modeling generally lacks a systematic method to evaluate a component or converter reliability and estimate its life span irrespective of the converter topology. Also, rapid prototyping tools for reliability modeling are not common, but

new applications requiring more reliable designs such as in aerospace and automotive systems will require such tools. It is important to note that reliability modeling and rapid prototyping in power electronic converters is beyond the scope of this thesis, but a brief literature review is presented here.

2.4 Summary of Literature Review Findings

Several conclusions can be drawn from the literature review in Sections 2.1-2.5:

1) Power loss models exhibit a number of ambiguities such as, parasitic elements not being considered and considering only specific component power losses while deriving system level power losses. Furthermore, PCBs and gate drive power losses are frequently ignored. Considering these elements can thus provide higher modeling accuracy.
2) Generalized power loss models are not commonly addressed in the literature.
3) Rapid prototyping methods for the above models are frequently ignored. Considering all these problems, a new power loss model is developed in further sections which should be a significant improvement over these limitations.
4) Cost models for components or converters observed in the literature are developed specifically for some components such as power MOSFETs while a generalized cost estimation tool based on all components in the converters is not developed.
5) Some cost models ignore essential elements of the system such as magnetic cores.
6) Cost models observed in the literature may not be able to evolve as per changes in technology or cost profiles over time.

Rapid prototyping cost estimation tools have also not been observed in the literature studied so far. Further sections will describe in detail the power loss and cost models proposed in this thesis

for power electronic components that are used as building blocks for converters. Rapid prototyping tools based on these models are also developed for individual components or building blocks, and in order to minimize the converter power loss or cost in an optimization mode.

CHAPTER 3: POWER LOSS MODELS FOR CONVERTERS

Power loss modeling is one of the essential steps in helping to improve the efficiency of a circuit by design. It is the most important tool to analyze the component power loss, its contribution towards the total system level power loss and its effect on the other components' power losses in order to determine the efficiency of the circuit. Inductors and MOSFETs are main components in boost and buck converters from a power loss perspective [79]. Similarly, the coupled inductor or transformer is a critical component of the flyback converter, which decides whether system's operation is in CCM or DCM, as well as overall flyback converter power loss [80]. Component non-idealities and parasitic elements also play a major role in increasing power losses of a component, so these parameters also have to be studied while developing a power loss model. Thus, to improve efficiency of the converter, each component power loss, along with its non-idealities and its contribution towards total system power loss, have to be analyzed.

In this chapter, components are considered as building blocks and the overall system-level power loss is obtained by configuring these building blocks as desired.

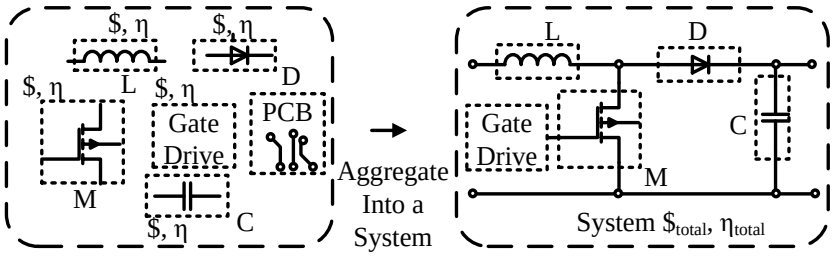

Figure 2 Example illustration on how to aggregate component level models into a system

The proposed approach is implemented on boost, buck and flyback converters and can be extended to buck-boost, Ćuk, and other converters. Figure 2 illustrates how to aggregate component level models into a system. This figure shows basic power electronic components

along with a gate drive circuit and PCB. A power loss model for each component is the same but variables such as voltage and current vary in value based on the converter topology.

Power loss models are based on converter voltage, current, power, and frequency ratings and operating conditions along with basic datasheet information. These models are derived on boost, buck in CCM and flyback converter in DCM. To derive power loss models for these converters, a generalized component-level approach is implemented. As the converter topology and its characteristics change, modifications are carried out in the power loss models for each converter. These power loss models are then aggregated in to a rapid prototyping tool to obtain simple, efficient and user friendly operation.

In this chapter, section 3.1 discusses generalized component level power loss models of each of the fundamental components in a power electronic converter. Section 3.2 explains the component level power losses for specific converter topologies and shows model derivation based on voltage and current values and/or waveforms for different converters. Section 3.3 shows experimental results to validate the proposed models.

3.1 Generalized Component-Level Power Loss Models

Generalized power loss models are derived based on equivalent circuit models of each major component by considering component non-idealities and parasitic elements irrespective of the converter topology.

In the upcoming model derivations, some assumptions are made to facilitate the modeling process: i) MOSFET C_{gs} is considered to calculate MOSFET gate drive losses, but the C_{gd} and the C_{ds} are neglected, because power losses in these capacitances are almost negligible; ii) In Figure 4, only the linear region of Δi is considered, however, sometimes the exponential region can also be observed for Δi; iii) For diodes, only the series resistance R_D is considered for

conduction loss, while the diode parallel capacitance is neglected because power loss within it is almost zero; iv) In an inductor, approximate value of P_{CORE} is obtained from the R_C value; this formula is based on actual empirical results; v) The inductor current waveform is not always linear as shown in Figure 7, but it is assumed to be linear in order to develop a power loss equation for the inductor; vi) For the capacitor, R_P and ESR are considered to model power losses in the capacitor, but ESL (i.e., equivalent series inductance) is ignored because it is usually only observed at high frequencies; vii) Gate drive losses are mainly observed within capacitances surrounding the gate drives ICs. CMOS capacitances contribute less power loss when bootstrap and supply capacitors are connected [85] and are thus ignored.

3.1.1 MOSFET Losses

In power electronic converters, MOSFETs operate as switching elements. Figure 3 shows a MOSFET model with its non-idealities.

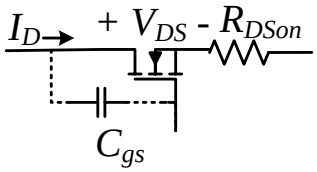

Figure 3 MOSFET model with non-idealities

MOSFET Conduction loss (P_{CM}) [79] is,

$$P_{CM} = R_{DSon} I_{Drms}^2 , \tag{31}$$

where I_D is represented as shown in Figure 4.

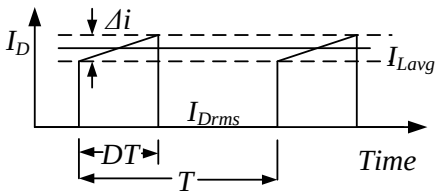

Figure 4 MOSFET drain current

In the conduction loss equation, R_{DSon} is drain-to-source resistance, I_{Drms} is drain-to-source RMS current. Switching losses of MOSFETs are mainly divided into two parts, the turn-on loss ($P_{ON(M)}$) and the turn-off loss ($P_{OFF(M)}$). Total switching losses in a MOSFET (P_{SW}) are thus [81],

$$P_{SW} = P_{ON(M)} + P_{OFF(M)} \tag{32}$$

where for a fixed f_{sw},

$$P_{ON(M)} = \frac{1}{2} V_{DS} I_{Don} t_r f_{sw}, \tag{33}$$

$$P_{OFF(\mathrm{M})} = \frac{1}{2} V_{DS} I_{Doff} t_f f_{sw}. \tag{34}$$

Gate losses (P_G) are usually observed at C_{gs} [79],

$$P_G = Q_{gs} V_{Supply} f_{sw}. \tag{35}$$

Thus, total power losses in a MOSFET ($P_{loss(MOSFET)}$) are,

$$P_{loss(\mathrm{MOSFET})} = P_{CM} + P_{SW} + P_G. \tag{36}$$

whereas, V_{DS} is drain-to-source voltage, I_{Don} is MOSFET on-state current, I_{Doff} is MOSFET off-state current, t_r is MOSFET rise time, t_f is MOSFET fall time, f_{sw} is switching frequency, Q_{gs} is gate-to-source charge and V_{Supple} is supply voltage.

3.1.2 Diode Losses

Diodes in power electronic converters act as rectifiers and also block reverse voltages. Figure 5 shows a diode model with its non-idealities.

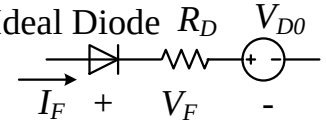

Figure 5 Diode model with non-idealities

Diode conduction loss (P_{CD}) is modeled as,

$$P_{CD} = V_{D0}(1-D)I_{Favg} + R_D(1-D)I_{Frms}^2 , \tag{37}$$

where typical values of V_{D0} and R_D are,

$$V_{D0} = \frac{V_{Dmax}}{V_{Dtyp}} \tag{38}$$

$$R_D = \frac{\Delta V_F}{\Delta I_F} \tag{39}$$

whereas, V_{D0} is diode initial state voltage, I_{Favg} is diode average forward current, I_{Frms} is diode RMS forward current, R_D is diode on-resistance, D is duty ratio, V_{Dmax} is diode maximum voltage, V_{Dtyp} is diode typical forward voltage, ΔV_F is change in diode forward voltage and ΔI_F is change in diode forward current.

There are two switching losses of a diode — turn-on loss and turn-off loss. The turn-on loss is usually ignored because the diode starts conducting from an off-state. The diode switching loss (P_{SWD}) is thus [82],

$$P_{SWD} = \frac{1}{2} Q_{rr} V_{rr} f_{sw} . \tag{40}$$

and the total diode power loss ($P_{loss(Diode)}$) is,

$$P_{loss(Diode)} = P_{CD} + P_{SWD} \tag{41}$$

In equation (40) and (41), Q_{rr} is diode reverse recovery charge, V_{rr} is diode reverse recovery voltage and f_{sw} is switching frequency.

3.1.3 Inductor Losses

An inductor stores energy in its magnetic field. Figure 6 shows an inductor along with its non-idealities and Figure 7 shows the inductor current waveform.

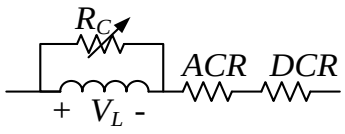

Figure 6 Inductor model with non-idealities

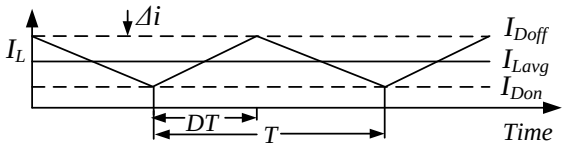

Figure 7 Inductor current waveform

The core loss (P_{CORE}) is obtained with the help of Steinmetz equation and given in [83, 84] as,

$$P_{CORE} = K_1 f^x B^y V_e . \tag{42}$$

If core loss coefficients are not supplied by a manufacturer, R_C can be used and P_{CORE} is estimated as,

$$P_{CORE} \approx \frac{V_L^2}{R_C} . \tag{43}$$

Resistive losses can also be estimated as shown in [83, 84],

$$P_{DCR} = I_{Lavg}^2 DCR , \tag{44}$$

$$P_{ACR} = I_{Lrms}^2 ACR . \tag{45}$$

Total power loss of an inductor ($P_{loss(Inductor)}$) is thus,

$$P_{loss(Inductor)} = P_{CORE} + P_{DCR} + P_{ACR} . \tag{46}$$

whereas, K_1 is the inductor core material constant, f is the inductor current frequency, B is the peak flux density, V_e is the effective core volume, V_L is the inductor voltage, R_C is the effective core impedance, ACR is the inductor AC resistance, DCR is the inductor DC resistance, P_{DCR} is the DC resistance power loss, P_{ACR} is the AC resistance power loss, I_{Lavg} is the inductor average current, I_{Lrms} is the inductor RMS current and x,y is core loss coefficients.

3.1.4 Capacitor Losses

Capacitors are another major storage element in power electronic converters. Figure 8 shows a capacitor equivalent model with its non-idealities.

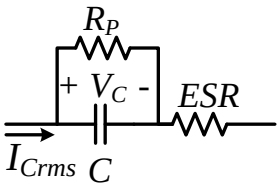

Figure 8 Capacitor model with non-idealities

Two major power losses in the capacitor are those in its AC and DC resistances [85]. The capacitor AC resistance loss (P_{ac}) is,

$$P_{ac} = I_{Crms}^2 ESR\,. \tag{47}$$

while the capacitor DC resistance loss (P_{dc}) is,

$$P_{dc} = \frac{V_C^2}{R_P}\,. \tag{48}$$

Total power loss of the capacitor ($P_{loss(Capacitor)}$) is thus,

$$P_{loss(Capacitor)} = P_{ac} + P_{dc}\,. \tag{49}$$

P_{dc} is small as compared to P_{ac} as capacitors are mainly used to pass current ripple, thus P_{dc} it is frequently ignored. In these equations I_{Crms} is the capacitor RMS current, ESR is the equivalent series resistance, V_C is the capacitor voltage, R_P is the capacitor parallel resistor,

3.1.5 PCB Losses

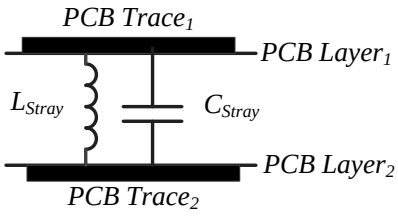

Figure 9 PCB equivalent model

Figure 9 shows PCB equivalent model. Stray inductances and capacitances are usually observed in multilayer PCBs [86, 87]. Trace power loss (P_{trace}) [88] is calculated as,

$$P_{trace} = I_{trace}^2 R_{trace}\,. \tag{50}$$

Stray inductance power loss (P_{Lstray}) is obtained [88] as,

$$P_{Lstray} = I_{trace} L_{stray} \left(\frac{di}{dt} \right). \tag{51}$$

where L_{stray} can be estimated in μH as,

$$L_{stray} = 2 \times 10^{-4} L_e \left[\ln\left(\frac{2L_e}{W+H} \right) + 0.2 \left(\frac{W+H}{Le} \right) + 0.5 \right]. \tag{52}$$

As presented in [88] stray capacitance is estimated as,

$$C_{stray} = \frac{0.085 E_r A}{d}, \tag{53}$$

and the stray capacitance power loss (P_{Cstray}) is,

$$P_{Cstray} = \frac{1}{2} V_d^2 C_{Stray} f_{sw}\,. \tag{54}$$

The total PCB power loss (P_{PCB}) is thus,

$$P_{PCB} = P_{trace} + P_{Lstray} + P_{Cstray}\,. \tag{55}$$

whereas, I_{trace} is PCB trace current, R_{trace} is PCB trace resistance, L_e is the length of PCB trace H is height of PCB trace, L_{stray} is the PCB stray inductance, C_{stray} is the PCB stray capacitance W is the width of PCB trace, E_r is the dielectric constant for air, A is the plate area in mm^2, d is the plate separation in mm.

3.1.6 Gate Drive Losses

Major power loss in the gate drive circuit is normally observed across its supply pin and bootstrap capacitor pin. Figure 10 shows a gate drive IC equivalent model.

Gate drive losses shown in this paper mainly focused on self-oscillating ICs or dedicated application ICs

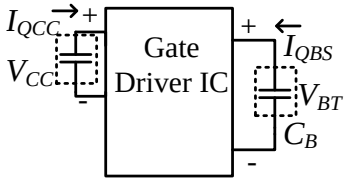

Figure 10 Gate drive ICs equivalent model

Gate drive power loss (P_{GDRV}) is calculated as in [89] to be,

$$P_{GDRV} = P_{VCC} + P_{BT}\,, \tag{56}$$

where ,

$$P_{VCC} = I_{QCC} V_{CC}\,, \tag{57}$$

$$P_{BT} = I_{QBS} V_{BT}\,. \tag{58}$$

whereas, I_{QBS}, I_{QCC} is the gate drive quiescent currents, V_{CC} is gate drive IC supply voltage, V_{BT} is the gate drive IC bootstrap voltage. The converter total power loss (P_{Total}) is thus:

$$P_{\text{Total}} = P_{loss(MOSFET)} + P_{loss(Inductor)} + P_{loss(Diode)} + P_{loss(Capacitor)} + P_{PCB} + P_{GDRV} \tag{59}$$

3.2 Power Loss Models for Several Converters

Equations explained in the previous section are common in the literature but are rarely presented for specific converter topologies. In this section, power loss models for boost and buck converter in CCM and flyback converter in DCM are explained in detail. These converters are used as examples due to their common use in any applications and their simple construction and analysis. All generalized equations are reformulated in terms of input and output parameters and datasheet information.

When power loss equations for a specific converter are prepared, some approximations are made, such as when MOSFET switching power losses in the boost converter are calculated, drain

to source voltage is assumed as V_{in} only. Ideally, while calculating drain to source voltage V_{DS}, the voltage across inductor V_L should be subtracted from input voltage V_{in}. However, since inductor contributes almost zero power loss in switching losses of the MOSFET, it can be excluded from measurement of MOSFET switching power loss. When the diode switching loss in the buck converter is calculated, the power loss across ESR is not considered. In Figure 12, the flyback transformer's primary current waveform is assumed to be linear, but sometimes it is exponential. Similarly, the flyback inductor switching waveform as shown in Figure 13 excludes the exponential region and the effect of disturbances on the linear region. These generalized assumptions are made because their effects on power loss models are insignificant and they cannot reduce the source of error in the estimated and the measured power losses.

3.2.1 Boost Converter in CCM

A typical non-ideal boost converter is shown in Figure 11. Derivations for boost converter in CCM are as follows,

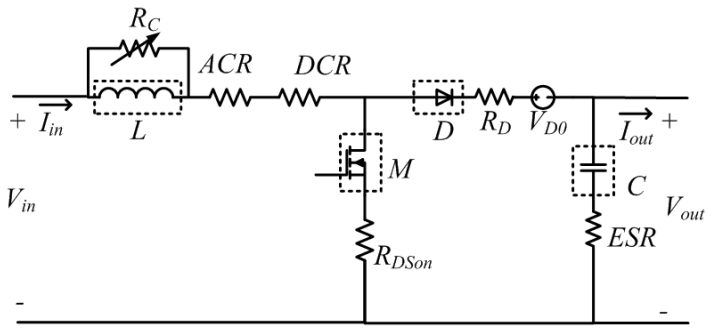

Figure 11 Boost converter with its non-idealities

3.2.1.1 MOSFETs Losses

P_{CM} is obtained from (31) and can be estimated [90,91] as,

$$P_{CM} = R_{DSon} D \left[I_{in}^2 + \frac{\Delta i^2}{12} \right] . \tag{60}$$

To calculate P_{SW}, I_{Don} and I_{Doff} can be obtained from Figure 7,

$$I_{Don} = I_{in} - \frac{\Delta i}{2}, \tag{61}$$

$$I_{Doff} = I_{in} + \frac{\Delta i}{2}, \tag{62}$$

$$V_{DS} = V_{in}. \tag{63}$$

Thus, $P_{ON(M)}$ and $P_{OFF(M)}$ are calculated as,

$$P_{ON(\mathrm{M})} = \frac{1}{2} V_{in} \left(I_{in} - \frac{\Delta i}{2} \right) t_r \, f_{sw}, \tag{64}$$

$$P_{OFF(\mathrm{M})} = \frac{1}{2} V_{in} \left(I_{in} + \frac{\Delta i}{2} \right) t_f \, f_{sw}. \tag{65}$$

whereas, V_{in} is the converter input voltage, Δi is the inductor ripple current, I_{in} is the converter input current, V_{DS} is the drain-to-source voltage, V_{out} is the converter output voltage and I_{out} is the converter output current and V_F is the diode forward voltage.

3.2.1.2 Diode Losses

P_{CD} and P_{SWD} are obtained by referring (37) and (40) as,

$$P_{CD} = V_{D0}(1-D) I_{in} + R_D (1-D) I_{in}^2, \tag{66}$$

$$P_{SWD} = \frac{1}{2} Q_{rr} \left(V_{out} - V_{in} - I_{in} DCR \right) f_{sw}. \tag{67}$$

3.2.1.3 Inductor Losses

P_{CORE}, P_{DCR} and P_{ACR} can be calculated as,

$$P_{CORE} \approx \frac{\left(V_{out} - V_{in} - I_{in} DCR - V_F \right)^2}{R_C}, \tag{68}$$

$$P_{DCR} = I_{in}^2 DCR, \tag{69}$$

$$P_{ACR} = \frac{\Delta i^2}{12} ACR \,. \tag{70}$$

3.2.1.4 Capacitor Losses

$P_{loss\,(Capacitor)}$ is obtained using (47) and Figure 8 as,

$$P_{loss(Capacitor)} = \frac{\Delta i^2}{12} ESR \,. \tag{71}$$

3.2.2 Buck Converter in CCM

A typical non-ideal buck converter is shown in Figure 12. Buck converter in CCM operation is considered for the following derivations:

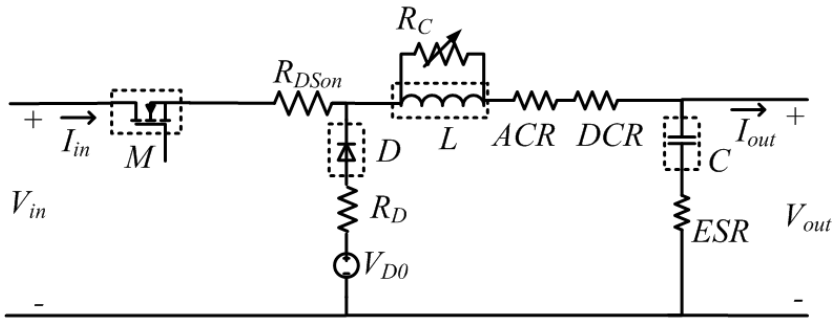

Figure 12 Buck converter topology for power loss model

3.2.2.1 MOSFETs Losses

P_{CM} is obtained from (31) and can be estimated from [91] as,

$$P_{CM} = R_{DSon} D \left[I_{out}^2 + \frac{\Delta i^2}{12} \right], \tag{72}$$

To calculate P_{SW}, I_{Don} and I_{Doff} can be obtained from figure 7 and V_{DS} is as (63) .Thus, P_{ON} and P_{OFF} are obtained as,

$$I_{Don} = I_{out} - \frac{\Delta i}{2} \,, \tag{73}$$

$$I_{Doff} = I_{out} + \frac{\Delta i}{2} \,, \tag{74}$$

$$P_{ON(\mathrm{M})} = \frac{1}{2} V_{in} \left(I_{out} - \frac{\Delta i}{2} \right) t_r \, f_{sw} \,, \tag{75}$$

$$P_{OFF(\mathrm{M})} = \frac{1}{2} V_{in} \left(I_{out} + \frac{\Delta i}{2} \right) t_f \, f_{sw} \,. \tag{76}$$

3.2.2.2 Diode Losses

P_{CD} and P_{SWD} are obtained by referring (37) and (40) as,

$$P_{CD} = V_{D0}(1-D) I_{out} + R_D (1-D) I_{out}^2 \,, \tag{77}$$

$$P_{SWD} = \frac{1}{2} Q_{rr} \left(V_{out} + I_{out} DCR \right) f_{sw} \,. \tag{78}$$

3.2.2.3 Inductor Losses

P_{CORE}, P_{DCR} and P_{ACR} can be calculated as,

$$P_{CORE} \approx \frac{\left(V_{in} - V_{out} - I_{in} R_{DSon} - I_{out} DCR \right)^2}{R_C} \,, \tag{79}$$

$$P_{DCR} = I_{out}^2 DCR \,, \tag{80}$$

$$P_{ACR} = \frac{\Delta i^2}{12} ACR \,. \tag{81}$$

3.2.2.4 Capacitor Losses

$P_{loss\,(Capacitor)}$ is obtained using (47) and Figure 8 as,

$$P_{loss(Capacitor)} = \frac{\Delta i^2}{12} ESR \,. \tag{82}$$

3.2.3 Flyback converter in DCM

Flyback converters are widely used in DCM. A non-ideal flyback converter in DCM is shown in the Figure 13.

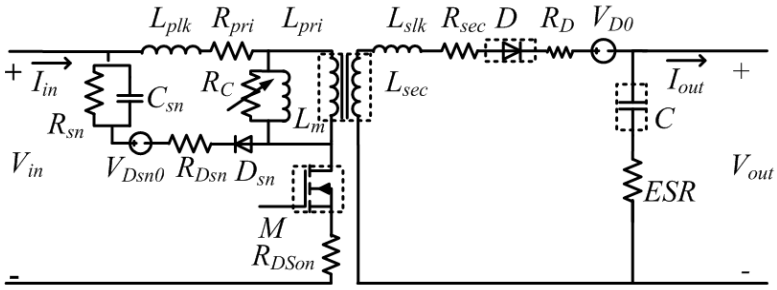

Figure 13 Flyback converter model with its non-idealities

3.2.3.1 MOSFET Losses

For this application MOSFET switching period was considered as $T_{ON}+T_{OFF}=0.8T_S$. MOSFET switching waveform is shown in Figure 14.

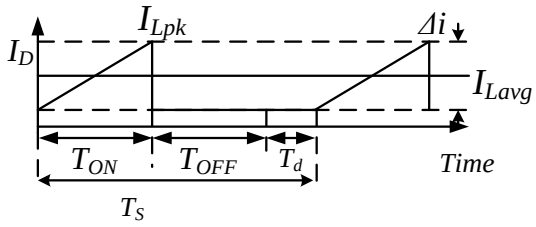

Figure 14 MOSFET switching waveform

Since,
$$T_{ON} = \frac{0.8T_S\left(V_{out}+V_F\right)}{V_F}\ , \tag{83}$$

$$V_{DS} = V_{in} + nV_{out}\,, \tag{84}$$

P_{CM} in the flyback converter is described in [91, 92] as,

$$P_{CM} = R_{DSon}\left(\frac{V_{in}}{\left(L_m+L_{pri}\right)f_{sw}}D\sqrt{0.26\left(1+\frac{V_{out}}{V_F}\right)}\right)^2 . \tag{85}$$

For a flyback converter in DCM, I_{Don} is zero but I_{Doff} and P_{SW} are determined using [93, 94] and Figure 15 as,

$$I_{Doff} = \frac{0.9V_{in}D}{2\left(L_m+L_{pri}\right)f_{sw}}\ , \tag{86}$$

$$P_{SW} = P_{OFF(\mathrm{M})} = \left(V_{in} + nV_{out}\right)\left[\frac{0.9V_{in}D}{2\left(L_m + L_{pri}\right)}\right]\frac{t_f}{2}. \tag{87}$$

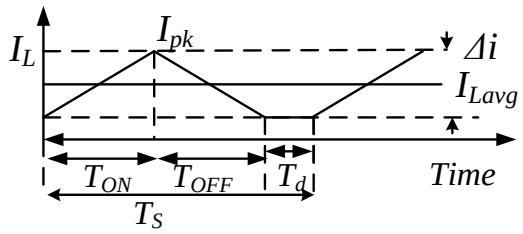

Figure 15 Inductor switching waveform

whereas, L_m is the mutual inductance, L_{pri} is the primary inductance, L_{sec} is the secondary inductance.

3.2.3.2 Diode Losses

P_{CD} and P_{SWD} of the flyback diode are calculated as,

$$P_{CD} = V_{D0}(1-D)I_{out} + R_D(1-D)\left[\frac{0.52nV_{in}D}{\left(L_m + L_{pri}\right)f_{sw}}\right]^2, \tag{88}$$

$$P_{SWD} = \frac{1}{2}Q_{rr}V_{out}f_{sw}. \tag{89}$$

3.2.3.3 Flyback Coupled-Inductor/Transformer Lossses

P_{CORE} is given in [92-94] as,

$$P_{CORE} = K_{fe}B_{AC}^{\beta}A_C L_m. \tag{90}$$

where,

$$B_{AC}^{\beta} = \frac{L_m \Delta i}{N_{\mathrm{Pr}i}A_C}. \tag{91}$$

Primary and secondary resistive losses are calculated [94] as,

$$P_{Rpri} = \left(\frac{0.4V_{in}D}{\left(L_m + L_{pri}\right)f_{sw}}\right)^2 R_{pri}, \tag{92}$$

$$P_{R\sec} = \left(\frac{0.4nV_{in}D}{\left(L_m + L_{pri}\right) f_{sw}} \right)^2 R_{\sec} . \tag{93}$$

In these equations, A_C is the cross-sectional area of core, B^{β}_{AC} is the AC component of flux density, K_{fe} is the inductor current material constant at switching frequency, N_{pri} is the primary windings number of turns, P_{Rpri} is the primary resistance loss, P_{Rsec} is the secondary resistance loss, R_{pri} is the primary DC resistance and R_{sec} is the secondary DC résistance.

3.2.3.4 Capacitor Losses

From (48), $P_{loss\,(Capacitor)}$ is calculated as,

$$P_{loss(Capacitor)} = \left\{ \left[\frac{0.52nV_{in}D}{\left(L_m + L_{pri}\right) f_{sw}} \right]^2 - I_{out}^2 \right\} ESR . \tag{94}$$

3.2.3.5 Snubber Circuit Losses

The main components in the snubber branch are snubber resistor (R_{sn}), snubber capacitor C_{sn} and snubber diode (D_{sn}). R_{sn} and C_{sn} form a clamp unit. Power loss in the clamp unit (P_{clamp}) is represented in [95] as,

$$P_{clamp} = \left(\frac{V_{clamp}}{R_{sn}} \right)^2 = \frac{\left(0.9V_{DSBR} - V_{in}\right)^2}{R_{sn}} , \tag{95}$$

P_{clamp} is also written as,

$$P_{clamp} = \frac{1}{2} f_{sw} L_{pri} \Delta i^2 \left(1 + \frac{V_{in}}{0.9V_{DSBR} - 2V_{in}} \right). \tag{96}$$

Snubber diode conduction loss (P_{CDsn}) is obtained from (41) as,

$$P_{CDsn} = V_{Dsn0}(1-D)nI_{out} + R_{Dsn}(1-D)nI_{Srms}^2 . \tag{97}$$

Snubber diode switching loss (P_{SWDsn}) is obtained as,

$$P_{SWDsn} = \frac{1}{2} Q_{rrsn} V_{in} f_{sw} . \tag{98}$$

whereas, R_{sn} is the snubber resistor, R_{Dsn} is the snubber diode on-state resistance, V_{DSBR} is the drain-to-source breakdown voltage, V_{clamp} is the clamp voltage rise, I_{Srms} is the flyback transformer secondary RMS current, V_{Dsn0} is the snubber diode initial state voltage, Q_{rrsn} is the snubber diode reverse recovery charge, $I_{Dsn(rms)}$ is snubber diode RMS current and $I_{Dsn(avg)}$ is snubber diode avg. current

Total snubber circuit power loss (P_{sn}) is represented as,

$$P_{sn} = P_{clamp} + P_{CDsn} + P_{SWDsn} . \tag{99}$$

3.3 Results

Basic boost, buck and flyback converters were experimentally developed to test the power loss models presented here. These converters were tested in open-loop mode. All parasitic elements and specific test condition examples are given in Table I. Figure 16 shows the board holding both the boost and buck converters. However, gate drive circuits are not powered from V_{in} thus their losses are not included. In addition to assumptions listed in sections 3.1 and 3.2, some approximations are made for testing these converters, e.g. R_C (when not given in a datasheet), and limited measurement accuracy. Each converter and its related results and waveforms are presented and discussed separately. In this section, detailed converter specification, each component power loss and specific converter power losses are organized. Measured power losses are calculated as the difference between measured input and output powers as recorded on the oscilloscope.

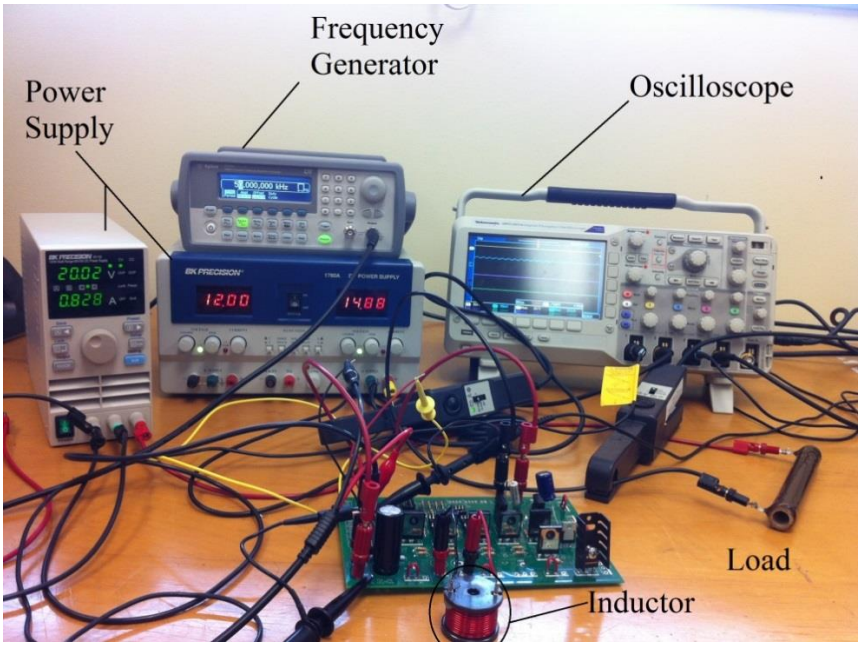

Figure 16 Experimental setup for the buck and boost converters

Table I Example testing conditions and parasitic elements in experimental prototypes

Parameter	**Boost**	**Buck**	**Flyback**
V_{in}	20V	62V	11.2V
I_{in}	3.5A	1.1A	0.38A
V_{out}	77.4V	24.6V	19.6V
I_{out}	0.85A	2.56A	0.15A
Δi	1.1A	2.95A	0.89A
f_{sw}	50KHz	50KHz	100KHz
D	0.75	0.4	0.5
ESR	0.603Ω	0.603Ω	0.603Ω
V_{D0}	1V	1V	1V
R_D	7mΩ	7mΩ	7mΩ
DCR/R_{pri}	0.06Ω	34mΩ	0.09
ACR/R_{sec}	0	1.5Ω	0.58
Q_{rr}	195nC	195nC	195nC
Q_{gs}	64nC	13nC	13nC
R_{DSon}	0.029Ω	0.18Ω	0.18Ω
t_r	100nsec	51nsec	51nsec
t_f	63nsec	36nsec	36nsec
$\approx R_{core}$	3325Ω	-	-
L_m, L_{pri}	-	-	59.4μH
B	-	3400mT	42.42mT
V_e/A_C	-	0.24cm^3	0.97cm^3

3.3.1 Boost Converter Results

Basic boost converter topology is built as shown in Figure 11 and operates in CCM. Table II explains boost converter results for different duty ratios along with actual measurements using a resistive load. Accuracy of the estimated power loss exceeds 92% with less than +/-8% estimation error. Table II represents the components, estimated and measured power losses. Table III presents detailed boost converter component power losses for different duty ratios. For the boost converter operation MOSFET-IRFP4332PBF, inductor-PCV-0-274-10L, diode-MURF860G and capacitor-EEU-EB2D221 are used. Inductor and capacitor values are selected from the rapid prototyping tool selection procedure for the boost converter as will be explained in Section 5.2.1.1 Figures 17-21 demonstrate operation of the boost converter from a 30% duty ratio to a 75% duty ratio. It is observed from Figure 17-21 that as duty ratio increases system performance decreases. The boost converter provides almost ideal performance at the 50% duty ratio but this is a drawback of the V-I measurement method [97] and oscilloscope which cannot capture the accurate results for higher disturbances. Measured power loss ($P_{measured}$) and estimated power loss ($P_{estimated}$) can provide percentage error. Estimation error shown in Table II and later tables is calculated as,

$$\% \text{ Error} = \left(\frac{P_{measured} - P_{estimated}}{P_{measured}} \times 100 \right). \quad (100)$$

Table II Estimated and measured power loss in boost converter

Duty	$P_{Measured}$	$P_{Estimated}$	**%Error**
30%	0.6	0.56	6.6%
40%	0.78	0.72	7.69%
50%	0.97	0.92	5.15%
60%	1.36	1.37	-0.74%
75%	4.21	4.19	0.43%

Table III Detailed boost converter component power losses for different duty ratios

Parameters	Duty Ratios				
	30%	40%	50%	60%	75%
V_{in}	20	20	20.1	20	20
I_{in}	0.45	0.6	0.88	1.35	3.50
V_{out}	28	33	39.8	49.3	77.4
I_{out}	0.3	0.34	0.42	0.52	0.85
f_{sw}	50KHz	50KHz	50KHz	50KHz	50KHz
D	0.3	0.4	0.5	0.6	0.75
$\boldsymbol{P_{Measured}}$	0.6	0.78	0.97	1.36	4.21
P_{loss_Mosfet}	0.10	0.11	0.14	0.19	0.61
P_{loss_Diode}	0.4	0.5	0.54	0.69	1.18
$P_{loss\_Inductor}$	0.03	0.06	0.15	0.34	1.67
$P_{loss\_Capacitor}$	0.01	0.02	0.03	0.04	0.062
P_{PCB}	0.02	0.03	0.06	0.1	0.67
$\boldsymbol{P_{Estimated}}$	0.56	0.72	0.92	1.37	4.19
%Error	**6.6**	**7.69**	**5.15**	**-0.74**	**0.43**

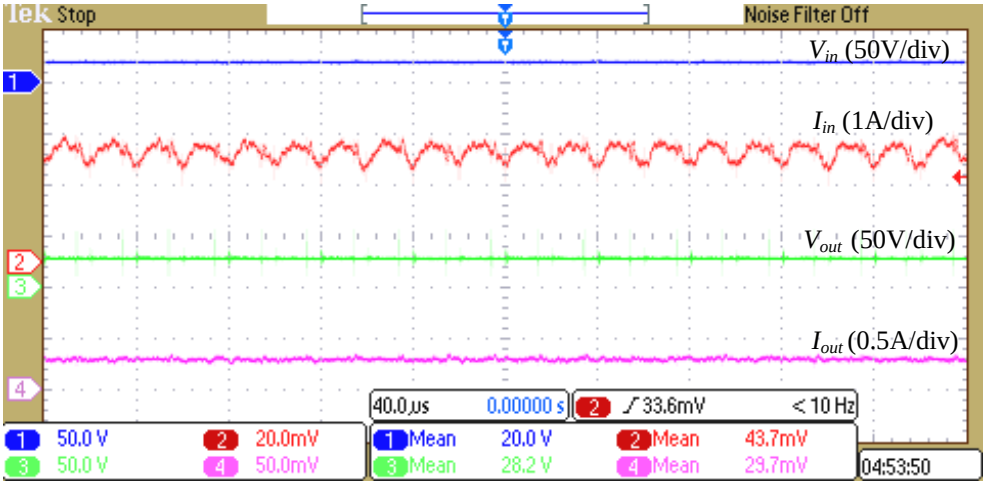

Figure 17 Boost converter results for 30% duty

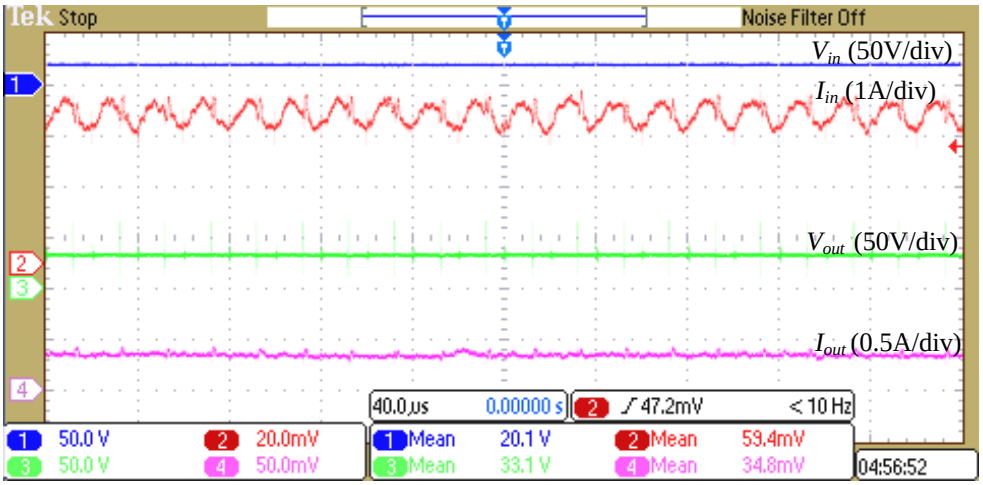

Figure 18 Boost converter results for 40% duty ratio

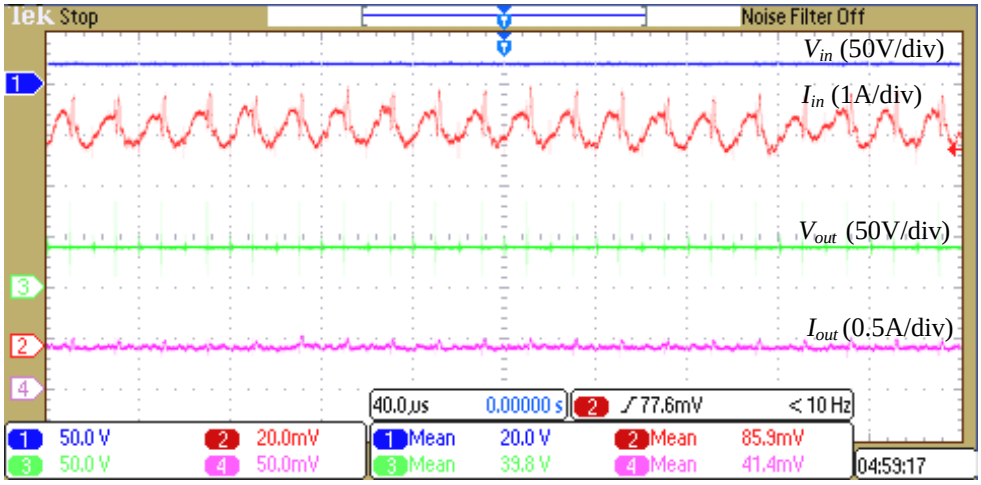

Figure 19 Boost converter results for 50% duty ratio

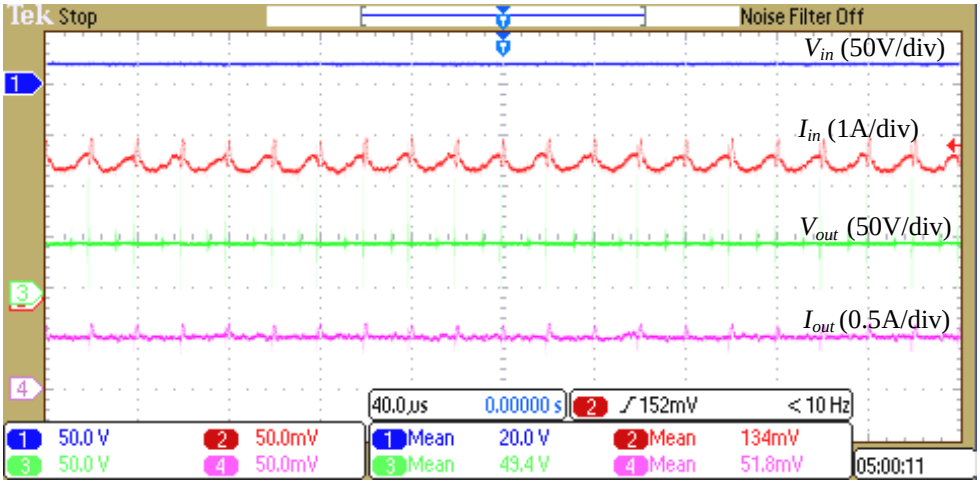

Figure 20 Boost converter results for 60% duty ratio

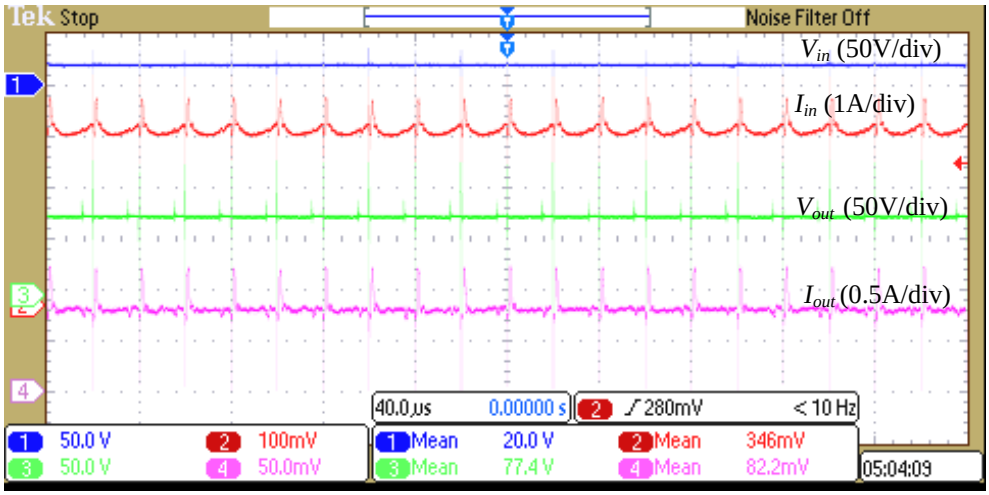

Figure 21 Boost converter results for 75% duty ratio

3.3.2 Buck Converter Results

The basic buck converter topology is built as shown in Figure 12 and operates in CCM. Table IV explains buck converter results for different duty ratios with actual measurements from an oscilloscope and the estimated power loss from the power loss model of the buck converter. The error between the measured power loss and the estimated power loss is less than 8%. Table IV represents components, estimated and measured power losses and Table V presents detailed buck converter component power losses for different duty ratios. For buck converter operation MOSFET- IRFP4332PBF, Inductor- AIRD-03-101k, Diode-MURF860G and capacitor- EEU-EB2D221 are used based on the component selection that will be described in Section 5.2.1.1. Figures 22-25 demonstrate operation of the buck converter from a 20% duty ratio to a 50% duty ratio.

Table IV. Estimated and measured power loss in buck converter

Duty	$P_{Measured}$	$P_{Estimated}$	**%Error**
20%	2.54	2.49	-1.96%
30%	3.76	3.78	0.53%
40%	5.22	5.20	-0.45%
50%	7.05	6.55	-7.09%

Table V Detailed buck converter component power losses for different duty ratios

Parameters	Duty Ratios				
	20%	30%	40%	50%	60%
V_{in}	60	60	62	61	46
I_{in}	0.28	0.6	1.1	1.65	1.6
V_{out}	12.4	18	24.6	30	27.1
I_{out}	1.15	1.79	2.56	3.12	2.55
f_{sw}	50KHz	50KHz	50KHz	50KHz	50KHz
D	0.2	0.3	0.4	0.5	0.6
$\boldsymbol{P_{Measured}}$	2.54	3.76	5.22	7.05	4.49
P_{loss_Mosfet}	0.23	0.45	0.87	1.36	1.01
P_{loss_Diode}	0.99	1.36	1.68	1.74	1.17
$P_{loss\_Inductor}$	0.95	1.31	1.51	1.87	1.22
$P_{loss\_Capacitor}$	0.20	0.32	0.44	0.45	0.24
P_{PCB}	0.13	0.19	0.70	1.13	0.83
$\boldsymbol{P_{Estimated}}$	2.49	3.78	5.2	6.55	4.47
%Error	**-1.96**	**0.52**	**-1.09**	**-7.09**	**-0.45**

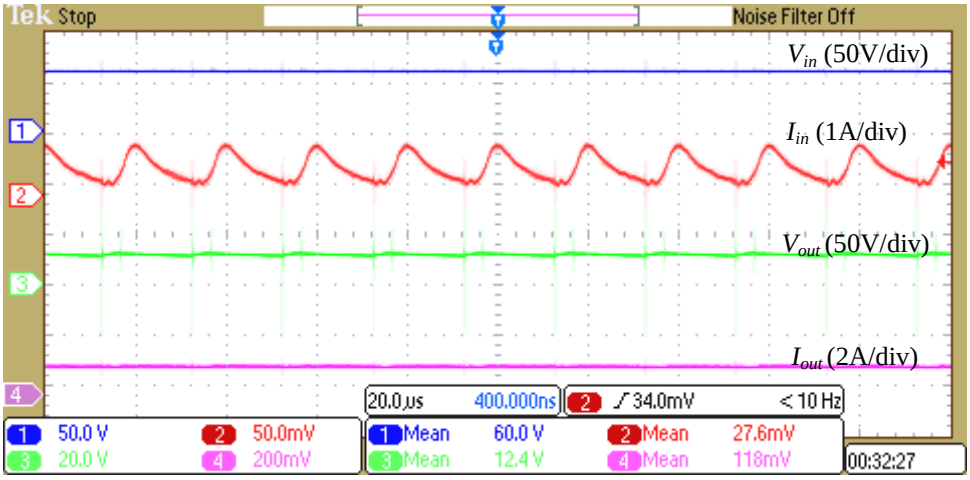

Figure 22 Buck converter results for 20% duty ratio

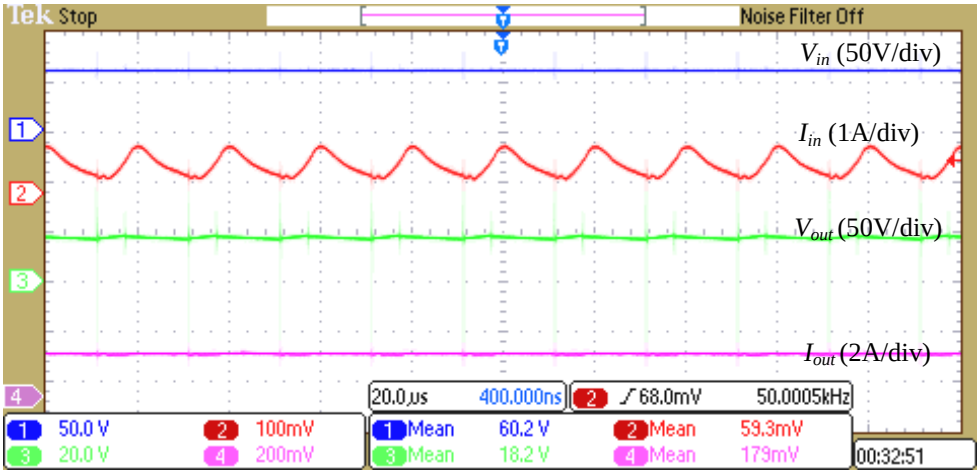

Figure 23 Buck converter results for 30% duty ratio

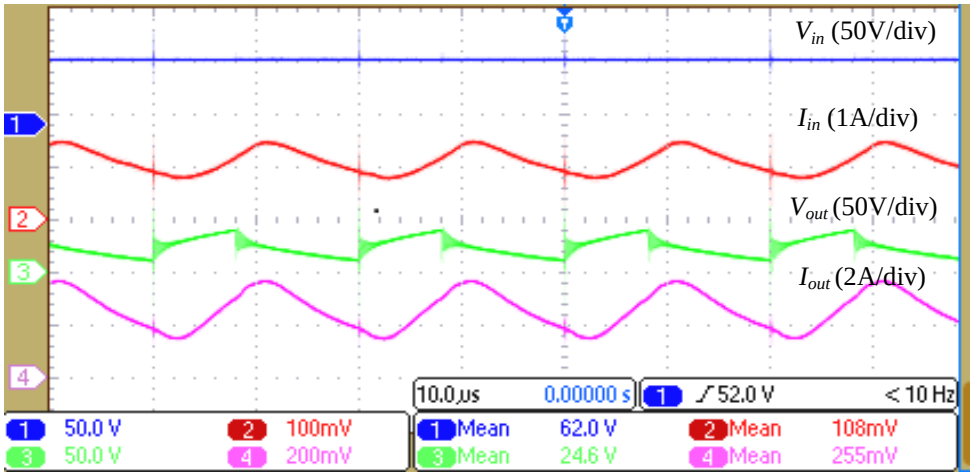

Figure 24. Buck converter results for 40% duty ratio

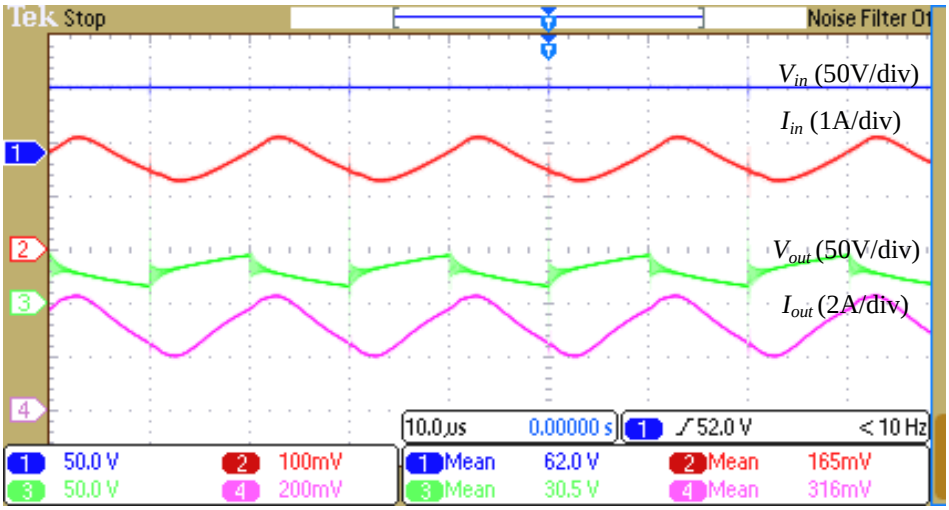

Figure 25 Buck converter results for 50% duty ratio

3.3.3 Flyback Converter Results

Basic flyback converter topology is built as shown in Figure 13 and operates in DCM Flyback converter results for different duty ratios are shown in Table VI with actual measurements from an oscilloscope and the estimated power loss from the power loss model of the flyback converter. The error between the measured power loss and the estimated power loss is less than 5%. Table VII represents components, estimated and measured power losses and Table VII presents detailed flyback converter component power losses for different duty ratios. For flyback converter operation MOSFET-IRFP4332PBF, flyback transformer-Q4338-BL, Diode-EGP10G and capacitor-EEU-EB2D221 are used. Figures 26-29 demonstrate operation of the flyback converter from a 20% duty ratio to a 50% duty ratio that is maximum duty ratio.

Table VI. Estimated & measured power loss in flyback converter

Duty Ratio	$P_{Measured}$	$P_{Estimated}$	**%Error**
20%	0.32	0.31	-3.13%
30%	0.55	0.56	1.81%
40%	0.85	0.82	-4.7%
50%	1.32	1.27	-3.78%

Table VII Detailed flyback converter component power losses for different duty ratios

Parameters	Duty Ratios			
	20%	30%	40%	50%
V_{in}	11.7	11.6	11.6	11.2
I_{in}	0.075	0.2	0.2	0.38
V_{out}	9.26	11.1	14.7	19.6
I_{out}	0.06	0.16	0.1	0.15
f_{sw}	100KHz	100KHz	100KHz	100KHz
D	0.2	0.3	0.4	0.5
$P_{Measured}$	0.32	0.55	0.85	1.32
P_{loss_Mosfet}	0.08	0.16	0.32	0.58
P_{loss_Diode}	0.14	0.22	0.20	0.27
$P_{loss\_Inductor}$	0.03	0.05	0.07	0.09
$P_{loss\_Capacitor}$	0.02	0.02	0.06	0.08
P_{sn}	0.04	0.10	0.14	0.21
P_{PCB}	0.004	0.01	0.02	0.04
$P_{Estimated}$	0.31	0.56	0.81	1.27
%Error	-3.13%	1.81%	-4.7%	-3.78

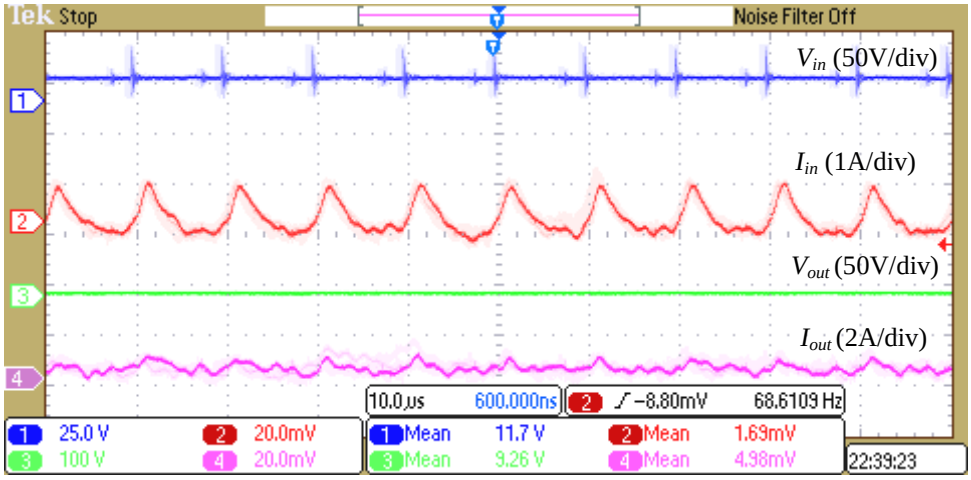

Figure 26 Flyback converter results for 20% duty ratio

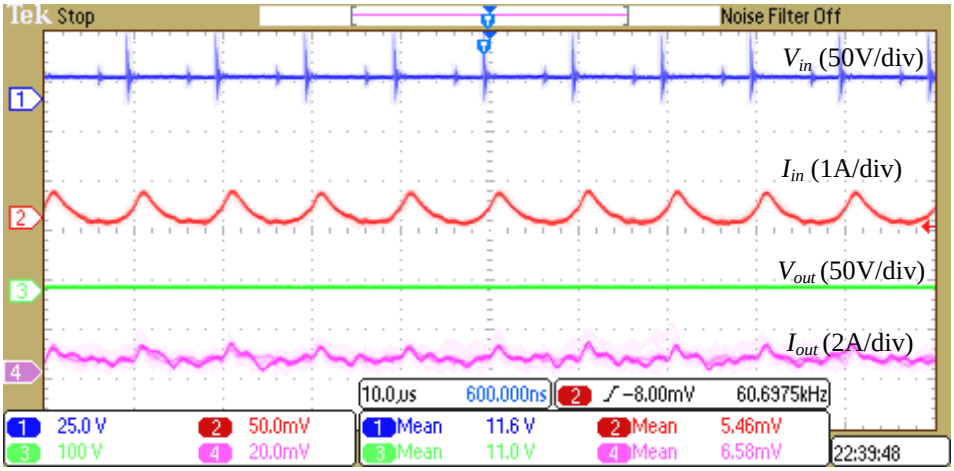

Figure 27 Flyback converter results for 30% duty ratio

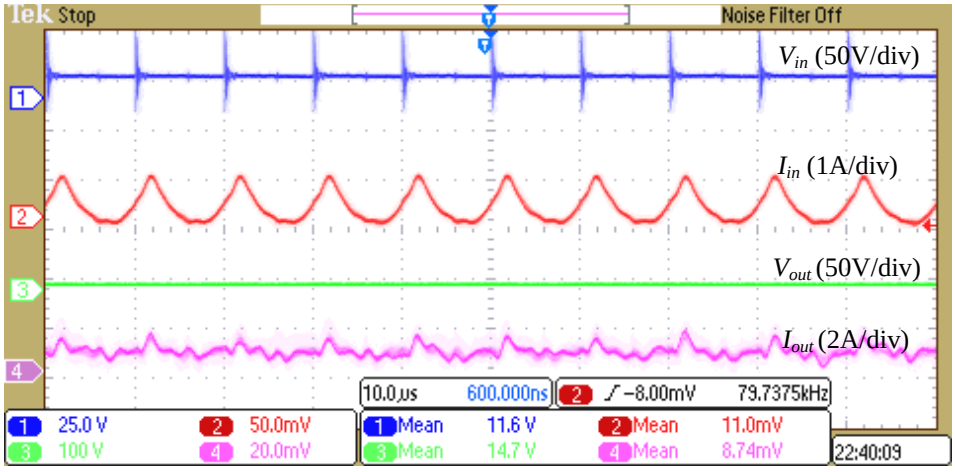

Figure 28 Flyback converter results for 40% duty ratio

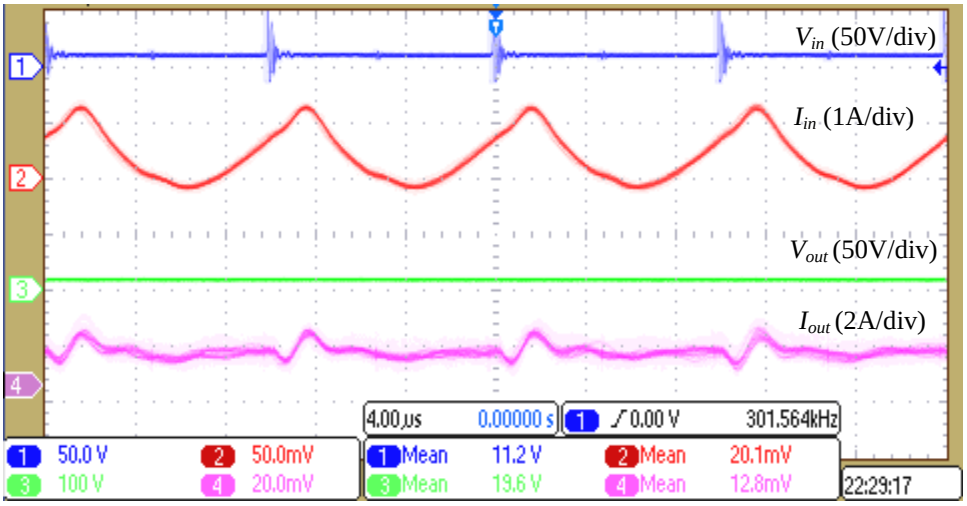

Figure 29. Flyback converter results for 50% duty ratio

Overall, results in Tables II, IV and VI are shown to be within 8% error and thus the power loss models established are proven to be more than 92% accurate. The accuracy of the power loss model is improved by considering the power loss of each component along with its non-idealities and parasitic elements. The estimation of PCB losses has also helped to improve the accuracy. The power loss model can be further improved if power loss of each component of the converter is estimated. This power loss model can also be developed for other components, converter topologies and systems with the same approach. Furthermore, power loss models for microcontrollers and DSP ICs can also improve accuracy and flexibility. Component power losses for each converter are provided in the Appendix I. Detailed derivation of RMS values of drain currents, capacitor RMS current of the flyback converter and inductor currents are given in the Appendix III.

CHAPTER 4: COST MODELS FOR CONVERTERS

The principal function and ultimate aim of industry is to make profitable products. Today's marketplace is full of new products and services changing at a very fast pace. In order to stay competitive in a rapidly changing consumer market, companies must focus on value generation for their customers. This value can be generated through new features and better functionality at lower costs. Cost has emerged as one of the most important attributes of a successful product and of a competitive industry in general.

When industry develops a new product with the customers' requirements in mind, the product has to go through numerous designs, engineering, manufacturing, testing and compliance procedures. All these factors contribute to the product cost and are indispensable to product success. While industry cannot avoid these critical operations in order to reduce cost, it still must remain focused on constantly lowering the cost while maintaining the product quality, reliability and availability at a high level. Developing prudent and practical cost reduction techniques based on raw material prices is thus a vital focus area for product designers and engineers.

In the particular case of electronics components, cost forms a major decision making factor. High-end electronics is an extremely competitive market and customer preferences are pushing developments towards more functionality at progressively lower cost. With the ever rising demand and constant cost pressure, it has become vitally important for electronic components to be designed and manufactured more efficiently and at lower costs.

The cost model developed in this research aims at solving this very important challenge facing a design engineer. These models are based on average prices related to component ratings obtained using an extensive market survey and surface-fitting tools. A large database of cost information for different elements was collected from common manufacturers and suppliers.

Average cost for each component at a certain rating combination was found by considering multiple options. This database was input to MATLAB to create an interpolated graph and the MATLAB surface fitting and the curve fitting tools were used to find a mathematical relationship between cost and component parameters. Cost per quantity was considered to avoid price discrepancy between manufacturers, purchase quantities, etc. It is important to note that component technology and cost profiles change over time as a result of changes in material and manufacturing techniques, but the methodology proposed here still applies.

In this chapter, sections 4.1-4.4 show cost models developed for MOSFETs, diodes, inductors, and capacitors, respectively. Section 4.5 elaborates on the importance of magnetic core cost estimation and shows the proposed core cost model. Section 4.6 discusses the cost model for magnet wire which is also critical to inductor and transformer design. Section 4.7 shows real against estimated prices of various components to validate the developed cost models.

4.1 MOSFET Cost Model

MOSFET selection procedure is based on its drain-to-source voltage, drain current, gate-to-source threshold voltage and switching time. These parameters decide the performance and the efficiency of the circuit. However, when the MOSFET is selected to develop any power electronic converter, its worst case current and voltage stress handling capacity has to be analyzed. Thus, to create a cost model equation for the MOSFET, a large database was prepared using drain to source voltage V_{DS}, drain current I_D and cost.

Figures 30 and 31 depict the mathematical relationship for this database as applicable to single as well as 1000 quantities. Cost per quantity is considered because the prices fluctuate with changing quantities. It can be observed that the structure of these two figures is almost identical. This indicates that even if this approach is implemented for different values of

quantity, the cost model equation from the surface fitting tool remains the same. Thus, the MOSFET cost model equation for multiple quantities ($Cost_M$) is represented as,

$$Cost_M(V_{DS}, I_D) = \sum_{i=0}^{i=13} \alpha_i V_{DS}^{\beta_i} I_D^{\gamma_i}, \tag{101}$$

Table VIII. α_i Coefficients and ranges

Coefficient	Values	Ranges	β_i	γ_i
α_0	1.622	(-9.142, 12.39)	0	0
α_1	0.034	(-0.087, 0.154)	1	0
α_2	-0.133	(-0.89, 0.63)	0	1
α_3	-0.0001	(-8, 25)	2	0
α_4	-0.0016	(-0.0047,-0.0163)	1	1
α_5	0.0058	(-0.01, 0.022)	0	2
α_6	1.3e-8	(-1.6e-6,1.6e-6)	3	0
α_7	8e-6	(-8.8e-7, 1.5e-5)	2	1
α_8	-2.95e-6	(-4.2e-5,3.6e-5)	1	2
α_9	-4.48e-5	(-1.4e-5,5.3e-5)	0	3
α_{10}	1.46e-10	(-1.2e-9,1.5e-9)	4	0
α_{11}	-5.3e-9	(-1.1e-8,5.6e-10)	3	1
α_{12}	-3.5e-8	(-6.9e-8, 1.3e-9)	2	2
α_{13}	1.3e-7	(-8.1e-8,3.4e-7)	1	3

In equation 101, $Cost_M$ is MOSFET cost, V_{DS} is MOSFET drain-to-source voltage, I_D is MOSFET drain-to-source current. α_i values are obtained from the surface fitting tool. Table VIII represents different α_i values and their ranges. To calculate exact cost α_i values must be varied within the specified range. These coefficients cannot change as per the quantity making this equation suitable for use with multiple quantities.

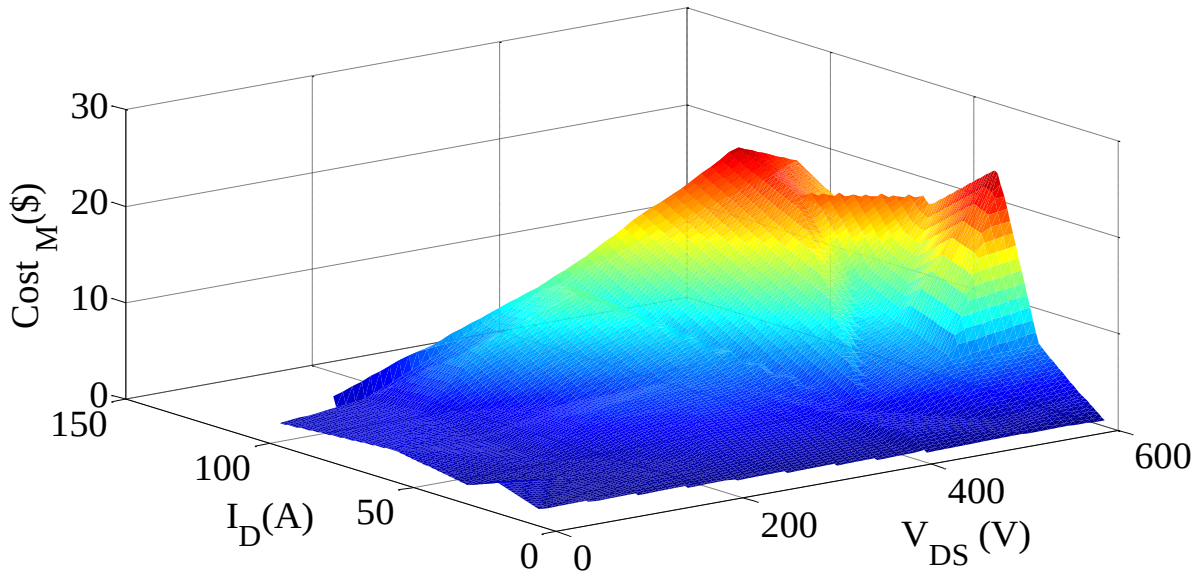

Figure 30 MOSFET cost model for one unit

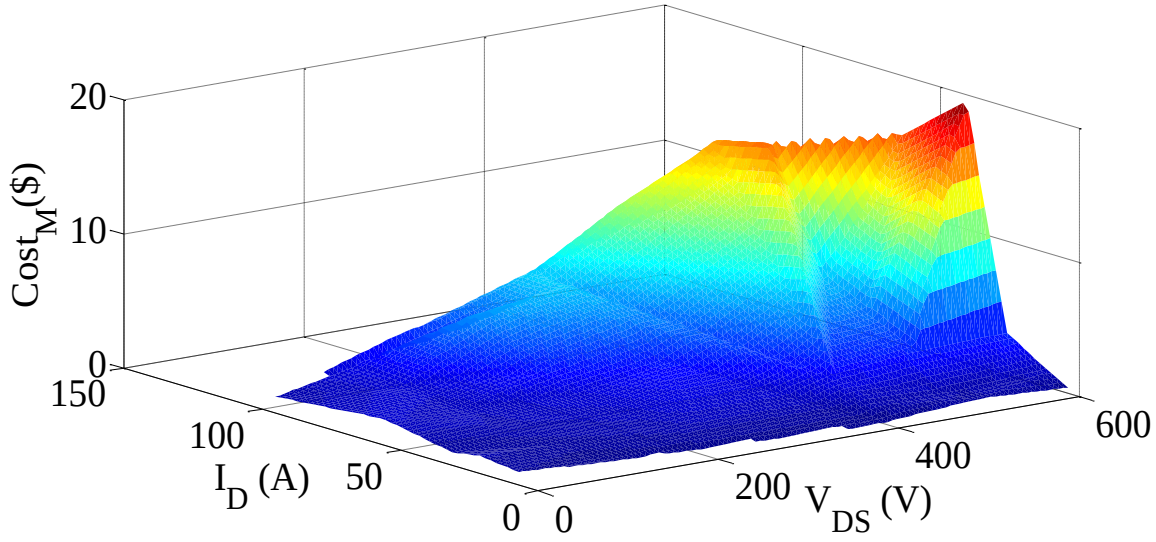

Figure 31 MOSFET cost model for 1000 units

4.2 Diode Cost Model

As described in the power loss model, it is necessary to analyze performance of a diode in 'ON' state as well as in 'OFF' state because when the diode is 'ON' it provides inductor current to the load and when it is 'OFF' it blocks reverse voltage from the load. When selecting a diode

for a power electronic converter, designers have to consider the ability of Diode to block the reverse voltage, capacity to handle peak current, forward voltage drop and the switching operation time. Out of these conditions, diode's selection procedure is mainly concerned with its reverse blocking voltage and its current capacity. With this consideration cost model equation for a diode was derived using DC blocking voltage (V_B), diode forward current (I_F) and the diode cost ($Cost_D$). Interpolated graphs of diodes for single and 1000 quantities are presented in Figure 32 and 33, respectively. These two interpolated graphs are almost identical thus establishing that cost model equation is independent of quantities.

The diode cost ($Cost_D$) is represented as,

$$Cost_D(V_B, I_F) = \sum_{j=0}^{j=2} \delta_j V_B^{\theta_j} I_F^{\kappa_j} . \tag{102}$$

Where δ coefficients are obtained as,

Table IX δ_j coefficients for diode cost model equations

Coefficients	Value	Range	θ_j	κ_j
δ_0	0.22	(-0.1, 0.3)	0	0
δ_1	7e-5	(-2.6e-4, 1.2e-4)	0	1
δ_2	0.1	(-0.08, 0.13)	1	0

In this equation δ_j values are obtained from surface fitting tool. Different δ values and their ranges are presented in Table IX. To calculate exact cost the δ values must be varied within the specified range. These coefficients cannot change as per the quantity so this equation can be used for multiple quantities.

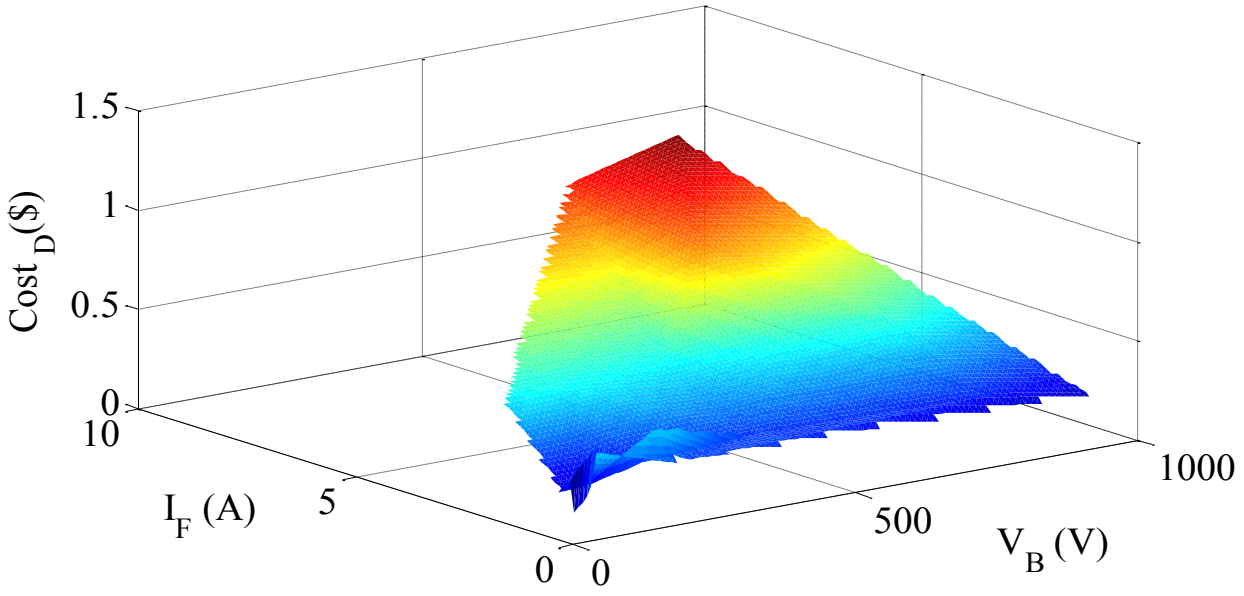

Figure 32 Diode cost model for one unit

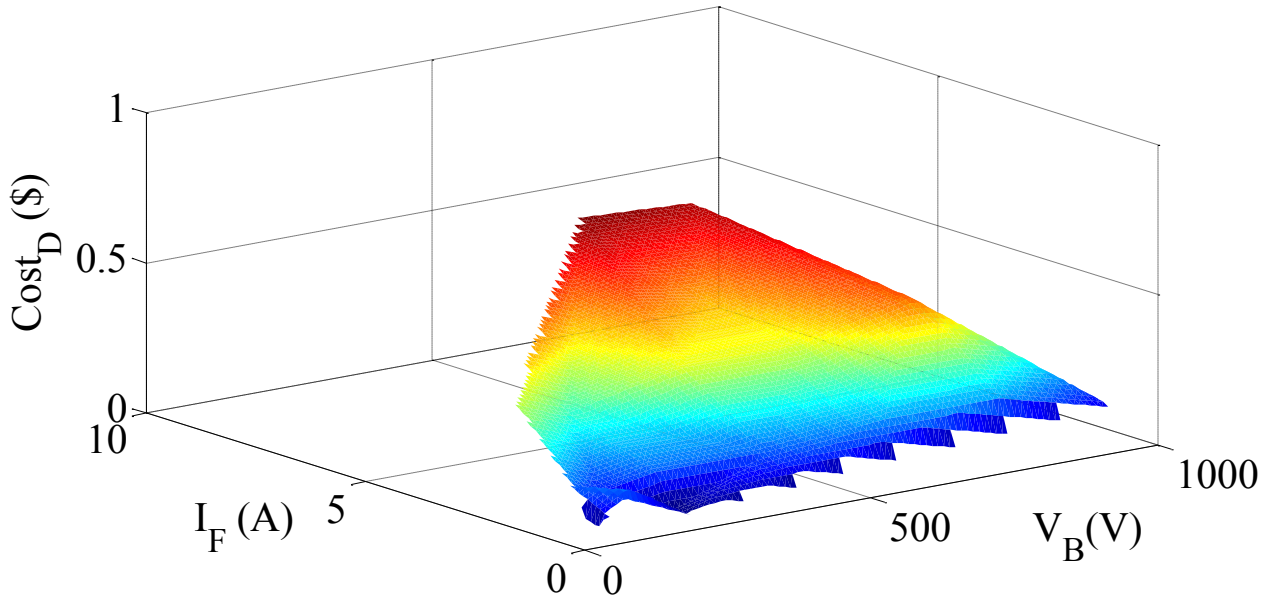

Figure 33 Diode cost model for 1000 units

4.3 Inductor Cost Model

Similar to the MOSFET and diode, an inductor also plays a vital role in the operation of the converter. Moreover, it is the value of the inductance that decides modes of operation for the converter. A smaller value of inductance results in failure of the inductor to operate in a specific mode whereas a higher value increases the start-up and settling times. The cost of an inductor is sometimes higher than that of other components in a converter. Designers may even opt to select the cores and the magnet wires to prepare an inductor as per the application requirement, but the cost model developed in this section is only for the ready-made inductors which are readily available in the market. Cost model for the inductors is based on inductance (L), inductor current (I_L) and cost as shown in Figures 34 and 35. Interpolated graphs are almost identical for single as well as multiple quantities. The inductor cost ($Cost_L$) is represented as,

$$Cost_L(L, I_L) = \chi + \mu \sin(\upsilon \pi L I_L) + \phi e^{-(\omega I_L)^2}, \tag{103}$$

Table X Inductor cost model coefficients

Coefficients	Value	Ranges
x	9.67	(-3.48, 24.83)
μ	61.64	(-25.68, 97.59)
ϕ	-8.246	(-20.63, 8.141)
ν	4.495	(-0.2334, 9.223)
ω	-0.08658	(-0.5143, 0.3411)

In Table X, the inductor cost model coefficients are obtained from surface fitting tool. These coefficients do not change as per the quantity so this equation can be used for multiple quantities. Similar approach can be implemented on the cores and magnet wires for the inductors. The cost models for flyback transformer cores and magnetic wires are based on this approach.

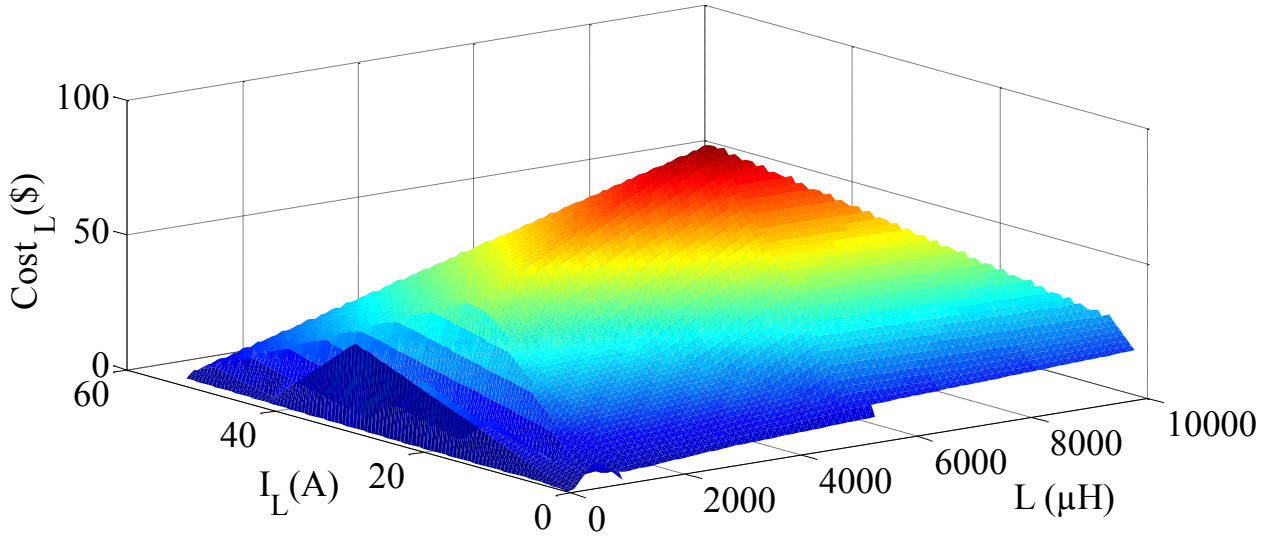

Figure 34 Inductor cost model for one unit

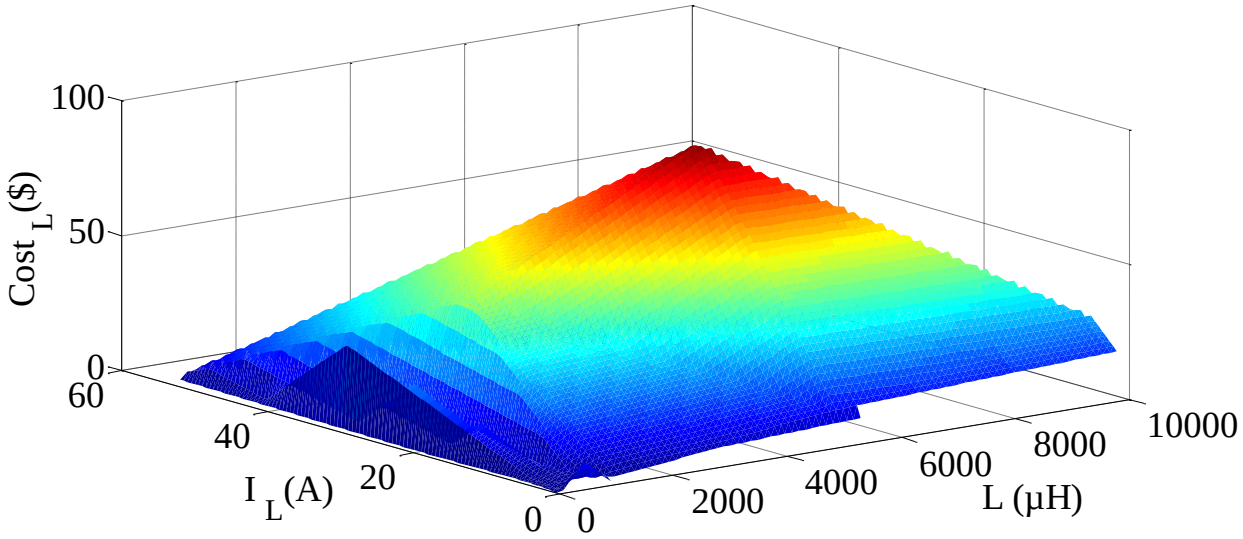

Figure 35 Inductor cost model for 1000 units

4.4 Capacitor Cost Model

A capacitor acts as a filter which is predominantly selected to suppress output voltage ripple and to handle output current ripples in the converter. As described in the previous section, capacitor power loss is dependent upon the ESR value. Thus, while selecting a capacitor for the converter, designers have to consider its capacitance value, capacity of handling the output voltage ripples and the ESR value.

In this cost model, a database was prepared for capacitance value (C), capacitor voltage (V_C) and the corresponding cost. Figures 36 and 37 show the interpolated graphs which are prepared from the capacitor database and the mathematical relationship for these graphs is also presented here.The capacitor cost ($Cost_C$) is represented as,

$$Cost_C(C,V_C) = \sum_{z=0}^{z=8} \eta_z C^{\sigma_z} V_C^{\xi_z}, \tag{104}$$

Table XI. η_z coefficients and ranges

Coefficients	Value	Ranges	σ_z	ξ_z
η_0	-0.5651	(-4.043, 2.913)	0	0
η_1	7.98e-4	(-0.017, 0.019)	1	0
η_2	0.03	(-0.022, 0.082)	0	1
η_3	5.1e-6	(-1.6e-5,1.74e-53)	2	0
η_4	3.2e-5	(-5e-5, 0.0001139)	1	1
η_5	-1.8e-4	(-4e-4,5.9e-5)	0	2
η_6	-4.9e-8	(-1.1e-7,1e-8)	2	1
η_7	1.6e-7	(4.2e-8,2.8e-7)	1	2
η_8	2.5e-7	(-5.5e-8, 5.6e-8)	0	3

Equation 104 represents the cost equation for capacitors, where Table XI presents the η_z coefficients obtained from MATLAB surface fitting tool. These coefficients are not affected by changes in quantity so this equation can be used for multiple quantities.

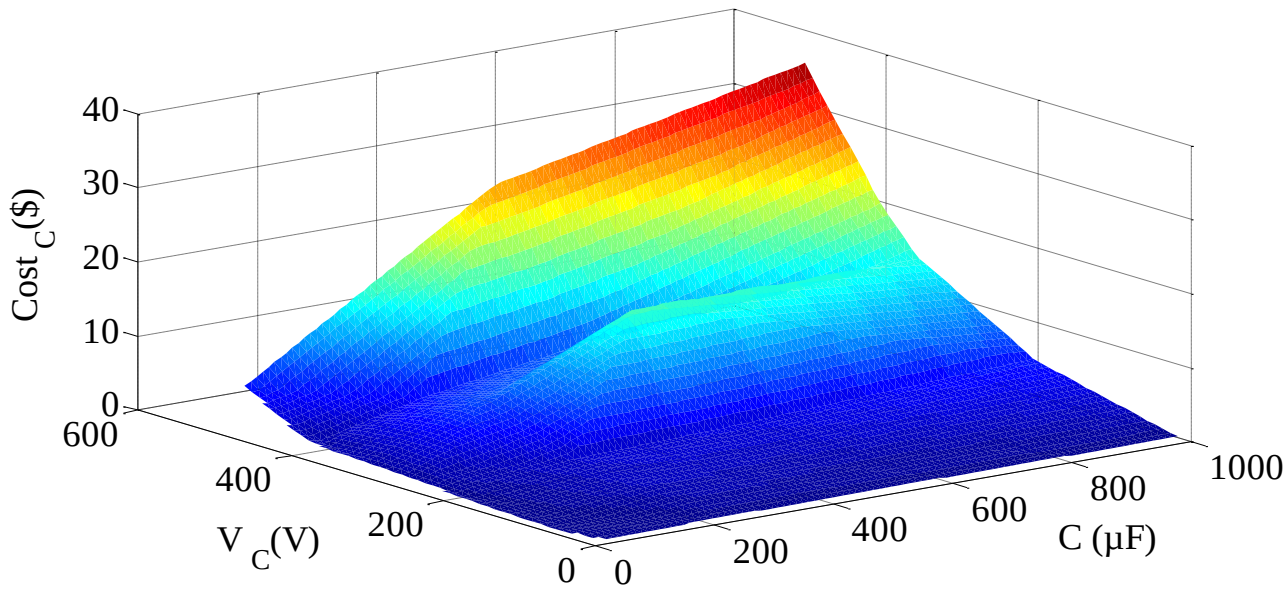

Figure 36 Capacitor cost model for one unit

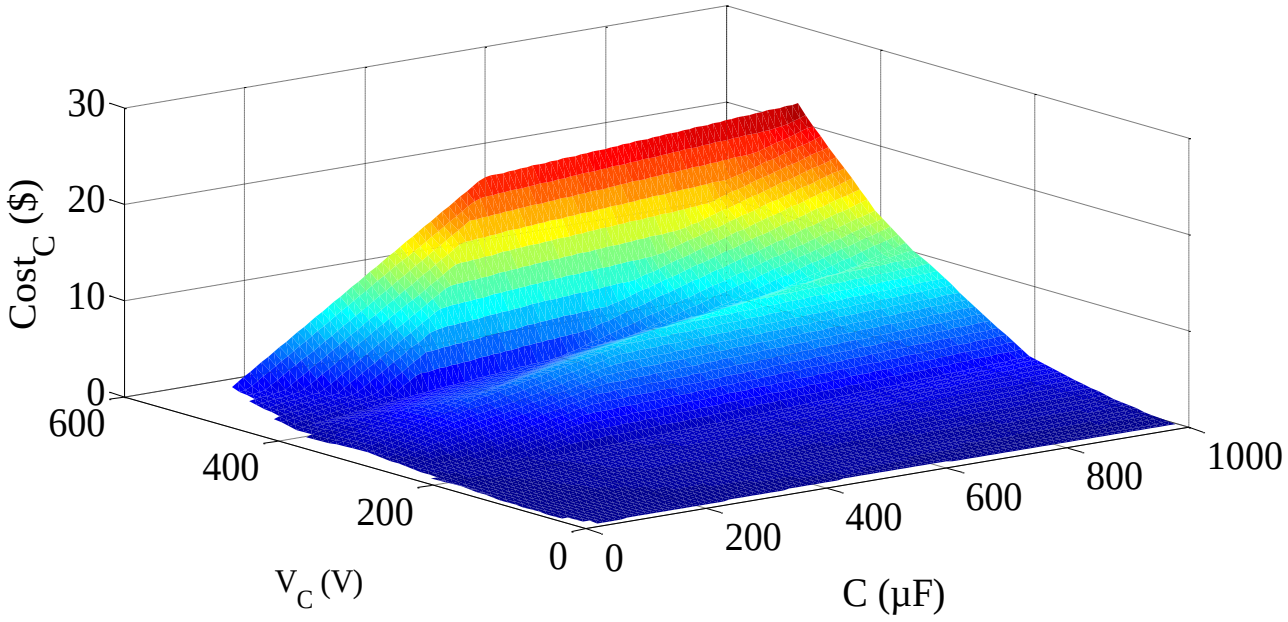

Figure 37 Capacitor cost model for 1000 units

4.5 Cost Model for Flyback Coupled-Inductor/Transformer Cores

Cores are vital elements when designing a flyback coupled inductor or transformer. They decide the mode of operation, performance and efficiency of a converter. Some manufacturers provide ready flyback transformers for commonly used applications, but even these commonly stem from custom designs. . There are two types of cores i.e. gapped and ungapped. In this cost model both these types are considered. Frequency range considered for the cores is 50 KHz to 500 KHz, and high frequency cores which are used for radio or telecommunications application are excluded from this research. Figures 38 and 39 show interpolated graph for core database. Cost model for the core is obtained on the basis of inductance factor value (A_L), switching frequency (f_{sw}) and cost. A_L value is considered because the inductance value is directly proportional to A_L. The core cost ($Cost_{Co}$) is represented as,

$$Cost_{Co}(A_L, f_{sw}) = \sum_{m=0}^{m=4} \tau_m A_L^{\psi_m} f_{sw}^{\rho_m}, \tag{105}$$

Table XII τ_m Coefficients and ranges

Coefficient	Value	Ranges	ψ_m	ρ_m
τ_0	1.204	(0.6736, 1.735)	0	0
τ_1	1.625	(1.31, 1.939)	1	0
τ_2	0.1432	(-0.6245, 0.9078)	0	1
τ_3	-0.007604	(-0.467, 0.4518)	1	1
τ_4	-0.1744	(-0.6827, 0.344)	0	2

Equation 105 represents the cost equation for the cores where τ_m coefficients obtained from MATLAB surface fitting tool are presented in Table XII. These coefficients are unchanged with respect to quantity so this equation can be used for multiple quantities.

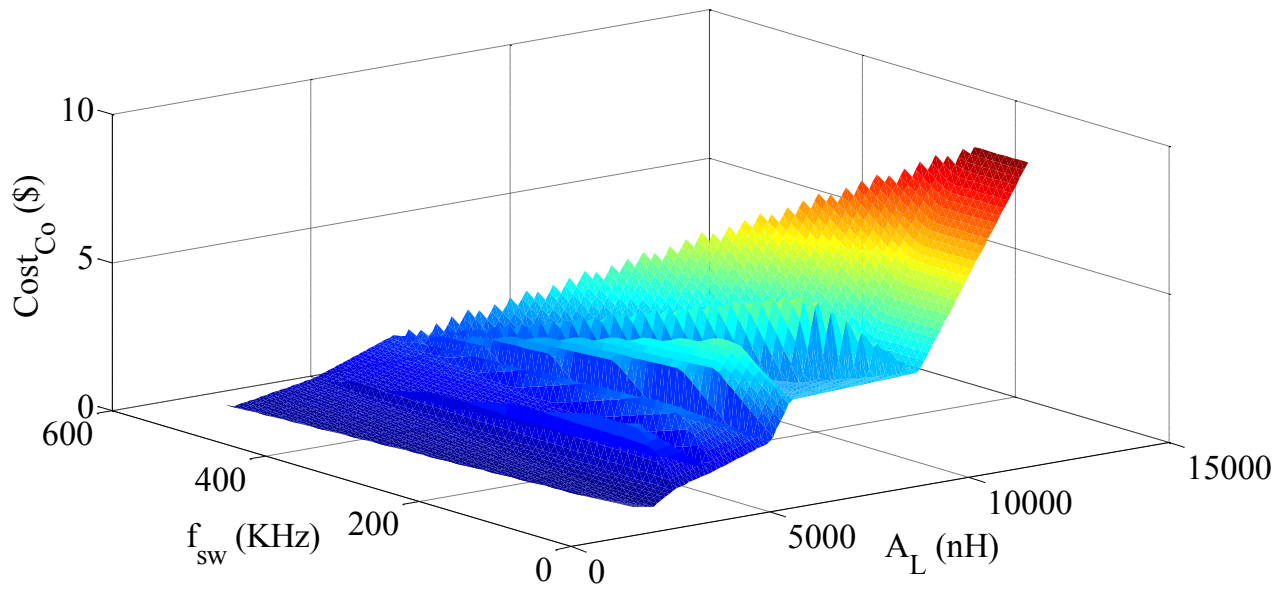

Figure 38 Flyback core cost model for one unit

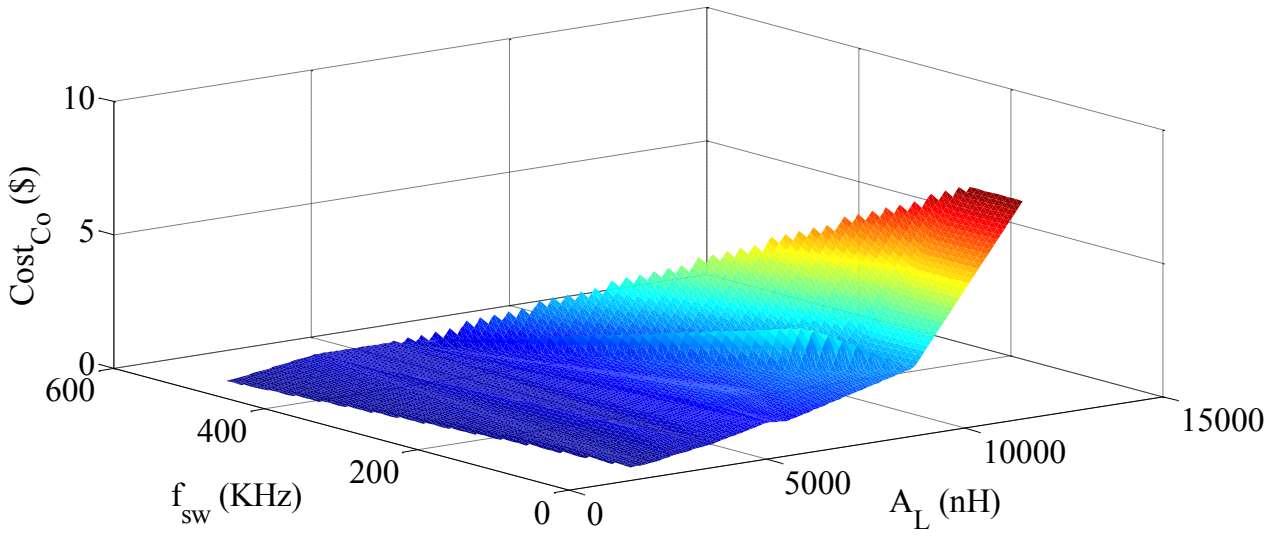

Figure 39 Flyback core cost model for 1000 units

4.6 Magnet Wire Cost Model

Magnet wire decides the current range of the flyback coupled inductor or transformer. Magnet wires are selected as per the gauge and total bundle cost where current requirement for a specific gauge is provided by the manufacturers. For the purpose of this section only a two dimensional graph is created to estimate cost equation since current and wire gauge are already established by standards for heat dissipation and safety. Table XIII described current requirement for specific gauge. The wire gauge and its corresponding current capacity are obtained from [83].

Table XIII Wire gauge and its current capacity [83]

Wire Gauge	Current Capacity
10	13.84
12	8.71
14	5.48
16	3.44
18	2.17
20	1.36
22	0.86
24	0.54
26	0.34
28	0.21
30	0.13
32	0.084
34	0.05
36	0.033
38	0.021
40	0.0132

Figure 40 shows magnet wire gauge (G) vs. cost graph where the cost model given here is developed for half pound bundles for consistency purposes. Cost equation for the magnet wire is obtained from the curve fitting tool .The capacitor cost ($Cost_W$) is represented as,

$$Cost_w(\mathrm{G}) = \sum_{q=0}^{q=6} \varphi_q G^{\varsigma q} , \tag{106}$$

Table XIV φ_q coefficients and ranges

Coefficient	Value	Ranges	ς_q
φ_0	0.0002906	(0.6736, 1.735)	5
φ_1	-0.03452	(1.31, 1.939)	4
φ_2	1.608	(-0.6245,	3
φ_3	-36.42	(0.5611, 1.106)	2
φ_4	396.6	(-0.467, 0.4518)	1
φ_5	-1583	(-0.6827, 0.344)	0

Equation (106) represents cost equation for the magnet wire where φ_q coefficients as presented in Table XIV are obtained using the MATLAB curve fitting tool. This equation is independent of quantities since the related coefficients do not vary with quantity.

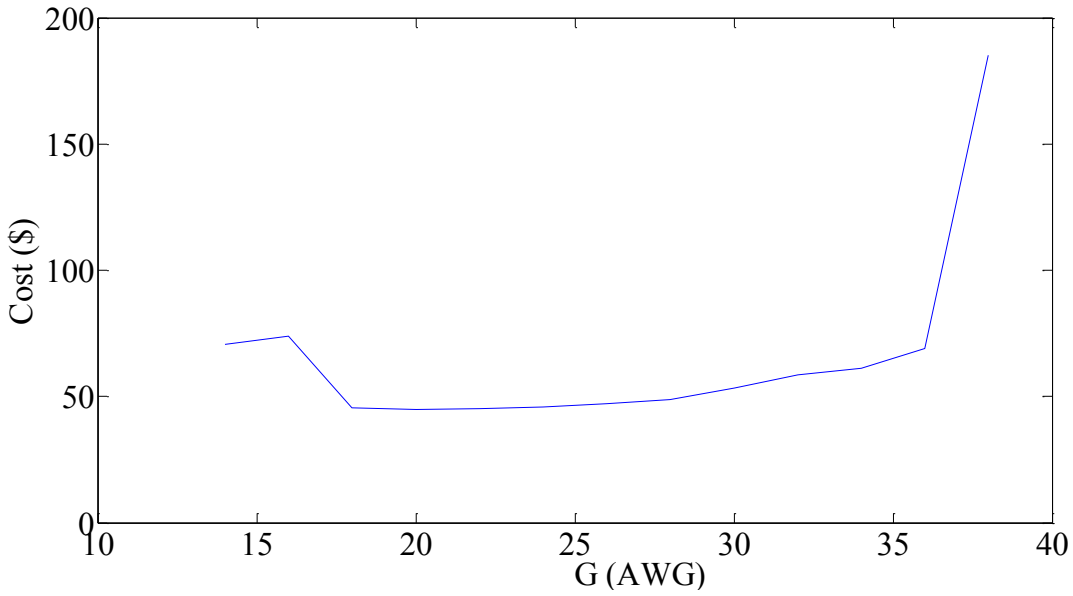

Figure 40 Magnet wire cost model for single bundle

Thus various cost models are prepared for estimating the cost of components and they can easily be extended for the purpose of system level cost estimation. Results are presented in the next section and are shown to be 90% accurate. The equation forms provided in section 4.1-4.6 were selected based on R^2 values as shown in Appendix IV. Next section includes a detailed analysis of results for the cost estimation of each component considered in this section.

4.7 Cost Models Results

A cost database for basic components was developed to test the cost models presented here.The cost estimates of components which are used for actual experiment are compared with actual prices from suppliers. Table XV summarizes components which are used for boost, buck and flyback converter development. The actual cost ($Cost_{actual}$) and the estimated cost ($Cost_{estimated}$) can provide percentage error. The error obtained from actual and estimated cost is shown as,

$$\% \text{ Error} = \left(\frac{C_{actual} - C_{estimated}}{C_{actual}} \times 100 \right) \tag{107}$$

Table XV. Detailed cost comparison for power components

Component	C_{actual}	$C_{estimated}$	**% Error**
MOSFET-FP4332PBF	$4.33	$4.37	-0.92%
Inductor-AIRD-03-101K	$5.97	$5.95	0.33%
Diode- MURF860G	$0.99	$1.03	-4.04%
Capacitor-220µF/250V	$0.723	$0.752	-4.01%
Core- B66421G0000X187	$0.69	$0.724	-4.93%
Wire-Belden wire 8051,	$49.03	$48.03	2.039%

Results in Table XV are shown to have less than 5% error and thus the cost models established prove that the results are more than 95% accurate. The accuracy of the cost model was improved with the help of interpolated graphs and surface fitting tools. An accurate surface fit can give better results of the interpolated graphs. Exact cost of the component can be obtained if coefficients are changed within specified range. The MATLAB surface fitting tools cannot provide exact surface fits but they can provide surface fitting estimates to some extent. Cost of the component changes as per trend and changes in technology and web based cost model can estimate component costs considering these changes. The cost model presented here can find ‘Ceiling cost’, that is the maximum cost of the component. Further improvement has to be made

in the cost model such that it can estimate a ‘Floor Cost’, that is the minimum cost of a component. This can be achieved if database of all available and active components is obtained from the manufacturers and distributors. Furthermore, a web based cost model can be developed following the approach presented here and an active database of manufacturer and distributor data can be incorporated into it to provide a robust, flexible and scalable cost modeling tool.

CHAPTER 5: RAPID PROTOTYPING TOOLS FOR POWER LOSS AND COST MODELS

Rapid prototyping is of interest for research, industrial, and commercial purposes as a major time and cost saving tool. Many engineers, researchers and designers use rapid prototyping tools to predict the results for their applications and designs. With the help of these tools they are able to evaluate several designs and tradeoffs in rapid iterations in order to decide on the most suitable design for their application before actual implementation. Rapid prototyping tools can help verify a concept, fix the design problems, and finalize the design before its actual implementation so as to avoid unnecessary cost burdens later in the development stage. These tools are found to be very helpful even for investors and customers to visualize the product performance and decide on further investment in the product before it goes to market.

Rapid prototyping tools or methods for power electronic converters are frequently ignored. Appropriate component selection is a crucial task for power electronics engineers or designers where they should consider cost, availability, performance, efficiency, and several other factors which is a very iterative and time-consuming process. Thus, developing rapid prototyping tools for power electronics applications will aid the designers and engineers in selecting suitable components for their application. Multiple rapid prototyping tools can be implemented to predict performance and operation along various parameters of a component or system, such as its cost, efficiency, reliability and operating conditions. This research is focused on efficiency and cost model estimation tools. The procedure used in rapid prototyping tools for cost and power loss models is illustrated in Figure 41.

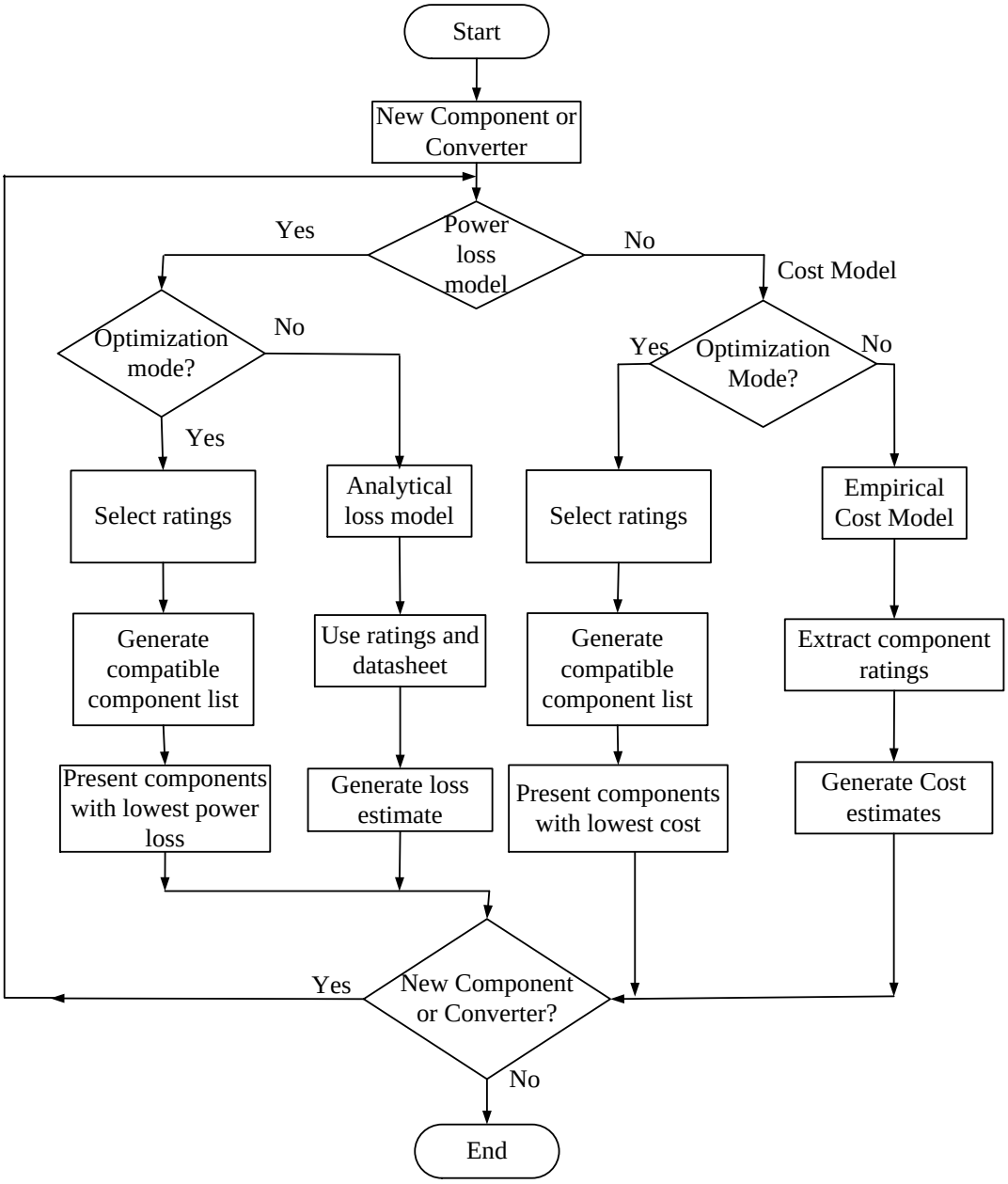

Figure 41 Procedure for the proposed rapid prototyping tools

Rapid prototyping tools for efficiency and cost models are further categorized into two modes: optimization mode and component-specific mode. In optimization mode, the tool takes converter ratings as inputs, then each component in a large database is checked to verify whether it is suitable for the application or not. Then the method automatically provides power loss and

cost estimates which help in identifying the best possible components for specific applications. The component-specific mode takes specific component parameters from datasheets and ratings, for example specific capacitor, inductor, MOSFET, diode, PCB, and gate drive parasitic elements and ratings, and then calculate power losses and costs of each component as well as the whole system. No optimal selection of these components is provided in the component-specific mode since all components and their related parameters are set by the user.

In this chapter, section 5.1 discusses rapid prototyping tools for the component-specific mode for both efficiency and cost estimation. This mode is especially useful for designers to check the effect of specific component choices on cost and efficiency in a converter. Section 5.2 presents the optimization mode for efficiency and cost models, which gives designers the freedom to choose from a number of components combinations. Thus, with the help of both the modes, a user can select a component, verify its performance and cost before its implementation or during the process of implementation of converters and also in already developed converters.

5.1 Rapid Prototyping Tool: Component-specific Mode

The power loss models developed in the Chapter 3 are implemented in a MATLAB GUI to obtain a user-friendly, simple, and efficient tool. This tool aids the designers to find out component and system level loss or cost estimates of already selected components.

5.1.1 Power Loss Modeling in the Component-specific Mode

Power loss models established in Chapter 3 for the buck and boost converters in CCM and flyback converter in DCM are embedded into a MATLAB GUI. Special entries are required for the flyback transformer: R_{core} , L_m and L_{pri}. The developed tool is explained with the help of a pseudo code and flowchart.

5.1.1.1 Pseudo Code for Power Loss Modeling in the Component-specific Mode

In this mode of operation, the user needs to input all specifications and datasheet information of known devices or components. Each component's power loss is then estimated with the help of power loss models derived in Chapter 3. Estimation error is calculated using equation (100) if power loss measurements are available.

Start;
Get input and output parameters;
if *boost or buck converter selected*
    Calculate P_{CM}, P_{SW} *and* P_G ;
        $P_{Loss\_MOSFET} = P_{CM}+P_{SW}+P_G$;
    Calculate P_{CD} *and* P_{SWD} ;
        $P_{Loss\_Diode} = P_{CD}+P_{SWD}$;
    Calculate P_{Core}, P_{DCR} *and* P_{ACR} ;
        $P_{Loss\_Inductor} = P_{Core}+P_{DCR}+P_{ACR}$;
    Calculate $P_{Loss\_Capacitor}$;
    Calculate P_{trace}, P_{Lstray}, P_{Cstray}
        $P_{PCB} = P_{trace}+P_{Lstary}+P_{Cstray}$;
    Calculate P_{GDRV};
else if *Flyback converter selected*
    Get L_m, L_{pri} *and* R_{Core} ;
    Calculate P_{CM}, P_{SW} *and* P_G
        $P_{Loss\_MOSFET} = P_{CM}+P_{SW}+P_G$;
    Calculate P_{CD} *and* P_{SWD}
        $P_{Loss\_Diode} = P_{CD}+P_{SWD}$;
    Calculate P_{Core}, P_{Pri} *and* P_{Sec}
        $P_{Loss\_Transformer} = P_{Core}+P_{Pri}+P_{Sec}$;
    Calculate $P_{Loss\_Capacitor}$;
    Calculate P_{trace}, P_{Lstray}, P_{Cstray} ;
        $P_{PCB} = P_{trace}+P_{Lstary}+P_{Cstray}$;
    Calculate P_{GDRV};
end if;
Calculate P_{Total};
if *experimental validation is required*
    Measure $P_{loss}=P_{in}-P_{out}$;
    Measure Error between P_{Total} *and* P_{Loss};
    Print error;
end if;
Print all power losses;

5.1.1.2 Flowchart for Power Loss Modeling in the Component-specific Mode

Figure 42 shows the overall procedure of power loss estimation technique in Component-specific mode.

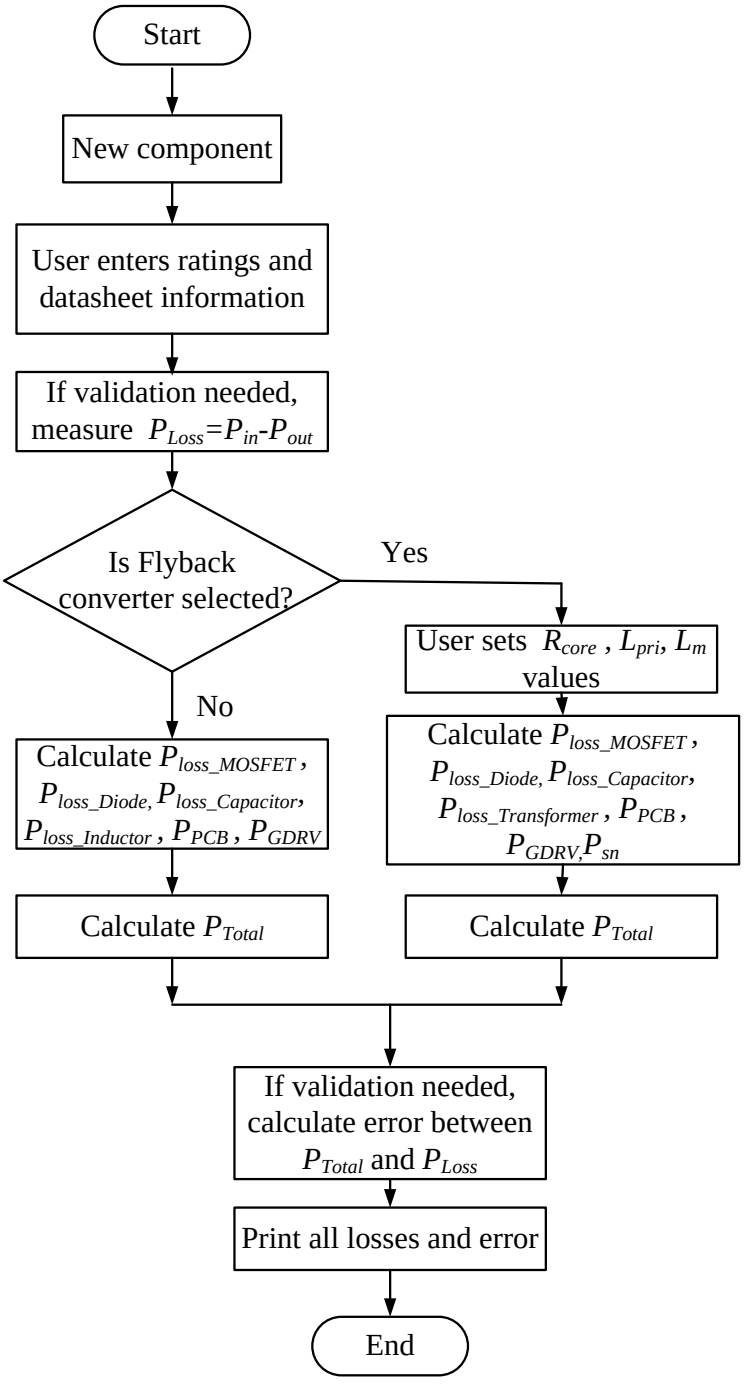

Figure 42 Overall procedure for power loss modeling in the component-specific mode

5.1.1.3 Results for Power Loss Modeling in the Component-specific Mode

Figures 43-45 present screenshots of the tool GUI in component-specific mode for the boost, buck and flyback converters, respectively,.

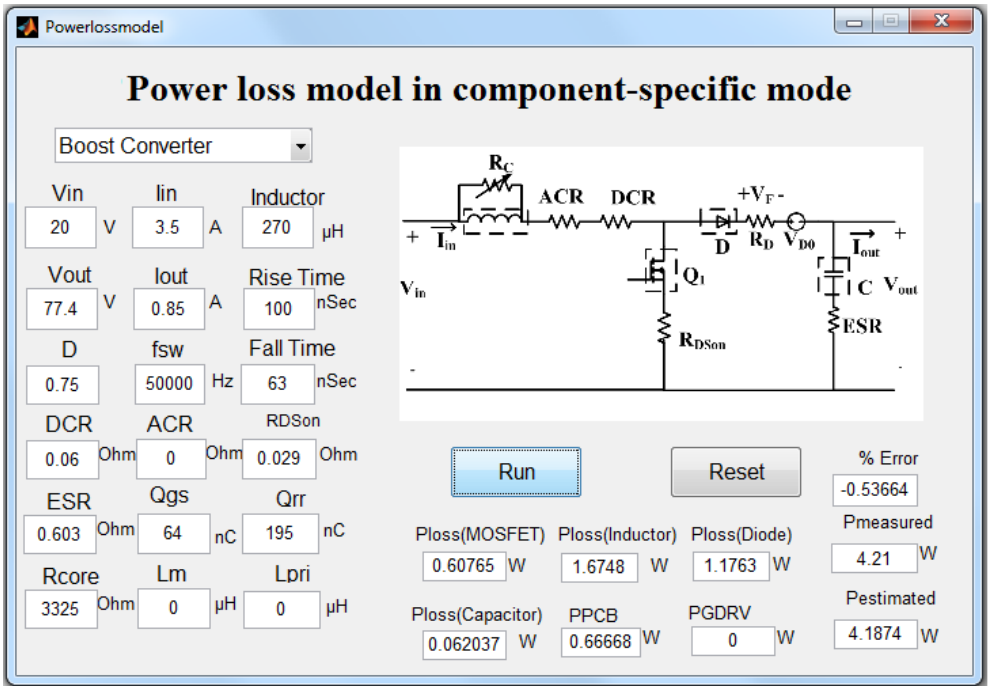

Figure 43 GUI showing component-specific mode boost converter power loss model

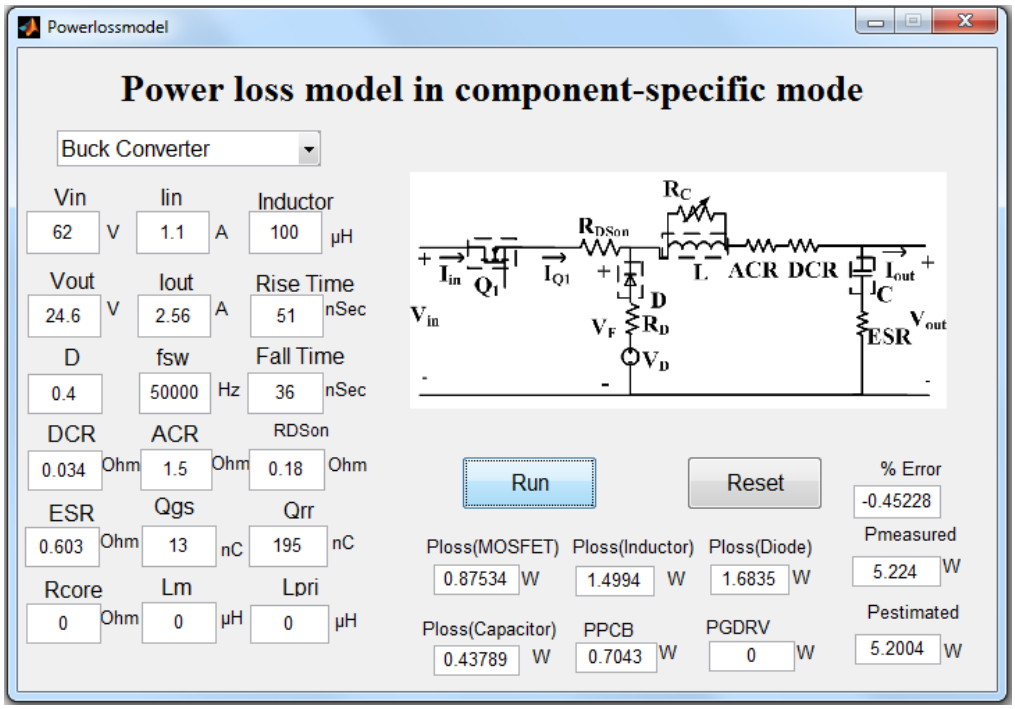

Figure 44 GUI showing component-specific mode buck converter power loss model

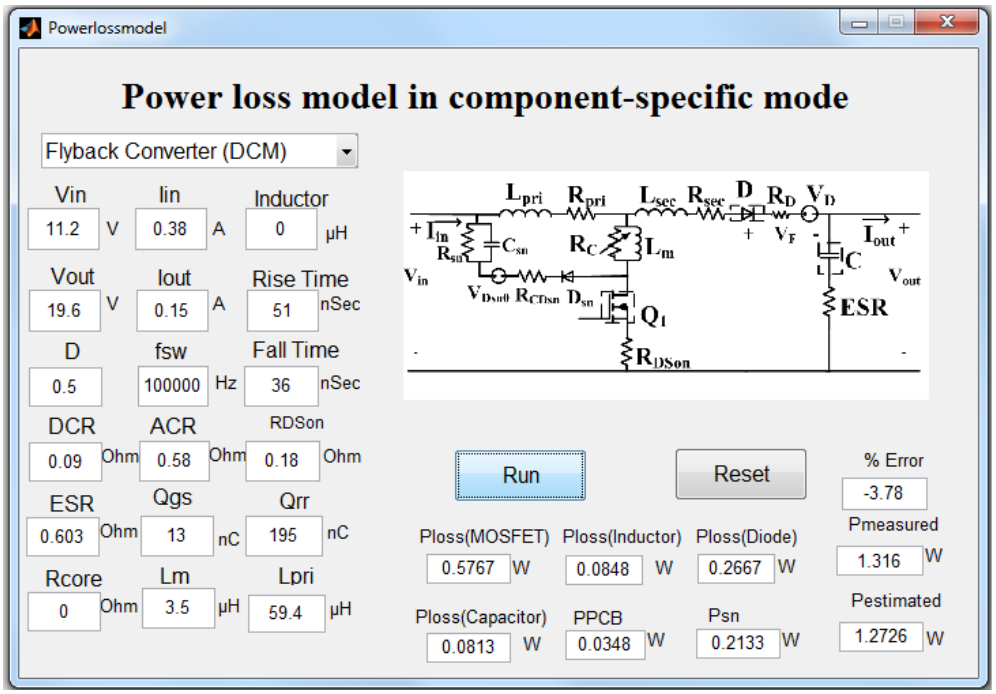

Figure 45 GUI showing component-specific mode flyback converter power loss model

This mode can accurately measure power losses in each component as well as whole system. Error between measured and estimated losses is also shown if measured losses are available from experiments. Note that error values shown in Tables II, IV and VI are reported using this tool and are shown to be less than 8% leading to accuracy over 92%. Note that this mode is advantageous when designers and engineers want to study the effect of specific components on converter power loss (sensitivity analysis), and when they have a selected set of components. But, the main drawback of this mode is that it cannot select components for the converter.

5.1.2 Cost Modeling in the Component-specific Mode

Cost of each component is obtained with the help of the cost model described in Chapter 4. This section gives cost estimates for basic power electronics components specified by the user. These estimates provide the user with a ‘ceiling’ cost such that cost of the selected component should not exceed the value obtained using the tool. The entire converter system cost is not

estimated because system cost also depends upon PCBs, gate drive circuits, soldering material and labor etc. The developed tool is further explained using pseudo code and flowchart.

5.1.2.1 Pseudo Code for Cost Modeling in the Component-specific Mode

Each component cost is estimated based on the cost models developed in Chapter 4. The error between actual and estimated cost is calculated using equation (107).

Start;
Select a component;
Get the component parameters and ratings;
Read Component.xlsx file and get the entire database
Put x-axis parameters from the 1st column of the database
Put y-axis parameters from the 2nd column of the database
Put z-axis parameters from the 3rd column of the database
Plot the 3D graph of cost model;
Calculate the cost for selected component with its dedicated cost equation;
Print the cost and interpolated graph;
Check whether new component is selected;
***if** new component is selected*
    Go to start;
end if;
end;

5.1.2.2 Flowchart for Cost Modeling in the Component-specific Mode

Figure 46 shows overall procedure of cost estimation technique in component-specific mode.

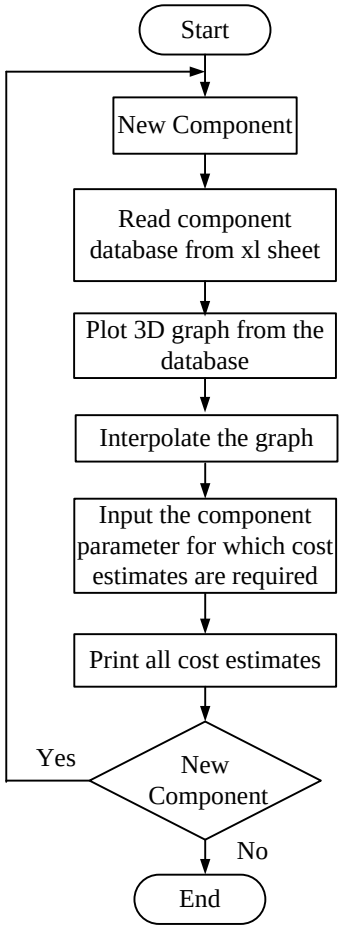

Figure 46 Flowchart for cost model in component-specific mode

5.1.2.3 Results for Cost Modeling in the Component-specific Mode

The cost model shown above was integrated into a user-friendly GUI developed in MATLAB for rapid-prototyping. Figure 47 presents cost modeling results from the component-specific mode. In this tool, a user can check each component cost estimates individually. The cost estimates given in Table XV are obtained from this cost model.

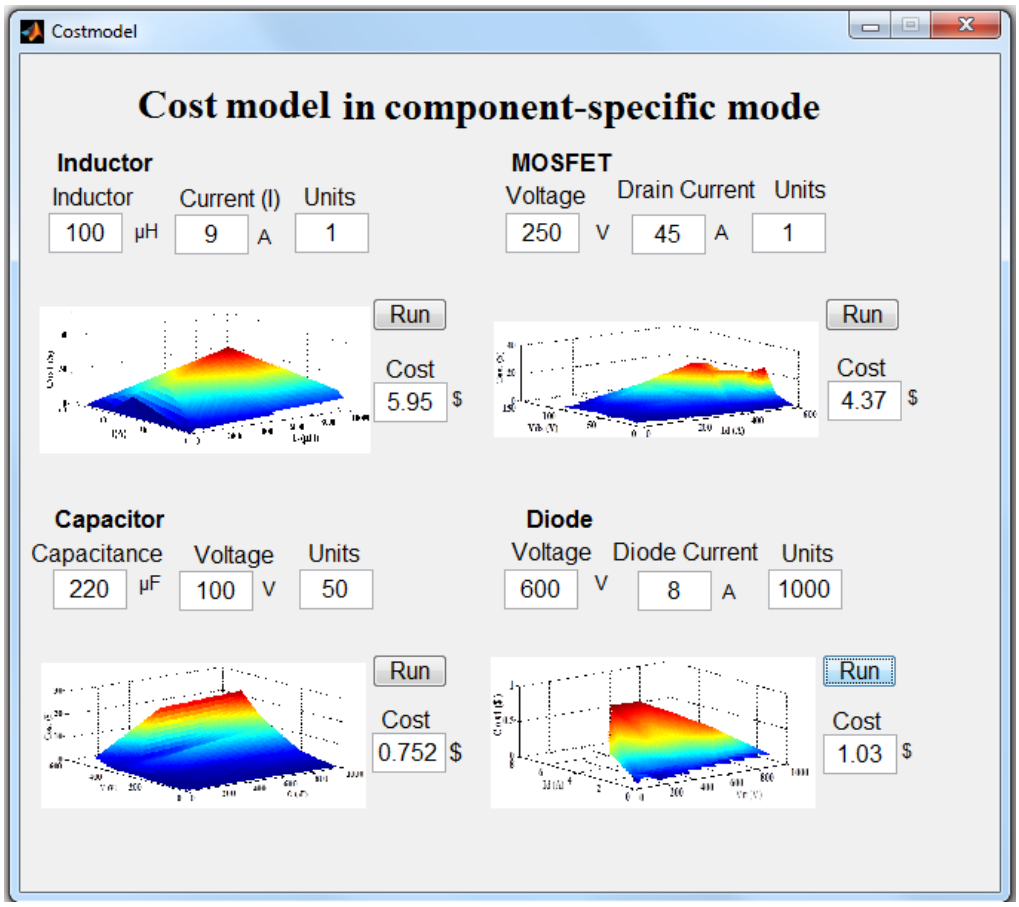

Figure 47 GUI for component cost estimates in Component-specific mode

Cost estimates shown in Figure 47 and %error values shown in Table XV are also within 8% error, leading to over 92% estimation accuracy. But, the main drawback of this mode is that it cannot select the lowest cost components for the converter by itself.

5.2 Rapid Prototyping Tools: Optimization Mode

Power loss models in the component-specific mode developed in the previous section is further optimized with the help of MATLAB GUI to obtain a user-friendly, simple, and more efficient tool. This tool aids designers in selecting components for their applications that avoid excess power loss in the circuit or have the lowest cost for a specific application. This subsection contains detailed analysis of the development of the efficiency and cost models.

5.2.1 Power Loss Modeling in the Optimization Mode

Power loss models developed in Chapter 3 are combined with converter ratings to automatically produce system-level minimum power loss and select the right components. This model reduces the manual effort in calculating component power losses to select a combination of components that minimizes power losses, which is a tedious and time consuming process. The selected component power loss is obtained and then minimum power loss component is selected for maximum efficiency. Considering this, the optimization techniques developed here are critical to facilitate rapid prototyping.

5.2.1.1 Component Selection Procedure

The component selection formulae are obtained from existing literature [96-98]. It is critically important to select inductor and capacitor values for various applications. If a smaller value of inductance is selected, it results in failure of the inductor to operate in a specific mode whereas a higher value increases the converter start-up and settling times. Similarly a smaller value capacitor cannot avoid unwanted ripples at the output. To avoid these discrepancies the exact values of components are estimated. Core and magnet wire size estimations are also provided for the flyback converters.

A. Component selection procedure for boost converters in CCM

To select boost converter components, input current ripple (ΔI_{in}) is calculated in [95] as,

$$\Delta I_{in} = 0.4 I_{out} \left(\frac{V_{out}}{V_{in}} \right), \tag{107}$$

whereas the inductor value (L) of the boost converter obtained in [97] is,

$$L = \frac{\left(V_{in} \left(V_{out} - V_{in} \right) \right)}{\left(\Delta I_{\text{in}} f_{sw} V_{out} \right)}. \tag{108}$$

Capacitance value (C) of the boost converter is given in [95] as,

$$C = \frac{\left(I_{out} D\right)}{\left(\Delta V_{out} f_{sw}\right)}. \tag{109}$$

The MOSFET and diode are selected based on values of the voltage and current flowing through them. In order to avoid the breakdown of these components due to excessive voltage and current, V_{DS} of the MOSFET should be greater than V_{out} of the converter and I_D should be greater than I_{in} of the converter [95]. Diode forward current I_F should be more than I_{in} and V_{rr} should be more than V_{out} [95].

B. Component selection procedure for buck converters in CCM

Inductor current ripple in a buck converter is obtained in [95] as,

$$\Delta i = \frac{\left(1-D\right)V_{out}}{L f_{sw}}, \tag{110}$$

Whereas inductor value of the buck converter is given in [96] as,

$$L = \frac{R_{Load}\left(1-D\right)}{2 f_{sw}}. \tag{111}$$

whereas, R_{Load} is load resistance of the converter.

The Capacitance value of the buck converter is given in [97] as,

$$C = \frac{V_{out}\left(1-D\right)}{\left(8L\Delta V_{out} f_{sw}^2\right)}. \tag{112}$$

In equation (112) ΔV_{out} is output voltage ripple of the converter.

MOSFET and diode are selected on similar criteria as described previously in the boost converter selection process.

C. Component selection procedure for flyback converters in DCM

The flyback converter component selection procedure is derived in [83], [85] and [97]. Inductor current ripples of buck converters are obtained in [97] as,

$$\Delta i = \frac{DV_{in}T_{on}}{L_m}, \tag{113}$$

whereas primary and secondary inductance value of the flyback converter are given in [83] as,

$$L_{pri} = \frac{2V_{in}I_{in}}{I_{pri}^2 f_{sw}}, \tag{114}$$

$$L_{\text{sec}} = \frac{V_{out}D}{f_{sw}\Delta i}. \tag{115}$$

whereas, primary current (I_{pri}). Inductance factor is obtained as,

$$A_{\text{L}} = \frac{L_{pri}}{N}. \tag{116}$$

In equation (116) A_L is inductance factor, N is transformation ratio.

Primary turns (N_{pri}) and secondary turns (N_{sec}) of the flyback converter are obtained from [85] as,

$$N_{pri} = \frac{L_m I_{\max}}{B_{\max} A_{\text{C}}}, \tag{117}$$

$$N_{\text{sec}} = nN_{pri}. \tag{118}$$

whereas, B_{max} is maximum peak flux density, A_C is cross sectional area of core, I_{max} is maximum mutual inductance current.

The output capacitance value of the flyback converter is similar to the boost converter capacitor as specified in equation (112). Primary and secondary windings resistances are obtained in [83] as,

$$R_{pri} = \frac{\rho_o N_{pri}(MLT)}{A_{wpri}}, \tag{119}$$

$$R_{\text{sec}} = \frac{\rho_o N_{\text{sec}} (MLT)}{A_{w\text{sec}}}. \tag{120}$$

Mean length per turn (*MLT*), conductivity of copper at room temperature (ρ_o), cross-sectional area of primary winding (A_{wpri}), cross-sectional area of secondary winding (A_{wsec}) and cross-sectional area of winding (A_w) are usually provided by manufacturers. If it is not given by manufacturers it can obtained as given in [83] as,

$$A_w = \frac{K_u W_A}{n}. \tag{121}$$

whereas, fill factor (K_u) is usually considered as, 0.5 for low voltage inductors and 0.65 for high voltage inductors. Window area (W_A) values are provided by the core manufacturers. MOSFET and diode are selected on similar criteria as described previously in the boost converter selection process.

While implementing these formulae in the software, more criteria are also implemented to select component within specified range. The current and voltage ranges are provided for component selection procedure to select appropriate component, if lowest value or highest value component may fails to perform specific applications. To avoid this discrepancy range for all components is prepared. This range provides final list to component selection procedure. The lowest power loss component is selected from this list.

To select MOSFET range is provided for V_{DS} and I_D. V_{DS} value should be selected as V_{DS} greater than and equal to double of V_{out} and less than four times V_{out}. I_D value should be selected as I_D greater than and equal to double of I_{in} and less than four times I_{in}. Similar approach is implemented for diode V_{rr} value should be selected as V_{rr} greater than and equal to double of V_{out} and less than four times V_{out} and I_F value should be selected as I_F greater than and equal to double of I_{in} and less than four times I_{in}. For inductors, the inductance value L should be less than

L_{max} and L_{max} value is equal to twice of L which is obtained from selection procedure. For capacitor selection criteria is put as, the capacitance value C should be less than C_{max} and C_{max} value is equal to twice of C which is obtained from selection procedure. This criteria can be changed for different application.

5.2.1.2 Pseudo Code for Power Loss Modeling in the Optimization Mode

The pseudo code provided here is specific to inductor selection and power loss estimation process only. Similar logic was developed for all components with the help of power loss model equations.

Start
Get input and output parameters;
$I_L = I_{in}$;
$L = ((V_{in} \times Duty \times (1-Duty))/(2 \times f_{sw} \times I_{out}))$;
$L_{max} = 2 \times L$;
Read inductor.xls file and get the entire database;
  for *i=1 to all database*
    if *L <=inductor values in database &&*
      L_{max} *> inductor values in database*
      if I_L *<= inductor current values in database*
        Extract ACR, DCR and RC values from the database;
      end if;
    end if;
  i=i+1;
  end if;
Calculate P_{ACR}, P_{DCR} *and* P_{CORE} *as described in power loss model*
$P_{loss\_inductor} = P_{ACR} + P_{DCR} + P_{CORE}$;
Print component name;

5.2.1.3 Flowchart for Power Loss Modeling in the Optimization Mode

Figure 48 shows the detailed flowchart of optimization mode for minimum power loss. .

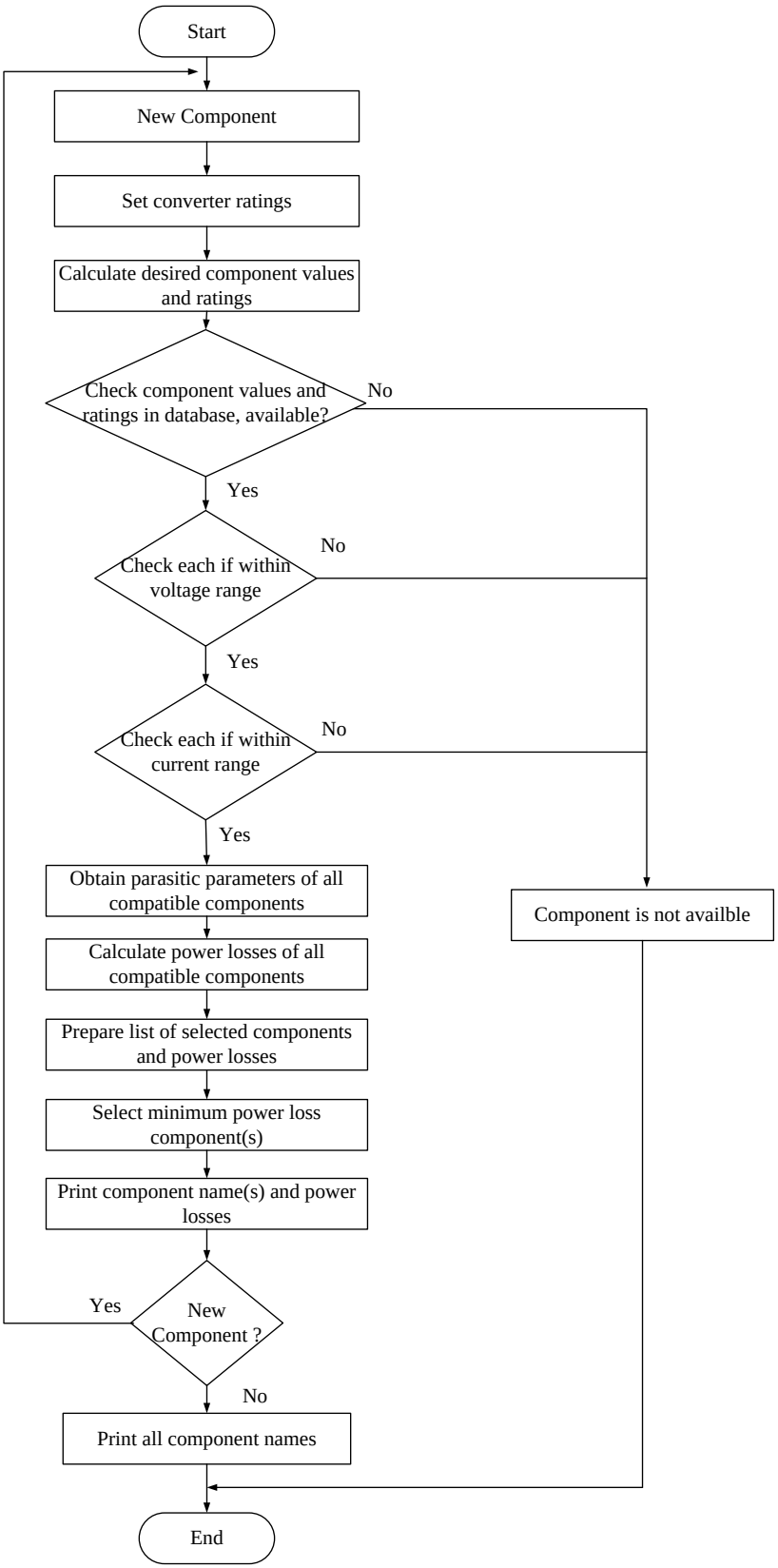

Figure 48 Optimization tool for minimum power loss component selection

5.2.1.4 Results for Power Loss Modeling in the Optimization Mode

Figures 49-51 show the optimization mode rapid prototyping tool developed for boost, buck, and flyback converters minimum power loss component selection, respectively. Results for these models are generated in a Microsoft Excel file through MATLAB and verified manually. Tables XVI-XVIII present results for boost, buck and flyback converters generated by the optimization tool. Power loss values of the components selected through optimization mode shown in Figures 49-51 are found to be the least values when compared with the component list shown in Table XVI–XVIII in which minimum power loss component selections are highlighted. The optimization tool thus performs as expected.

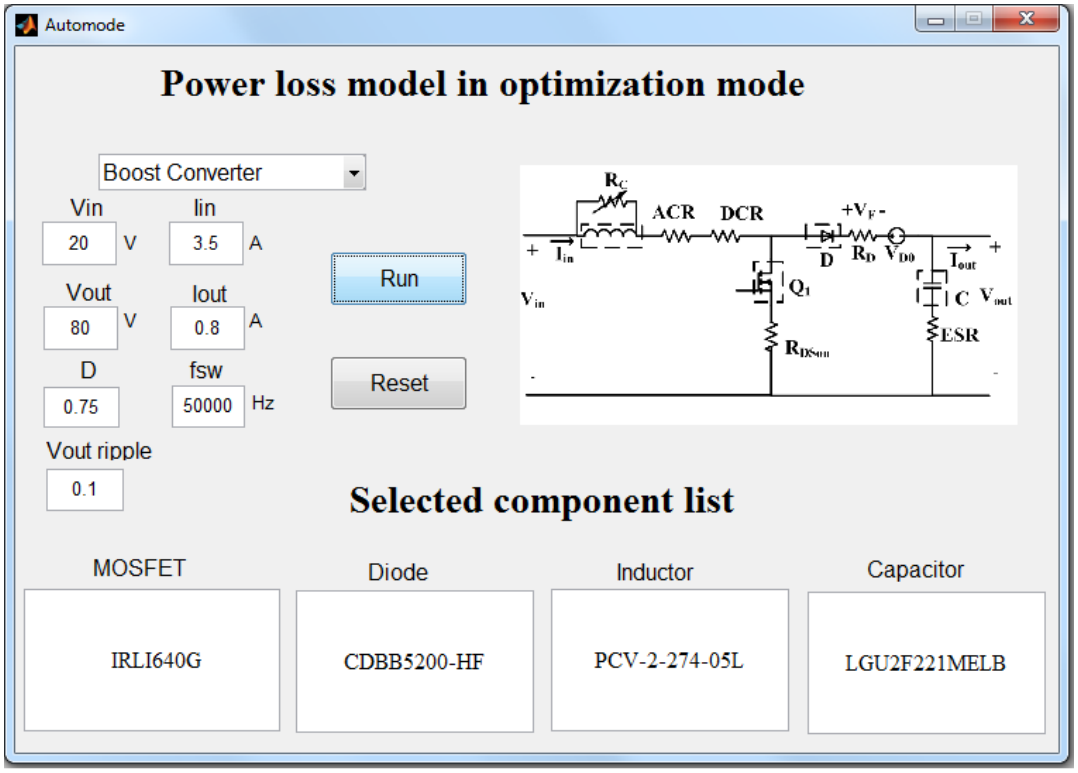

Figure 49 Optimization mode boost converter power loss modeling and component selection

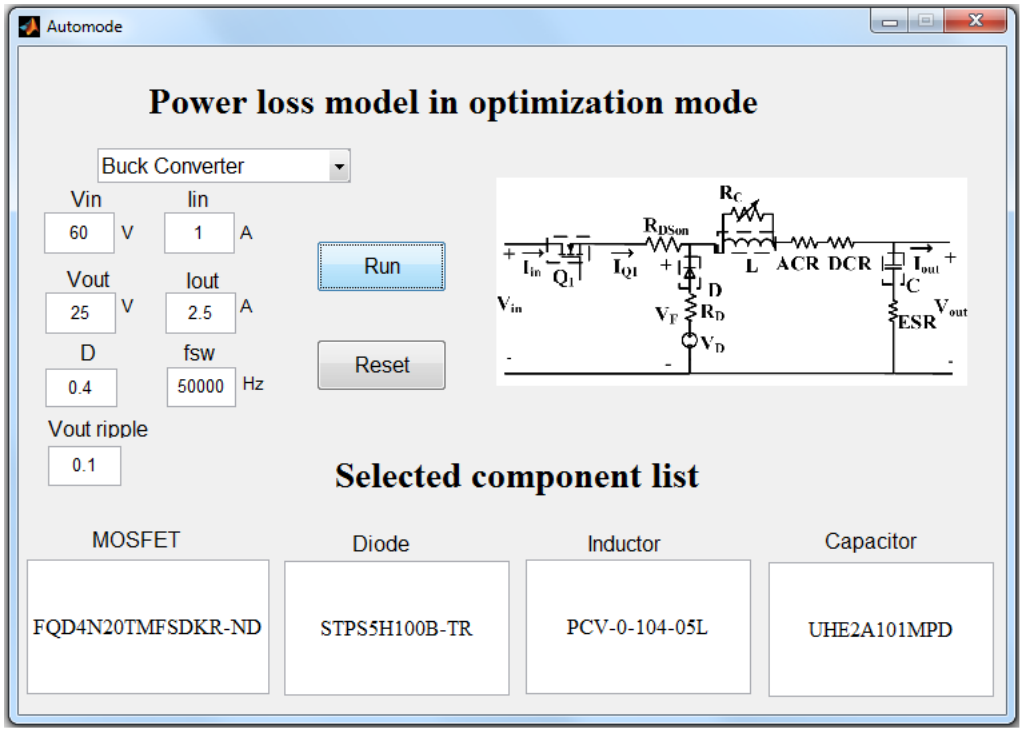

Figure 50 Optimization mode buck converter power loss modeling and component selection

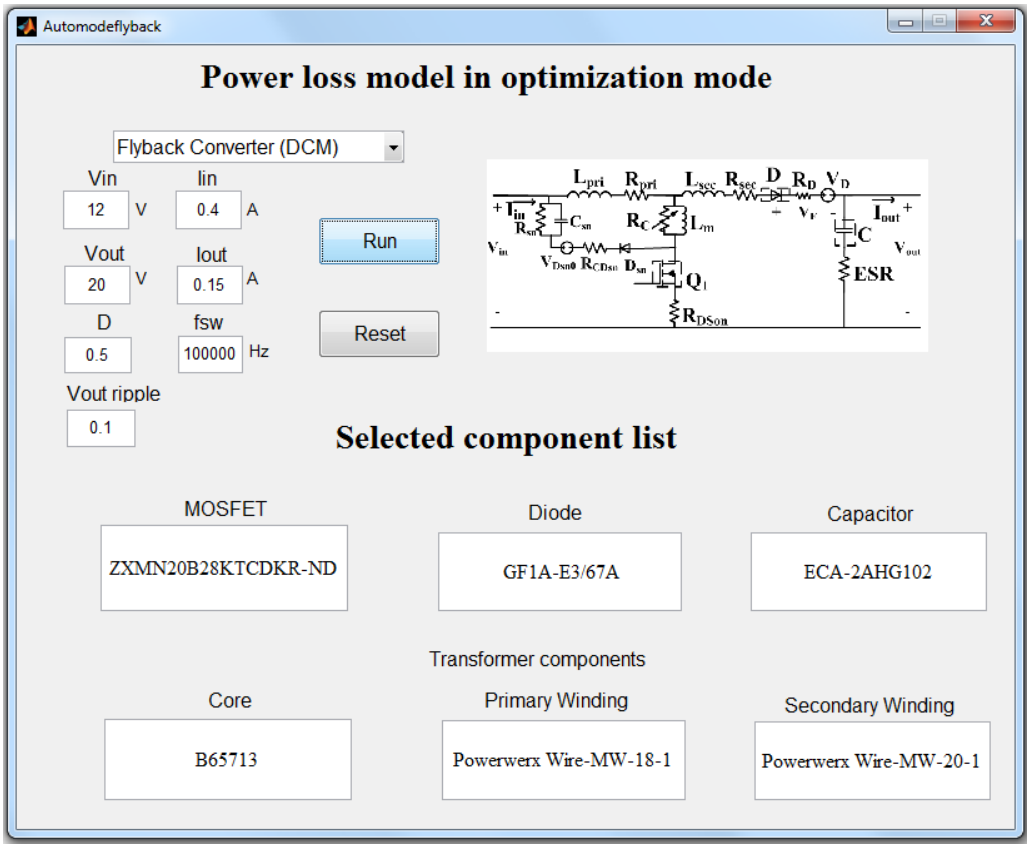

Figure 51 Optimization mode flyback converter power loss modeling and component selection

Table XVI Boost converter results generated by power loss modeling tool

MOSFET		Capacitor	
Suitable Components	P_{Loss}(W)	Suitable Components	P_{Loss}(W)
RDN100N20FU6-ND	3.436527	EEU-EB2D221	0.000223251
RDN100N20-ND	3.436527	LGU2F221MELB	0.000223251
IRLI640GPBF	1.898888	ECO-S2GB221EA	0.027160494
IRLI640G	1.898888	Inductor	
FQP9N30	4.466997	Suitable Components	P_{Loss}(W)
STP12NK30Z	3.76386	PCV-0-274-10L	2.983625744
Diode		PCV-2-274-03L	3.302118631
Suitable Components	P_{Loss}(W)	PCV-2-274-05L	1.171902331
CDBB5200-HF	1.495	PCV-2-274-10L	1.528307208
		PCV-2-394-05L	3.299376352

Table XVII Buck converter results generated by power loss modeling tool

MOSFET		Diode	
Suitable Components	P_{Loss}(W)	Suitable Components	P_{Loss}(W)
FQD4N20TMFSCT-ND	5.03508831		
FQD4N20TMFSDKRND	5.03508831	SK35A-LTP	2.878770625
Capacitor		STPS5H100B-TR	2.0371
Suitable Components	P_{Loss}(W)	B350A-13-F	2.881284375
UHE2A101MPD	0.00574182	SS35	2.87751375
ESH107M200AM7AA	1.07828776	B550C-13-F	2.331017472
UVZ2F101MHD	0.01446759	SB550-E3/54	2.397534375
UPT2G101MHD6	0.01446759	SK55L-TP	2.46423892
Inductor		SB550	2.2554836647
Suitable Components	P_{Loss}(W)	CDBC580-G	2.45870867
PCV-0-104-01L	0.94052368	SB580	2.258625852
PCV-0-104-03L	0.35827212	SB580-T	2.21386
PCV-0-104-05L	0.27427803	HSM580G/TR13	2.464077
		RGP30B-E3/73	3.186462933
		SK310A-LTP	2.890710938
		CDBA3100-G	2.734426563
		B3100-13-F	2.586175679
		CDBC5100-G	2.46423892
		SS5P10-M3/86A	2.301881552
		SB5100-T	2.2188875

Table XVIII Flyback converter results generated by power loss modeling tool

MOSFET		Capacitor	
Suitable Components	P_{Loss}(W)	Suitable Components	P_{Loss}(W)
ZXMN20B28KTCCT-ND	1.293020308	EEU-FC2A220	0.003203172
ZXMN20B28KTCDKRND	1.293020308	EEU-EB2D220	0.006851628
Primary winding		UPJ2F220MHD1TN	0.009106776
Suitable Components	P_{Loss}(W)	EKXG401ELL220MK	0.01097266
Powerwerx Wire-MW-18-1	8.7940e-04	ECA-2AM470	9.72443E-05
Secondary winding		EEU-ED2C470	0.000145076
Suitable Components	Suitable	UPB2E470MHD1TO	0.000145076
Powerwerx Wire-MW-20-1	8.7940e-04	ECO-S2GA470BA	0.014191632
Cores		380LX470M500H012	0.003591
Suitable Components	P_{Loss}(W)	UHE2A101MPD	3.64846E-05
B65713	0.000263	ESH107M200AM7A	0.006851628
B65805	0.002582	UVZ2F101MHD	9.19296E-05
B66361	0.00216	UPT2G101MHD6	9.19296E-05
B66285	0.002582	EEU-FC2A221	0.001249668
B65814	0.001417	EEU-EB2D221	3.11699E-05
B66288	0.001759	LGU2F221MELB	3.11699E-05
B66287	0.00098	ECO-S2GB221EA	0.003792096
B66291	0.00098	ECA-2AHG471	7.77092E-06
B66387	0.000562	SLP471M200E1P3	0.006075972
B65684	0.000562	ELXM3B1VSN471M	0.006075972
Diode		EET-HC2G471LA	1.46513E-05
Suitable Components	P_{Loss}(W)	EKMS501VSN471M	1.93914E-05
SS15	0.115716	ECA-2AHG102	3.64846E-06
GF1A-E3/67A	0.102843	EET-UQ2D102EA	0.00129276
SS15E-TP	0.104059	350LSQ1000MNB36	0.00129276
SK15-13-F	0.107342	B43508A9108M000	0.00172368
SS18-TP	0.108761	ALS30A102KF500	0.001378944
SS18	0.116216		
B180-13-F	0.104988		
CDBA180-G	0.11361		

5.2.2 Cost Modeling in the Optimization Mode

Designers have to review vast amounts of catalog and web content in order to select low cost components that fit their design and budget. This iterative process adds a significant burden in terms of time and effort. Using the optimized mode the cost modeling tool, components in a database are automatically filtered on the basis of various ratings and operating conditions, and components with minimum cost are selected

5.2.2.1 Pseudo Code for Cost Modeling in the Optimization Mode

Start
Get input and output parameters;
$L=((V_{in}\times Duty\times(1-Duty))/(2\times f_{sw}\times I_{out}))$; $Lmax=2\times L$;
Read inductor.xls file and get all the database;
  for *i=1 to all database*
    if *L <=inductor values in database && Lmax > inductor values in database*
      Extract ACR, DCR and RC values from database;
      Extract unit costs and multiple unit costs data base;
    end *i=i+1;*
  end
Find minimum cost of the component for unit quantity;
Find minimum cost of the component for multiple quantities;
 if *minimum quantity=1;*
   print minimum cost of the component for unit quantity;
 else if *minimum quantity=1000;*
   print minimum cost of the component multiple quantities;
end elseif;
end if;
Calculate P_{ACR}, P_{DCR} and P_{CORE} as described in power loss model;
$P_{loss\_inductor}= P_{ACR}+ P_{DCR} +P_{CORE}$;
Print component name; Print component cost;

5.2.2.2 Flowchart for Cost Modeling in the Optimization Mode

Figure 52 shows the detailed flowchart of the optimization technique implementation for the cost modeling tool.

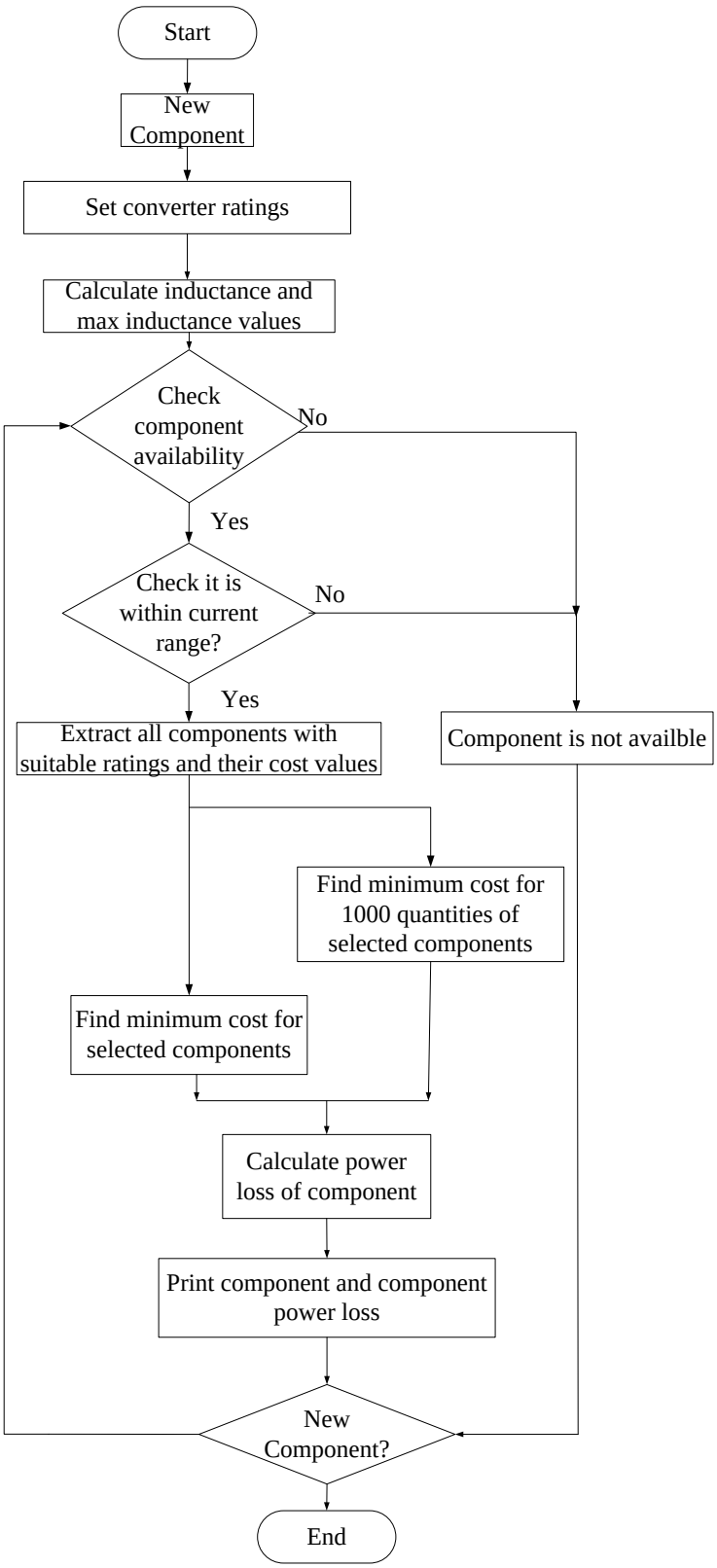

Figure 52 Optimization mode flowchart for the cost modeling tool

5.2.2.3 Results for Cost Modeling in the Optimization Mode

The cost model shown above was integrated into a user-friendly GUI developed in MATLAB to establish a rapid-prototyping tool. The optimization mode cost model generates the component list and lowest price of the selected components. Figures 53-55 present the boost, buck, and flyback converter cost estimates in optimization mode. Costs of the components selected through this mode are found to be the least values when compared with the component list shown in Table XIX. An example of the tradeoff between minimum power loss and minimum cost is shown in Table XIX and XX for the boost converter. If a component is selected on the basis of minimum cost, then it may not result in a power efficient circuit. Similarly when a component is selected only based on lowest power loss it may lead to an efficient but expensive solution. Table XIX shows those selected components that have a higher power loss at the lowest available cost while table XX shows the selected components with lowest power loss and highest cost. Table XXI and XXII show the selected components for buck and flyback converters.

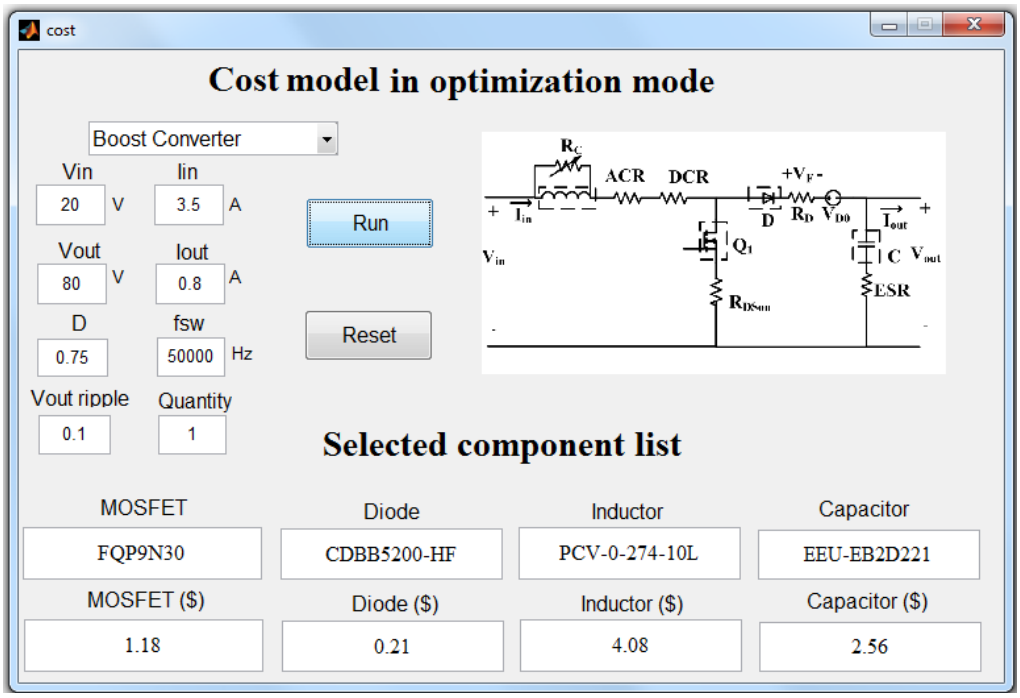

Figure 53 Boost converter Optimization mode cost modeling tool

Table XIX Boost converter results generated by optimization mode cost modeling tool with minimum cost as the optimization objective

MOSFET		
Suitable	*Cost*($)	P_{Loss}(W)
RDN100N20FU6-	2.73	3.436527778
RDN100N20-ND	2.73	3.436527778
IRLI640GPBF	2.88	1.898888889
IRLI640G	2.88	1.898888889
FQP9N30	1.18	4.466997222
STP12NK30Z	1.95	3.763864198
Diode		
Suitable	*Cost*($)	P_{Loss}(W)
CDBB5200-HF	0.21	1.495020814
Inductor		
Suitable	*Cost*($)	P_{Loss}(W)
PCV-0-274-10L	4.08	2.983625744
PCV-2-274-03L	4.15	3.302118631
PCV-2-274-05L	4.56	1.171902331
PCV-2-274-10L	7.39	1.528307208
PCV-2-394-05L	5.1	3.299376352
Capacitor		
Suitable	*Cost*($)	P_{Loss}(W)
EEU-EB2D221	2.56	0.000223251
LGU2F221MELB	7.022	0.000223251
ECO-S2GB221EA	4.68	0.027160494

Table XX Boost converter results generated by optimization mode cost modeling tool with lowest power loss as the optimization objective

MOSFET		
Suitable	*Cost*($)	P_{Loss}(W)
RDN100N20FU6-	2.73	3.436527778
RDN100N20-ND	2.73	3.436527778
IRLI640GPBF	2.88	1.898888889
IRLI640G	2.88	1.898888889
FQP9N30	1.18	4.466997222
STP12NK30Z	1.95	3.763864198
Diode		
Suitable	*Cost*($)	P_{Loss}(W)
CDBB5200-HF	0.21	1.495020814
Inductor		
Suitable	*Cost*($)	P_{Loss}(W)
PCV-0-274-10L	4.08	2.983625744
PCV-2-274-03L	4.15	3.302118631
PCV-2-274-05L	4.56	1.171902331
PCV-2-274-10L	7.39	1.528307208
PCV-2-394-05L	5.1	3.299376352
Capacitor		
Suitable	*Cost*($)	P_{Loss}(W)
EEU-EB2D221	2.56	0.000223251
LGU2F221MELB	7.022	0.000223251
ECO-S2GB221EA	4.68	0.027160494

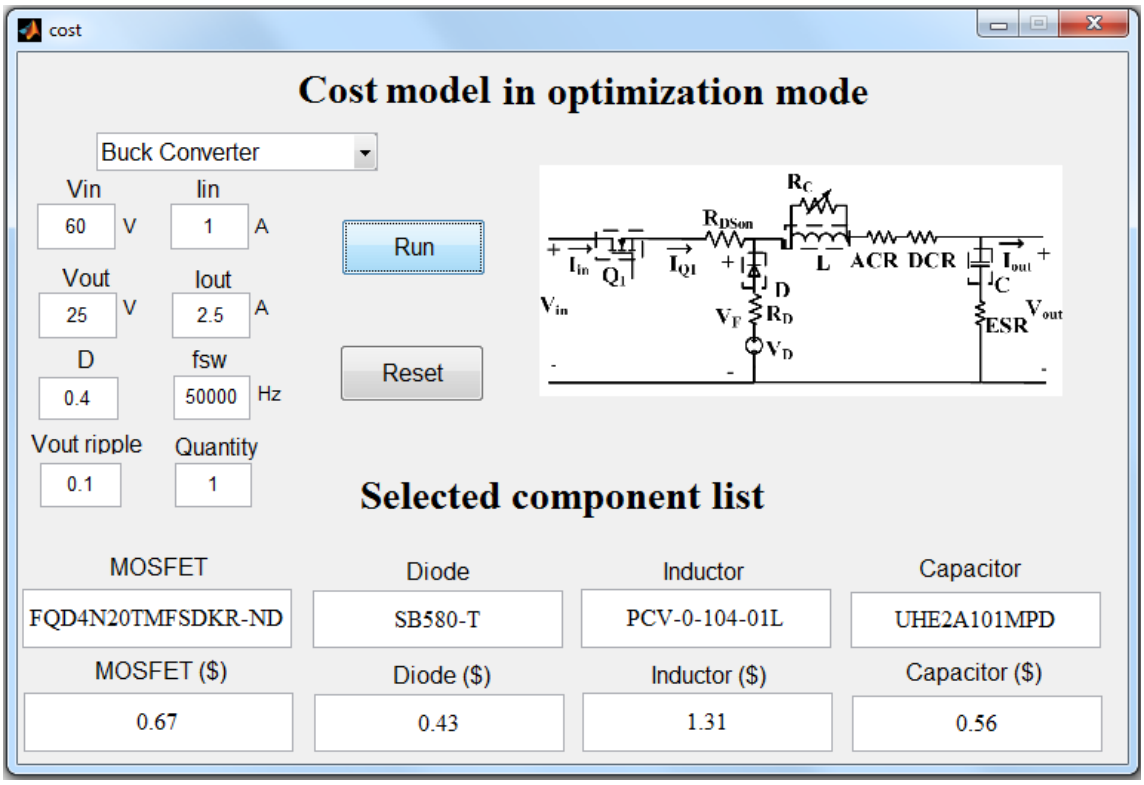

Figure 54 Buck converter optimization mode cost modeling tool

Table XXI Buck converter results generated by optimization mode cost modeling tool

MOSFET		Diode	
Suitable Components	*Cost*($)	Suitable Components	*Cost*($)
FQD4N20TMFSCT-ND	0.67	SK35A-LTP	0.57
FQD4N20TMFSDKR-ND	0.67	STPS5H100B-TR	1.4
Capacitor		B350A-13-F	0.46
Suitable Components	*Cost*($)	SS35	0.63
UHE2A101MPD	0.56	B550C-13-F	0.95
ESH107M200AM7AA	1.02	SB550-E3/54	0.61
UVZ2F101MHD	1.85	SK55L-TP	0.49
UPT2G101MHD6	2.68	SB550	0.56
Inductor		CDBC580-G	0.74
Suitable Components	*Cost*($)	SB580	0.59
PCV-0-104-01L	1.31	SB580-T	0.43
PCV-0-104-03L	1.48	HSM580G/TR13	1.34
PCV-0-104-05L	2.37	RGP30B-E3/73	0.476
		SK310A-LTP	0.57
		CDBA3100-G	0.63
		B3100-13-F	0.68
		CDBC5100-G	0.74
		SS5P10-M3/86A	0.77
		SB5100-T	0.74

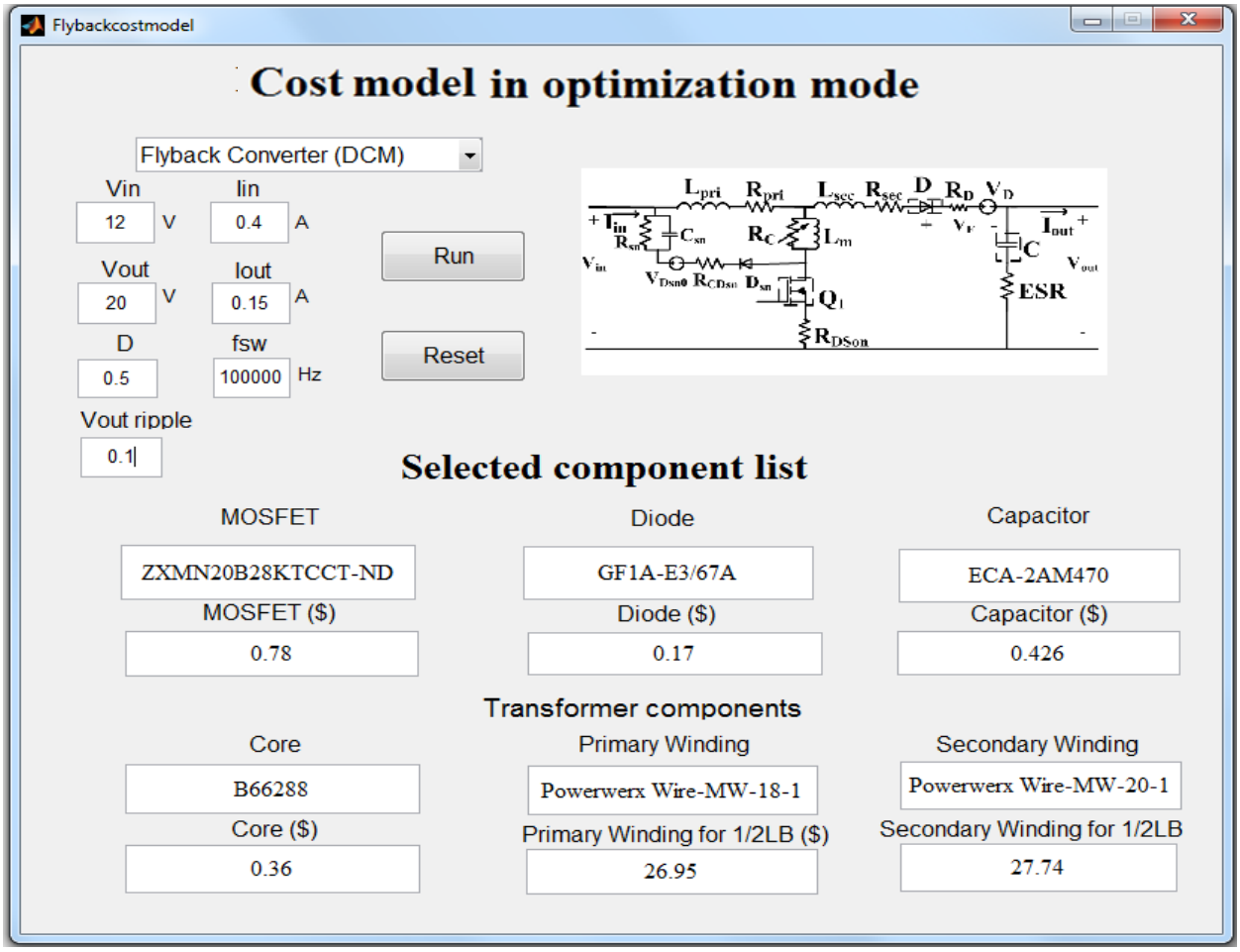

Figure 55 Flyback converter optimization mode cost modeling tool

Table XXII Flyback converter results generated by optimization mode cost modeling tool

MOSFET		Capacitor	
Suitable Components	*Cost*($)	Suitable Components	*Cost*($)
ZXMN20B28KTCCT-	0.78	EEU-FC2A220	0.502
ZXMN20B28KTCDKR	0.78	EEU-EB2D220	0.69
Primary winding		UPJ2F220MHD1TN	1.32
Suitable Components	*Cost*($) per ½ lb	EKXG401ELL220MK	1.72
Powerwerx Wire-MW-	26.95	ECA-2AM470	0.426
Secondary winding		EEU-ED2C470	0.724
Suitable Components	*Cost*($) per ½ lb	UPB2E470MHD1TO	1.668
Powerwerx Wire-MW-	27.74	ECO-S2GA470BA	1.314
Cores		380LX470M500H012	5.41
Suitable Components	*Cost*($)	UHE2A101MPD	0.56
B65713	10.08	ESH107M200AM7AA	1.02
B65805	0.43	UVZ2F101MHD	1.85
B66361	0.51	UPT2G101MHD6	2.68
B66285	1.07	EEU-FC2A221	2.018
B65814	1.07	EEU-EB2D221	2.56
B66288	0.36	LGU2F221MELB	7.022
B66287	2.72	ECO-S2GB221EA	4.68
B66291	2.72	ECA-2AHG471	1.69
B66387	5.6	SLP471M200E1P3	3.198
B65684	3.54	ELXM3B1VSN471M	15.88
Diode		EET-HC2G471LA	7.904
Suitable Components	*Cost*($)	EKMS501VSN471M	26.83333333
SS15	0.41	ECA-2AHG102	2.762
GF1A-E3/67A	0.17	EET-UQ2D102EA	5.264
SS15E-TP	0.4	350LSQ1000MNB36	14.244
SK15-13-F	0.95	B43508A9108M000	20.305
SS18-TP	0.39	ALS30A102KF500	36.1
SS18	0.46		
B180-13-F	0.82		
CDBA180-G	0.54		

Thus, the rapid prototyping tools developed here can provide two modes of operation for designers. In this chapter these modes have been explained with the help of GUI models and the results obtained from these models are verified experimentally and manually. The results shown in Tables II, IV, VI and XV are obtained from component-specific mode while Tables XVI-XXII provide results for manual mode. Results for component-specific mode operation are verified

with the help of experimentally implemented boost, buck and flyback converters and the results for optimization mode are verified manually. These two modes of operation help in selecting the components such that they are useful in maximizing the efficiency of the circuit or provide a cost effective solution.

CHAPTER 6: CONCLUSION AND FUTURE WORK

Rapid prototyping tools are presented here in optimization mode and component-specific mode. With these two modes of operation the users can estimate power loss or cost of the components as well as that of the overall system. These two modes of operation aid in component selection process by estimating the cost and performance of the component within the converter system before finalizing it. The rapid prototyping tools can be useful for engineers and designers. The power loss and cost models are found to be 92% accurate. These tools have been verified as major time and cost saving applications and they can be easily scaled up to include many other applications such as in inverters, motor drives, and lighting applications.

The review of existing literature was instrumental in providing insights about developing more accurate power loss and cost models. Since most of the existing research did not consider non-idealities and parasitic elements while calculating power loss of components. Moreover, PCBs and gate drive losses are also not considered in the existing power loss models. The power loss models presented here are based on non-idealities and parasitic elements including PCB and gate drive losses to develop more accurate models. Derivation for all power loss models are presented and discussed in detail. These models are based on converter specifications and datasheet information so that the users can predict power losses in the circuits before finalizing their converter design.

Cost models were derived based on an extensive survey of the commercial devices followed by a cost surface fitting and curve fitting exercise. Component cost equations are obtained with the help of these tools and further verified with actual cost of the components. The error observed in this verification was less than 10%. Existing literature does not discuss the core and magnet wire cost estimation models which are important for flyback transformers. These models

derived here can be helpful for designers while designing flyback transformers as well. It is important to note that component technology and cost profiles change over time as a result of changes in material and manufacturing techniques. The rapid prototyping tools developed in this research intend to develop power loss and cost modeling methodologies that can evolve with time and changes in technology.

The rapid prototyping tools are prepared as with the aim of saving time and cost. These tools are divided into two categories to improve selection process. Optimization mode for power loss models helps to select components based on the least power loss whereas component-specific mode can provide power losses of each selected components. Similarly optimization mode for cost models selects the components based on lowest costs while the component-specific mode can provide cost estimates for a specific range of component parameters. Although the techniques for component selection process developed here are shown to be successful, the models presented here cannot provide power loss or cost estimates for other applications. However, they can be easily scaled and extended for other applications based on a similar methodology and approach. Similarly, the rapid prototyping tools are limited to power loss and cost models, but can be extended not only for other applications but also for other models such as reliability models.

The component-specific mode work well with power losses for basic power electronic components, PCBs and gate drive circuits, but further work should be done to estimate power losses within microcontroller or DSP. The cost model with component-specific mode can estimate the ceiling prices of components, however further work is needed in order to obtain a minimum value of ‘floor’ price of the component. In conclusion, this research provides a simple, flexible and user-friendly way of selecting components to design systems by considering the

vital elements of power loss and cost in the design phase itself. These methods and models are highly accurate and scalable considering the early stage of their application in the overall system design process. Finally, this research will be helpful to all designers and engineers to prepare their own rapid prototyping tools for the applications of their choice. The prepared tools can also be useful for component distributors who can implement these tools in a web-based environment.

APPENDIX I COMPONENT-SPECIFIC MODE RESULTS FOR DIFFERENT DUTY RATIOS

Table A1 Boost converter component-specific mode results for different duty ratios

Parameters	Duty Ratios				
	30%	40%	50%	60%	75%
V_{in}	20	20	20.1	20	20
I_{in}	0.45	0.6	0.88	1.35	3.50
V_{out}	28	33	39.8	49.3	77.4
I_{out}	0.3	0.34	0.42	0.52	0.85
F_{sw}	50KHz	50KHz	50KHz	50KHz	50KHz
D	0.3	0.4	0.5	0.6	0.75
P_{in}	9.00	12.00	17.69	27	70
P_{out}	8.4	11.22	16.72	25.63	65.79
P_{loss}	0.6	0.78	0.97	1.36	4.21
P_{CM}	0.002	0.005	0.012	0.03	0.27
P_{SW}	0.03	0.04	0.07	0.10	0.28
P_{GD}	0.06	0.06	0.064	0.06	0.064
P_{loss_Mosfet}	0.10	0.11	0.14	0.19	0.61
P_{CD}	0.32	0.4	0.44	0.55	0.89
P_{SWD}	0.08	0.1	0.1	0.14	0.28
P_{loss_Diode}	0.4	0.5	0.54	0.69	1.18
P_{CORE}	0.02	0.04	0.1	0.23	0.93
P_{DCR}	0.01	0.02	0.05	0.11	0.74
P_{ACR}	0	0	0	0	0
$P_{loss\_Inductor}$	0.03	0.06	0.15	0.34	1.67
$P_{loss\_Capacitor}$	0.01	0.02	0.03	0.04	0.062
P_{GDRV}	0	0	0	0	0
P_{PCB}	0.02	0.03	0.06	0.1	0.67
P_{Total}	0.56	0.72	0.92	1.37	4.19
%Error	**6.6**	**7.69**	**5.15**	**-0.74**	**0.43**

Table A2 Buck converters component-specific mode results for different duty ratios

Parameters	Duty Ratios				
	20%	30%	40%	50%	60%
V_{in}	60	60	62	61	46
I_{in}	0.28	0.6	1.1	1.65	1.6
V_{out}	12.4	18	24.6	30	27.1
I_{out}	1.15	1.79	2.55	3.12	2.55
F_{sw}	50KHz	50KHz	50KHz	50KHz	50KHz
D	0.2	0.3	0.4	0.5	0.6
P_{in}	16.80	36	68.20	100.65	73.60
P_{out}	14.03	32.22	62.73	93.6	69.11
P_{loss}	2.54	3.76	5.47	7.05	4.49
P_{CM}	0.06	0.20	0.52	0.94	0.75
P_{SW}	0.13	0.21	0.31	0.38	0.24
P_{G}	0.04	0.04	0.04	0.04	0.03
P_{loss_Mosfet}	0.23	0.45	0.87	1.36	1.01
P_{CD}	0.93	1.27	1.56	1.59	1.04
P_{SWD}	0.06	0.09	0.12	0.15	0.13
P_{loss_Diode}	0.99	1.36	1.68	1.74	1.17
P_{CORE}	0.41	0.41	0.41	0.41	0.41
P_{DCR}	0.05	0.11	0.22	0.33	0.22
P_{ACR}	0.49	0.79	1.09	1.13	0.59
$P_{loss\_Inductor}$	0.95	1.31	1.72	1.87	1.22
$P_{loss\_Capacitor}$	0.20	0.32	0.44	0.45	0.24
P_{GDRV}	0	0	0	0	0
P_{PCB}	0.13	0.19	0.70	1.13	0.83
P_{Total}	2.49	3.78	5.41	6.55	4.47
%Error	**1.96**	**-0.52**	**0.45**	**7.09**	**0.45**

Table A3 Flyback converters component-specific mode results for different duty ratios

Parameters	Duty Ratios			
	20%	30%	40%	50%
V_{in}	11.7	11.6	11.6	11.2
I_{in}	0.075	0.2	0.2	0.38
V_{out}	9.26	11.1	14.7	19.6
I_{out}	0.06	0.16	0.1	0.15
F_{sw}	100KHz	100KHz	100KHz	100KHz
D	0.2	0.3	0.4	0.5
P_{in}	0.88	2.32	2.32	4.26
P_{out}	0.56	1.78	1.47	2.94
P_{loss}	0.32	0.55	0.85	1.32
P_{CM}	0.05	0.12	0.28	0.52
P_{SW}	0.01	0.02	0.03	0.04
P_{GD}	0.02	0.02	0.02	0.02
P_{loss_Mosfet}	0.08	0.16	0.32	0.58
P_{CD}	0.05	0.11	0.06	0.08
P_{SWD}	0.09	0.11	0.14	0.19
P_{loss_Diode}	0.14	0.22	0.20	0.27
P_{CORE}	0.02	0.02	0.02	0.02
P_{pri}	0.002	0.004	0.01	0.01
P_{sec}	0.01	0.02	0.04	0.05
$P_{loss\_Inductor}$	0.03	0.05	0.07	0.09
$P_{loss\_Capacitor}$	0.02	0.02	0.06	0.08
P_{sn}	0.04	0.10	0.14	0.21
P_{PCB}	0.004	0.01	0.02	0.04
P_{Total}	0.31	0.56	0.81	1.27
%Error	**3.13**	**-1.81**	**4.7**	**3.78**

APPENDIX II OPTIMIZATION MODE RESULTS FOR DIFFERENT DUTY RATIOS

Table A4 Boost and buck converter parameters for GUI model

	Boost Converter			Buck Converter		
Parameters	Case 1	Case 2	Case 3	Case 1	Case 2	Case 3
V_{in} (V)	50	40	20	50	200	200
I_{in} (A)	4	2.1	2	0.5	2	1.5
V_{out} (V)	120	80	130	25	160	120
I_{out} (A)	2.1	0.9	0.3	1	2.5	2.5
Duty	0.6	0.5	0.85	0.5	0.8	0.6
f_{sw} (KHz)	100	100	50	50	50	100
$V_{outripple}$(V)	0.1	0.1	0.1	0.2	0.1	0.2

Table A5 Boost converter power loss model results for Case 1

MOSFET		Diode	
Suitable Components	P_{Loss}(W)	Suitable Components	P_{Loss}(W)
FQP9N30	6.0472777	RD0504T-TL-H	3.633955
STP12NK30Z	4.1921913	BY229B-400HE3/45	5.533324
IRF740PBF	5.8689506	STTH5L04DEE-TR	3.2627
IRF740STRLPBF	5.8689506	Capacitor	
SiHB10N40D	6.1370370	Suitable Components	P_{Loss}(W)
Inductor		LGU2F221MELB	0.000223
Suitable Components	P_{Loss}(W)	ECO-S2GB221EA	0.027160
PCV-2-274-03L	4.4202524		
PCV-2-274-05L	1.5975424		
PCV-2-274-10L	2.0457273		

Table A6 Boost converter power loss model results for Case 2

MOSFET		Inductor	
Suitable Components	P_{Loss}(W)	Suitable Components	P_{Loss}(W)
FQD7N20LTMDKR-	2.4663682	PCV-2-394-05L	1.318871
BUZ73AL H-ND	1.8637325		
JAN2N6798U-MIL	1.2855430		
FQD7N30TMTR-ND	2.0267703	Capacitor	
Diode		Suitable Components	P_{Loss}(W)
Suitable Components	P_{Loss}(W)	EEU-ED2C470	0.000221
S320	1.774	UPB2E470MHD1TO	0.000221
PDS3200-13	1.659	ECO-S2GA470BA	0.021652
GI912-E3/73	2.007	380LX470M500H012	0.005478

Table A7 Boost converter power loss model results for Case 3

MOSFET		Diode	
Suitable Components	P_{Loss}(W)	Suitable Components	P_{Loss}(W)
FQD7N30TMTR-ND	2.5106656	UVZ2F101MHD	0.00019
IRF730PBF	3.4607854	UPT2G101MHD6	0.00019
IRF730STRRPBF	3.4607854	Inductor	
STP7NK40Z	3.4570348	Suitable Components	P_{Loss}(W)
STD9NM40N	2.7229388	PCV-2-564-02L	12.71139
STD6NK50ZT4	4.1627202	PCV-2-564-06L	8.046394
FDD6N50FTM	4.0036300	PCV-2-564-08L	4.245614
NDF05N50ZH	5.1767546	DO5040H-684KLB	37.92929
Diode			
Suitable Components	P_{Loss}(W)		
RGP30G-E3/73	0.6374304		

Table A8 Buck converter power loss model results for Case 1

MOSFET		Inductor	
Suitable Components	P_{Loss}(W)	Suitable Components	P_{Loss}(W)
FQT7N10LTFCT-ND	0.4254166	PCV-2-223-05L	0.0503284
FQT7N10LTFDKR-ND	0.4254166	PCV-2-223-10L	0.0490967
FQT7N10TFTR-ND	0.3047916	PCH-27X-223-LT	56.996215
ZXMN20B28KTCCT-	0.6625	RFB1010-221L	3.4780687
ZXMN20B28KTCDKR	0.6625	PCV-0-224-03L	0.1401287
Diode			
Suitable Components	P_{Loss}(W)W)		
SS15	0.9509380	Capacitor	
GF1A-E3/67A	1.0959235	Suitable Components	P_{Loss}(W)
SS15E-TP	0.8867728	EEU-FC2A220	0.0743333
SK15-13-F	0.9124580	EKXG401ELL220MK	0.2546333
SS18-TP	0.8416144	EEU-EB2D220	0.159
SS18	0.9512507	UPJ2F220MHD1TN	0.2113333
B180-13-F	0.9214661		
CDBA180-G	0.9575686		
RS1B-E3/5AT	1.1698561		
CDBM1100-G	0.9575045		
SS110-TP	0.8429902		
SB1100	0.9568791		

Table A9 Buck converter power loss model results for Case 2

MOSFET		Diode	
Suitable Components	P_{Loss}(W)	Suitable Components	P_{Loss}(W)
IRF730PBF	7.0840833	RGP30G-E3/73	1.1569199
IRF730STRRPBF	7.0840833	RD0504T-TL-H	1.0370262
STP7NK40Z	7.0379166	STTH5L04DEE-TR	0.8737418
STD9NM40N	5.4708333	BYC5DX-500,127	1.0616713
STD6NK50ZT4	8.6292083	RGP30J-E3/73	1.0753008
FDD6N50FTM	8.4104166	CN649	0.9847395
NDF05N50ZH	10.466041	LXA03B600	1.7456863
STP8N80K5	6.9358333	BYV25D-600,118	0.9804920
SPD06N80C3	6.72875	LQA05TC600	1.2823453
IXTH6N80A	10.775	Capacitor	
Inductor		Suitable Components	P_{Loss}(W)
Suitable Components	P_{Loss}(W)	UPT2G101MHD6	0.0133333
PCV-2-223-05L	0.1884615		
PCV-2-223-10L	0.1685322		
PCH-27X-223_LT	136.29945		
PCV-0-224-03L	1.0476876		

Table A10 Buck converter power loss model results for Case 3

MOSFET		Diode	
Suitable Components	P_{Loss}(W)	Suitable Components	P_{Loss}(W)
IRF720	9.7368333	RGP30G-E3/73	2.2659598
IRF720SPBF	9.7368333	RD0504T-TL-H	2.0181925
IRF720STRRPBF	9.7368333	STTH5L04DEE-TR	1.7395036
IRF730PBF	5.8348333	Inductor	
IRF730STRRPBF	5.8348333	Suitable Components	P_{Loss}(W)
STP7NK40Z	5.7425	PCV-0-104-01L	4.6252808
STD9NM40N	4.3583333	PCV-0-104-03L	1.7468856
STD6NK50ZT4	7.2584166	PCV-0-104-05L	1.3359644
FDD6N50FTM	7.2375	Capacitor	
NDF05N50ZH	8.4320833	Suitable Components	P_{Loss}(W)
STP8N80K5	5.955	UPB2E470MHD1TO	0.021042
SPD06N80C3	5.9575	ECO-S2GA470BA	2.058333
IXTH6N80A	9.8833333	380LX470M500H012	0.520833

Table A11 Boost converter cost model results for Case 1

MOSFET		Diode	
Suitable Components	*Cost*($)	Suitable Components	*Cost*($)
FQP9N30	1.18	RD0504T-TL-H	1.05
STP12NK30Z	1.95	BY229B-400HE3/45	1.03
IRF740PBF	1.63	BYC5DX-500,127	0.35
IRF740STRLPBF	1.63	BYV25D-600,118	0.848
SiHB10N40D	1.79	LQA05TC600	1.41
Inductor		BY229B-600HE3/45	5.5333244
Suitable Components	*Cost*($)	LQA08TC600	1.93
PCV-2-274-03L	4.15	QH08TZ600	1.85
PCV-2-274-05L	4.56	MURF860G	0.99
PCV-2-274-10L	7.39	Capacitor	
		Suitable Components	*Cost*($)
		LGU2F221MELB	7.022
		ECO-S2GB221EA	4.68

Table A12 Boost converter cost model results for Case 2

MOSFET		Diode	
Suitable Components	*Cost*($)	Suitable	*Cost*($)
FQD7N20LTMDKR-	0.98	GI912-E3/73	0.48
BUZ73AL H-ND	1.26	RGP30G-E3/73	0.45
JAN2N6798U-MIL	4.34	RD0504T-TL-H	1.05
RDN100N20FU6-ND	2.73	Capacitor	
RDN100N20-ND	2.73	Suitable	*Cost*($)
IRLI640GPBF	2.88	EEU-ED2C470	0.724
IRLI640G	2.88	UPB2E470MHD1T	1.668
FQD7N30TMTR-ND	1.04	ECO-S2GA470BA	1.314
FQP9N30	1.18	380LX470M500H01	5.41
STP12NK30Z	1.95	Inductor	
		Suitable	*Cost*($)
		PCV-2-394-05L	5.1

Table A13 Boost converter cost model results for Case 3

MOSFET		Inductor	
Suitable Components	*Cost*($)	Suitable	*Cost*($)
FQD7N30TMTR-ND	1.04	PCV-2-564-02L	3.78
FQP9N30	1.18	PCV-2-564-06L	6.46
STP12NK30Z	1.95	PCV-2-564-08L	10.79
IRF730PBF	1.26	Capacitor	
IRF730STRRPBF	1.51	Suitable	*Cost*($)
STP7NK40Z	1.56	UVZ2F101MHD	1.85
STD9NM40N	1.67	UPT2G101MHD6	2.68
IRF740PBF	1.63		
IRF740STRLPBF	1.63	Diode	
SiHB10N40D	1.79	Suitable	*Cost*($)
STD6NK50ZT4	1.18	LQA05TC600	1.41
FDD6N50FTM	1.1	RGP30G-E3/73	0.45
NDF05N50ZH	0.94	RD0504T-TL-H	1.05
TK10A50D	1.89	BYC5DX-500,127	0.35
STP11NK50ZFP	1.93	RGP30J-E3/73	0.495
IPA50R350CP	1.12	LXA03B600	0.81
FDPF12N50UT	1.73	BYV25D-600,118	0.848

Table A14 Buck converter cost model results for Case 1

MOSFET		Inductor	
Suitable Components	*Cost*($)	Suitable	*Cost*($)
FQT7N10LTFCT-ND	0.54	PCV-2-223-05L	2.12
FQT7N10LTFDKR-	0.54	PCV-2-223-10L	2.06
FQT7N10TFTR-ND	0.54	PCH-27X-223_LT	1.91
Diode		RFB1010-221L	0.68
Suitable Components	*Cost*($)W)	PCV-0-224-03L	1.46
SS18-TP	0.39	Capacitor	
SS18	0.46	Suitable	*Cost*($)
B180-13-F	0.82	EEU-FC2A220	0.502
CDBA180-G	0.54	EKXG401ELL220M	1.72
RS1B-E3/5AT	0.178	EEU-EB2D220	0.69
CDBM1100-G	0.57	UPJ2F220MHD1TN	1.324
SS110-TP	0.39		
SB1100	0.52		

Table A15 Buck converter cost model results for case 2

MOSFET		Diode	
Suitable Components	*Cost*($)	Suitable Components	*Cost*($)
IRF730PBF	1.26	RGP30G-E3/73	0.45
IRF730STRRPBF	1.51	RD0504T-TL-H	1.05
STP7NK40Z	1.56	STTH5L04DEE-TR	1.49
STD9NM40N	1.67	BYC5DX-500,127	0.35
STD6NK50ZT4	1.18	RGP30J-E3/73	0.495
FDD6N50FTM	1.1	CN649	0.448
NDF05N50ZH	0.94	LXA03B600	0.81
Inductor		BYV25D-600,118	0.84
Suitable Components	*Cost*($)	LQA05TC600	1.41
PCV-2-223-05L	2.12		
PCV-2-223-10L	2.06	Capacitor	
PCH-27X-223_LT	1.91	Suitable Components	*Cost*($)
PCV-0-224-03L	1.46	UPT2G101MHD6	2.68

Table A16 Buck converter cost model results for case 3

MOSFET		Diode	
Suitable	P_{Loss}(W)	Suitable Components	P_{Loss}(W)
IRF720	3.18	RGP30G-E3/73	0.45
IRF720SPBF	1.51	RD0504T-TL-H	1.05
IRF720STRRPBF	1.51	STTH5L04DEE-TR	1.49
IRF730PBF	1.26	Inductor	
IRF730STRRPBF	1.51	Suitable Components	P_{Loss}(W)
STP7NK40Z	1.56	PCV-0-104-01L	1.31
STD9NM40N	1.67	PCV-0-104-03L	1.48
STD6NK50ZT4	1.18	PCV-0-104-05L	2.37
FDD6N50FTM	1.1	Capacitor	
NDF05N50ZH	0.94	Suitable Components	P_{Loss}(W)
		UPB2E470MHD1TO	1.668
		ECO-S2GA470BA	1.314
		380LX470M500H012	5.41

APPENDIX III DETAILED DERIVATIONS OF EQUATIONS

For equation (60) and (72) I_{Drms} is obtained by taking RMS value of I_D where I_D is represented as shown in Figure 4.

I_{Drms} is represented as

$$I_{Drms} = \sqrt{\frac{1}{T}\int_0^{DT}\left[\left(Iout - \frac{\Delta i}{2}\right) + \frac{\Delta i}{DT}t\right]^2 dt}\,, \tag{A1}$$

$$I_{Drms} = \sqrt{\frac{1}{T}\int_0^{DT}\left[\left(I_{out} - \frac{\Delta i}{2}\right)^2 + \frac{\Delta i^2 t^2}{D^2T^2} + \frac{2\Delta i t}{DT}\left(I_{out} - \frac{\Delta i}{2}\right)\right]dt} \tag{A2}$$

$$I_{Drms} = \sqrt{DI_{out}^2 + \frac{\Delta i^2 D}{4} - DI_{out}^2\Delta i + \frac{\Delta i^2 D}{3}t + \Delta i D I_{out}t + \frac{\Delta i^2 t}{2}\Big|_0^{DT}} \tag{A3}$$

$$I_{Drms} = \sqrt{DI_{out}^2 + \frac{3\Delta i^2 D + 4\Delta i^2 D - 6\Delta i^2 D}{12}} \tag{A4}$$

$$I_{Drms} = \sqrt{D\left[I_{out}^2 + \frac{\Delta i^2}{12}\right]} \tag{A5}$$

Similar approach is implemented to calculate I_{Drms} of the boost converter.

I_{Drms} represented in (85) and Figure 14 is calculated as,

$$I_{Drms} = I_{Lpk}\sqrt{\frac{D_1}{3}}\,, \tag{A6}$$

$$I_{Drms} = I_{Lpk}\sqrt{\frac{D_1 T_s}{3T_s}}\,, \tag{A7}$$

but
$$T_{ON} = D_1 T_s\,, \tag{A8}$$

$$T_{ON} = \frac{0.8T_S\left(V_{out} + V_F\right)}{V_F}\,, \tag{A9}$$

$$I_{Drms} = \frac{V_{in}D}{f_{sw}\left(L_{pri}+L_m\right)}\sqrt{\frac{1}{3T_S}\left(\frac{0.8T_S\left(V_{out}+V_F\right)}{V_F}\right)}, \tag{A10}$$

$$I_{Drms} = \frac{V_{in}D}{f_{sw}\left(L_{pri}+L_m\right)}\sqrt{0.26\left(1+\frac{V_{out}}{V_F}\right)}, \tag{A11}$$

To calculate I_{Doff} of the flyback transformer current (86), I_{Lavg} in (92) and (93) is calculated with the help of (84) as,

$$I_{Lavg} = \frac{I_{LPK}}{2}\left(D_1+D_2\right), \tag{A12}$$

$$I_{Lavg} = \frac{0.8}{2}\left(\frac{V_{in}D}{\left(L_m+L_{pri}\right)f_{sw}}\right), \tag{A13}$$

$$I_{Lavg} = I_{Lpri} = \left(\frac{0.4V_{in}D}{\left(L_m+L_{pri}\right)f_{sw}}\right), \tag{A14}$$

$$I_{Lsec} = \left(\frac{0.4nV_{in}D}{\left(L_m+L_{pri}\right)f_{sw}}\right), \tag{A15}$$

$$I_{Doff} = \left[\frac{0.8}{2}\left(\frac{V_{in}D}{\left(L_m+L_{pri}\right)f_{sw}}\right)-\left(\frac{V_{in}D}{2\left(L_m+L_{pri}\right)f_{sw}}\right)\right] \tag{A16}$$

$$I_{Doff} = \frac{0.9V_{in}D}{\left(L_m+L_{pri}\right)f_{sw}} \tag{A17}$$

RMS value of triangular waveform is given in Figure 14 calculated as,

$$I_{rms(pri)} = I_{LPK}\left(\sqrt{\frac{D_1T_S+D_2T_S}{3T_S}}\right) \tag{A18}$$

$$I_{rms(pri)} = I_{LPK}\left(\sqrt{\frac{T_{ON}+T_{OFF}}{3T_S}}\right) \tag{A19}$$

$$I_{rms(pri)} = I_{LPK}\left(\sqrt{\frac{0.8T_S}{3T_S}}\right) \tag{A20}$$

$$I_{rms(pri)} = I_{LPK}\left(\sqrt{0.26}\right) \tag{A21}$$

$$I_{rms(pri)} = 0.52I_{LPK} \tag{A22}$$

$$I_{rms(\sec)} = 0.52nI_{LPK} \tag{A23}$$

Capacitor current I_{crms} in (94) flyback converter

$$I_{Crms(\sec)} = \left[\left(\frac{0.52nV_{in}D}{\left(L_m + L_{pri}\right)f_{sw}}\right)^2 - I_{out}^2\right] \tag{A24}$$

APPENDIX IV COST MODEL EQUATIONS WITH DIFFERENT SURFACE FITS

Table A17 Surface fitting tool equations for MOSFET

Surface fitting tool results	Cost Models
Lowess- quadratic	SSE-51.44, R-square-0.9436 No explicit model was provided by MATLAB tool
Polynomial –x degree four and y degree three	$Cost_M(V_{DS}, I_D) = \sum_{i=0}^{i=13} \alpha_i V_{DS}^{\beta_i} I_D^{\gamma_i}$ SSE-194.2, R-square-0.6717
Customize equation	$Cost_M(V_{DS}, I_D) = a + b\sin(m\pi V_{DS} I_D) + ce^{(-(\omega I_D)^2)}$ SSE-898.4, R-square-0.01473

Table A18 Surface fitting tool equations for diode

Surface fitting tool results	Cost Models
Lowess- quadratic	SSE: 0.07198, R-square: 0.9502 No explicit model was provided by MATLAB tool
Polynomial –x degree one and y degree one	$Cost_D(V_B, I_F) = \sum_{j=0}^{j=2} \delta_j V_B^{\theta_j} I_F^{\kappa_j}$ SSE-0.1591, R-square-0.8899
Customize equation	$Cost_D(V_B, I_F) = a + b\sin(m\pi V_B I_F) + ce^{(-(\omega I_F)^2)}$ SSE-0.2563, R-square-0.8039

Table A19 Surface fitting tool equations for inductors

Surface fitting tool results	Cost Models
Lowess- linear or quadratic	Out of surface fit box No explicit model was provided by MATLAB tool
Polynomial –x degree one and y degree one	$Cost_L(L, I_L) = \mathrm{a} + \mathrm{b}L + \mathrm{c}I_L$ SSE-7693, R-square-0.3261
Customize equation	$Cost_L(L, I_L) = \chi + \mu\sin(\upsilon\pi L I_L) + \phi e^{-(\omega I_L)^2}$ SSE-3408, R-square-0.7014

Table A20 Surface fitting tool equations for capacitor

Surface fitting tool results	Cost Models
Lowess- linear	SSE: 139.8, R-square: 0.9091 No explicit model was provided by MATLAB tool
Polynomial –x degree two and y degree three	$Cost_C(C,V_C)=\sum_{z=0}^{z=8}\eta_z C^{\sigma_z} V_C^{\xi_z}$ SSE: 265.5, R-square: 0.8274
Customize equation	$Cost_C(C,V_C)=a+b\sin(m\pi CV_C)+ce^{(-(\omega V_C)^2)}$ SSE: 1245, R-square: 0.19

Table A21 Surface fitting tool equations for Cores

Surface fitting tool results	Cost Models
Lowess- linear	SSE: 1.196 R-square: 0.9882 No explicit model was provided by MATLAB tool
Polynomial –x degree two and y degree two	$Cost_{Co}(A_L, f_{sw})=\sum_{m=0}^{m=4}\tau_m A_L^{\psi_m} f_{sw}^{\rho_m}$ SSE: 6.448 R-square: 0.9365
Customize equation	$Cost_{Co}(A_L, f_{sw})=a+b\sin(m\pi A_L f_{sw})+ce^{(-(\omega f_{sw})^2)}$ SSE: 74.43 R-square: 0.2669

Table A22 Curve fitting tool equations for Magnet wire

Curve fitting tool results	Cost Models
Linear polynomial	$Cost_w(\mathrm{G})=\sum_{q=0}^{q=1}\varphi_q G^{\varsigma q}$
Quadratic polynomial	$Cost_w(\mathrm{G})=\sum_{q=0}^{q=2}\varphi_q G^{\varsigma q}$
Cubic polynomial	$Cost_w(\mathrm{G})=\sum_{q=0}^{q=3}\varphi_q G^{\varsigma q}$
Polynomial 5th degree	$Cost_w(\mathrm{G})=\sum_{q=0}^{q=6}\varphi_q G^{\varsigma q}$

REFERENCES

[1] S.M.Cuk, R.D. Middlebrook, "DC-DC switching converters," U.S. Patent 4 184 197A, Jan 15, 1980.

[2] E. Biagi, G. Pasetti, F. Tinfena, ; R. Serventi, L. Fanucci, "A High Voltage High Power high frequency Boost/Flyback DC-DC converter for automotive applications," in *Proc. IEEE Power Electronics, Electrical Drives, Automation and Motion conference,* 2012, pp. 1166 – 1171.

[3] N.G. Ziesse, "High frequency DC-DC converter," U.S. Patent 4 449 174A, May 15, 1984.

[4] Gu, Bin, Lin, Chien-Yu Chen, Bai Feng,Jason Dominic, Cong Zheng, Jih-Sheng Lai, "A high efficiency hybrid resonant PWM zero-voltage-switching full-bridge DC-DC converter for electric vehicle battery chargers ," in *Proc. IEEE Applied Power Electronics Conference and Exposition,*2013, pp. 23 – 30.

[5] M.C.W. Lindmark, " Switched mode power supply," U.S. Patent 4 097 773A, June 27, 1978.

[6] Dan Dai, Jing Liu, "Design of a practical human-powered contactless charger for cellphone," *IEEE Transactions on Consumer Electronics*, vol. 59, pp. 476 – 482, August 2013.

[7] W.G. Borland, " Resonant switching converter," U.S. Patent 4 945 466A, May 15, 1984.

[8] Ying-Chun Chuang, Yu-Lung Ke ; Hung-Shiang Chuang ; Yung-Shan Wang, "A novel single-switch resonant power converter for renewable energy generation applications," in *Proc. IEEE Industrial & Commercial Power Systems Technical Conference,* 2013, pp.1-9.

[9] H. Wang, P. Zanchetta, J. Clare, C. Ji, "Modelling and control of a zero current switching high-voltage resonant converter power supply for radio frequency sources," *IEEE Transactions on Power Electronics,* vol.5, pp. 401 – 409, April 2012.

[10] Jinjun Liu, Weiyun Chen, Jindong Zhang, Dehong Xu , F.C.Lee, "Evaluation of power losses in different CCM mode single-phase boost FC converters via a simulation tool," in *Proc. IEEE Industry Applications Conference,* 2001, pp. 2455 - 2459.

[11] J.P.M.Figueiredo, F.L.Tofoli, R.L.Alves, "Comparison of non-isolated DC-DC converters from the efficiency point of view," in Proc. IEEE Power Electronics Conference, 2011, pp. 14-19.

[12] N. Yamashita, N. Murakami, T. Yachi, "Conduction power loss in MOSFET synchronous rectifier with parallel-connected Schottky barrier diode," *IEEE Transactions on Power Electronics,* vol.13, pp. 667 - 673, Jul 1998.

[13] Jiaxin Chen, Ge Chen, Youguang Guo, Jianguo Zhu "Comprehensive analysis of power loss in the output diode of flyback switching converter operating in DCM and CCM," in *Proc. IEEE Electrical Machines and Systems, 2008,* pp. 1865 – 1870.

[14] Yang Chen, P. Asadi, P. Parto, "Comparative analysis of power stage losses for synchronous Buck converter in Diode Emulation mode vs. Continuous Conduction Mode at light load condition," in *Proc. IEEE Applied Power Electronics Conference and Exposition, 2010,* pp. 1578 – 1583.

[15] Jinjun Liu, T.G. Wilson, R.C. Wong,R. Wunderlich, F.C. Lee, "A method for inductor core loss estimation in power factor correction applications," in *Proc. IEEE Applied Power Electronics Conference and Exposition, 2002,* pp. 439 - 445.

[16] H.Y. Chung, M.H. Pong, "Effect of switching frequency and number of winding layers on copper loss of an inductor," in *Proc. IEEE Power Electronics and Motion Control Conference, 2000,* pp. 1312 – 1317.

[17] A. Braham, A. Lahyani, P.Venet, N. Rejeb, "Recent Developments in Fault Detection and Power Loss Estimation of Electrolytic Capacitors," *IEEE Transactions on Power Electronics,* vol.25, pp. 33 - 43, Jan. 2010.

[18] I.Lope, C.Carretero, J.Acero, J.M.Burdio, R.Alonso, "Practical issues when calculating AC losses for magnetic devices in PCB implementations," in *Proc. IEEE Applied Power Electronics Conference and Exposition, 2012*, pp. 1017 - 1022.

[19] P. Pathmanathan, C.M. Jones, S.G. Pytel, D.L. Edgar, P.G. Huray, "Power loss due to periodic structures in high-speed packages and Printed Circuit Boards," in *Proc. IEEE Microelectronics and Packaging Conference, 2011*, pp. 1 - 8.

[20] Ren-Huei Tzeng, Chern-Lin Chen, "A Low-Consumption Regulated Gate Driver for Power MOSFET," *IEEE Transactions on Power Electronics,* vol.24, pp. 532 - 539, Feb. 2009.

[21] Zhiliang Zhang, W. Eberle, Zhihua Yang ; Yan-Fei Liu, P.C. Sen, "Optimal Design of Current Source Gate Driver for a Buck Voltage Regulator Based on a New Analytical Loss Model," in *Proc. IEEE Power Electronics Specialists Conference, 2007*, pp. 1 - 8.

[22] M.M. Jovanovic, "A technique for reducing rectifier reverse-recovery-related losses in high-power boost converters," *IEEE Transactions on Power Electronics,* vol.13, pp. 932 - 941, Sep. 1998.

[23] Jun Wang, Jun Li, Xiaohu Zhou, Tiefu Zhao, A.Q. Huang, R. Callanan, F. Husna, A. Agarwal, "10 kV SiC MOSFET Based Boost Converter," in *Proc. IEEE Industry Applications Society Annual Meeting, 2008*, pp.1-6.

[24] Z.Ivanovic, B.Blanusa, M.Knezic, "Power loss model for efficiency improvement of boost converter," in *Proc. IEEE Information, Communication and Automation Technologies*, 2011, pp. 1-6.

[25] Weiping Zhang, Yuanchao Liu, Zhi Li, Xiaoqiang Zhang, "The dynamic Power Loss analysis in Buck Converter," in *Proc. IEEE Power Electronics and Motion Control Conference, 2009*, pp. 362 - 367.

[26] T.Lopez, R.Elferich, "Method for the Analysis of Power MOSFET Losses in a Synchronous Buck Converter," in Proc. IEEE Power Electronics and Motion Control Conference, 2006, pp. 44-49.

[27] Jong-Hyun Kim, Myung hyo Ryu, Byung Duk Min, Eui Ho Song, "A Method to Reduce Power Consumption of Active-Clamped Flyback Converter at No-Load Condition," in *Proc. IEEE Industrial Electronics, 2006*, pp. 2811 – 2814.

[28] D. Murthy-Bellur, M.K. Kazimierczuk, "Winding losses caused by harmonics in high-frequency flyback transformers for pulse-width modulated DC-DC converters in discontinuous conduction mode," *IEEE Transactions on Power Electronics,* vol.3, pp. 804 - 817, Sep. 2010.

[29] A. Causo, A. Salati, E. Lorenzani, F. Immovilli, C. Bianchini, "Power losses analysis in interleaved flyback based PV grid connected micro-inverters," in *Proc. IEEE Industrial Electronics, 2013*, pp. 1833 - 1838.

[30] P.Bartal, I.Nagy, "On-line efficiency estimation for DC-DC converter cluster by dedicated software," in Proc. Energy Conference and Exhibition, 2012, pp. 800-805.

[31] Ying-Win Bai and Wei-Chih Kuo, "Design and implementation of an automatic measurement system for DC-DC converter efficiency on a motherboard," in *Proc. IEEE Industrial Electronics Society Conference, 2010,* pp. 1323 –1328.

[32] K. Viswanathan, R. Oruganti, "Evaluation of Power Losses in a Boost PFC Unit by Temperature Measurements," *IEEE Transactions on Industry Applications,* vol.43, pp. 1320 - 1328, Sept.-Oct. 2007.
[33] A. Shahin, A. Payman, J. Martin, S. Pierfederici, F. Meibody-Tabar,"Approximate Novel Loss Formulae Estimation for Optimization of Power Controller of DC-DC Converter," in *Proc. IEEE Industrial Electronics Society,2010,* pp. 373 – 378.
[34] Pill-Soo Kim, Yong Kim, "A future cost trends of magnetizer systems in Korea," in *Proc. IEEE Industrial Electronics, Control, and Instrumentation, 1996* , pp. 991 – 996.
[35] A.M. Roldan, A. Barrado, J. Pleite, J. Vazquez,E. Olias, "Size and cost reduction of the energy-storage capacitors," in *Proc. IEEE Applied Power Electronics Conference and Exposition, 2004,* pp. 723 – 729.
[36] Pill-Soo Kim, Yong Kim, "Part I-circuit, thermal and cost modeling of impulse magnetizer," in *Proc. IEEE Power Electronics and Drive Systems, 1999,* pp. 371 – 376.
[37] Bruno Burger, Dirk Kranzer, Olivier Stalter, "Cost Reduction of PV-Inverters with SiC-DMOSFETs," in *Proc. IEEE Integrated Power Systems, 2008,* pp. 1 – 5.
[38] R. Burkart, J.W.. Kolar, "Component cost models for multi-objective optimizations of switched-mode power converters," in *Proc. IEEE Energy Conversion Congress and Exposition, 2013,* pp. 2139 – 2146.
[39] Xiangyu Dong, Jishen Zhao, Yuan Xie, "Fabrication Cost Analysis and Cost-Aware Design Space Exploration for 3-D ICs," *IEEE Computer-Aided Design of Integrated Circuits and Systems,* vol.29, pp. 1959 - 1972, Dec. 2010.
[40] A.K. Coskun, A.B. Kahng, T.S. Rosing, "Temperature- and Cost-Aware Design of 3D Multiprocessor Architectures," in *Proc. IEEE Digital System Design, Architectures, Methods and Tools, 2009,* pp. 183 – 190.
[41] Pill-Soo Kim, "Cost modeling of battery electric vehicle and hybrid electric vehicle based on major parts cost," in *Proc. IEEE Power Electronics and Drive Systems, 2003,* pp. 1295 – 1300.
[42] P. Manimekalai, R. Harikumar, "Design, cost estimation and simulation of a standalone PV power generation system using interleaved converter," in *Proc. IEEE Emerging Trends in Science, Engineering and Technology , 2012,* pp. 416 – 421.
[43] K. Kim, S. Lertburapa, C. Xu, and P. Krein, "Efficiency and Cost Trade- Offs for Designing Module Integrated Converter Photovoltaic Systems," in *Proc. IEEE Power and Energy Conference at Illinois, 2012,* pp. 1–7, 2012.
[44] B. Azzopardi, J. Mutale, D. Kirschen, "Cost boundaries for future PV solar cell modules," in *Proc. IEEE Sustainable Energy Technologies, 2008,* pp. 589 – 594.
[45] P.I. Muoka, M.E. Haque,M. Negnetvitsky, "A new tool for design optimization and cost estimation of stand-alone photovoltaic power plants," in *Proc. IEEE Power and Energy Society General Meeting, 2011,* pp. 1 – 7.
[46] Tian Weidong, "The principle of minimum production cost model for multiple area interconnected power systems," in *Proc. IEEE Computer, Communication, Control and Power Engineering., 1993,* pp. 339 – 343.
[47] Weiwei Pan, Guowei Wu, Hui Zhou, Chong Wang, Yunhe Hou, "Risk-based life cycle cost analysis method for transmission systems," in *Proc. IEEE Innovative Smart Grid Technologies, 2012,* pp. 1 – 5.

[48] Xu Xinsheng, Fang Shuiliang, Gu Xinjian, "A model for manufacturing cost estimation based on machining feature," in *Proc. IEEE Technology and Innovation Conference, 2006,* pp. 273 – 278.
[49] K. Ma, F. Blaabjerg, "Reliability-cost models for the power switching devices of wind power converters," in *Proc. IEEE Power Electronics for Distributed Generation Systems, 2012*, pp. 820 – 827.
[50] G.A.Klutke, P.C. Kiessler, M.A.Wortman, "A critical look at the bathtub curve", *in Proc. IEEE transaction on Reliability,* vol. 52, pp. 125 – 129, Mar 2003.
[51] F. Jensen, "Component failures based on flaw distributions," in *Proc Reliability and Maintainability Symposium, 1989*, pp. 91 – 95.
[52] J. Fussel, E. Aber, and R. Rahl, "On the quantitative analysis of priorty- and failure logic," IEEE Transactions on Reliability, vol. 31, pp. 219–254, June 1982.
[53] Military handbook; Reliability prediction of Electronic equipments (MIL-HDBK-217),Jan 1991.
[54] K. Shenai, "Power MOSFET screening to improve field-reliability of power supplies," *in Proc. IEEE Energytech, 2013,* pp. 1 – 3.
[55] V. Banu, X. Jorda, J. Montserrat, P. Godignon, J. Millan, Pierre Brosselard, "Accelerated test for reliability analysis of SiC diodes," *Power Semiconductor Devices & IC's, 2009,* pp 267-270.
[56] E. A. Herr, A. Poe, A. Fox, "Reliability Evaluation and Prediction for Discrete Semiconductors," *in Proc. IEEE transaction on Reliability*, vol. 29, pp. 208 - 216, Aug 1980.
[57] C.Rodriguez, G. Amaratunga, "Long-Lifetime Power Inverter for Photovoltaic AC Modules", *IEEE transaction on industrial electronics*, 2008 pp. 2593 – 2601.
[58] S. V. Dhople, A. Davoudi, P. L. Chapman and A. D. Domínguez- García, "Reliability Assessment of Fault-Tolerant DC-DC Converters for Photovoltaic Applications," in *Proc. IEEE Energy Conversion Congress and Exposition, 2009,* pp. 2271 – 2276.
[59] T. Kobayashi, H. Ariyoshi, A. Masuda, "Reliability Evaluation and Failure Analysis for Multilayer Ceramic Chip Capacitors," *in Proc. IEEE transaction on Reliability*, vol. 1, pp. 316 - 324, Sep 1978.
[60] A. Cavallini, I. Ghinello, G. Maszanti, G.C. Montanari, "Accelerated capacitor degradation due to nonsinusoidal voltage supply and reliability of insulation systems,"*in Proc. IEEE Harmonics and Quality of Power Proceedings, 1998,* pp.720-726.
[61] Juha-Veikko Voutilainen, Tuomas Happonen, Juha Hakkinen, "Reliability of silkscreen printed planar capacitors and inductors under accelerated thermal cycling and humidity bias life testing," *in Proc. IEEE Electronic System-Integration Technology Conference, 2012* pp.1-6.
[62] Dan Zhou, Chengrong Li, Zhongdong Wang, "Power transformer lifetime modeling," *in Proc. IEEE Prognostics and System Health Management, 2012,* pp.1-7.
[63] Na Liu, Wensheng Gao, Kexiong Tan, Liufang Wang, Guodong Liang, Wei Li , "Decision on Maintenance Period for Power Transformer based on Monte Carlo Simulation of Reliability," *in Proc. IEEE Properties and Applications of Dielectric Materials, 2003.* pp. 479 - 482.
[64] M.K. Alam, F.H. Khan, "Reliability analysis and performance degradation of a Boost converter," *in Proc. IEEE Energy Conversion Congress and Exposition, 2013* pp. 5592 - 5597.

[65] S. V. Dhople, A. Davoudi, P. L. Chapman and A. D. Domínguez- García, "A Unified Approach to Reliability Assessment of Multiphase DC–DC Converters in Photovoltaic Energy Conversion Systems," *IEEE Transactions on Power Electronics*, vol. 27, pp. 739 - 751, Feb 2012.
[66] R.D. Kulkarni, V. Agarwal, "Reliability analysis of a modern power supply under nuclear radiation effects," in *Proc. IEEE Power Electronics and Drive Systems, 2003*, pp. 71 – 76.
[67] Boyi Yang, Jiann-Shiun Yuan, Z. Shen, "Reliability and failure mechanisms of lateral MOSFETs in synchronous DC-DC buck converter," in *Proc. IEEE Physical and Failure Analysis of Integrated Circuits, 2009*, pp. 1946-1542.
[68] A. Rahnamaee, J. Milimonfared, K. Malekian, M. Abroushan, "Reliability consideration for a high power zero-voltage-switching flyback power supply," in *Proc. IEEE Power Electronics and Motion Control Conference, 2008*, pp. 365 - 371.
[69] Jiaxin Chen, Youguang Guo, Jianguo Zhu, Jianxun Jin, "Heavy Load Simulation Model of Flyback Switching DC-DC Converters and its Application for Reliability Improvement," in *Proc. IEEE Industry Applications Conference, 2007*, pp. 2295 - 2302.
[70] H. Wang, M. Liserre, and F. Blaabjerg, "Toward reliable power electronics: challenges, design tools, and opportunities," IEEE Industrial Electronics Magazine, vol. 7, no. 2, pp. 17-26, Jun. 2013.
[71] Military handbook; Reliability prediction of Electronic equipment (MIL-HDBK-338B), Oct. 1998.
[72] A. Ranjbar, M. Kiani,B. Fahimi, "Dynamic Markov Model for Reliability Evaluation of Power Electronic Systems", in *Proc. Power Engineering, Energy and Electrical Drives,2011*,pp.1-6.
[73] A. Aal, T. Polte, "On component reliability and system reliability for automotive applications", in *Proc. Integrated Reliability Workshop Final Report, 2012*, pp. 168-170.
[74] Qingyu Yang, Yong Chen, "Monte Carlo Methods for Reliability Evaluation of Linear Sensor Systems," *IEEE transaction on Reliability*, vol. 60, pp. 305-314, Mar 2011.
[75] S M. Molhanec, "Model based FMEA method for solar modules," in *Proc. Electronics Technology conference 2013*, pp. 183 – 188.
[76] A.M. Bazzi, Xiangyu Ding ; A. Dominguez-Garcia, P.T. Krein, "Circuit-based induction motor drive reliability under different control schemes and safe-mode operation', in *Proc. Applied Power Electronics Conference and Exposition 2011*, pp. 653 – 660.
[77] J. Mora-Flórez, J. Bedoya-Hernandez, S. Perez-Londono," Fault tree based methodology to evaluate the reliability of converter transformers," ," in *Proc. Transmission and Distribution Conference and Exposition*, 2008, pp. 1-7.
[78] B. Edson, Xijin Tian, "A prediction based design-for-reliability tool," in *Proc. Reliability and Maintainability Annual Symposium*, 2004, pp. 412-417.
[79] P.T.Krein "Elements of Power Electronic," 2nd edition, Oxford University –Press, Inc. New York, 1997.
[80] Shuai Shao, Xinke Wu, Min Chen,F. Peng, "Design considerations of a self-biased current driven SR in DCM flyback DC-DC converter," in *Proc. IEEE Energy Conversion Congress and Exposition, 2010*, pp. 242 – 248.
[81] Jingdong Chen, "Need to estimate buck converter efficiency in portable apps," *eetimes-India*, Jan. 2008.

[82] A.M.Bazzi, P.T.Krein, J.W.Kimball, and K.Kepley, "IGBT and Diode Loss Estimation under Hysteresis Switching," *IEEE Transactions on Power Electronics*, vol. 27, pp. 1044-1048, Mar 2012.
[83] R.W.Erickson, "Fundamentals of Power Electronics," 2nd edition, Kluwer Academic Publishers, 2001.
[84] Gary L. Johnson, "Solid State Tesla Coil," Chapter 3, Dec 2001.
[85] X.Zhang, X.Ruan, H.Kim, and C.K.Tse, "Adaptive Active Capacitor Converter for Improving Stability of Cascaded DC Power Supply System," *IEEE Transactions on Power Electronics*, vol.28, pp. 1807-1816, Apr 2012.
[86] A.Haider, P.Variyam, A.Chatterjee, J.Ridley, "Measuring stray capacitance on tester hardware," in *Proc. IEEE VLSI test symposium,* 2002, pp. 351-356.
[87] Yang Chen, Guozhu Chen, K.Smedley, "Analysis and measurement of small inductance of loops and vias on printed circuit board," in *Proc. IEEE Industrial Electronics Society,* 2003, pp. 1661 – 1666.
[88] H.Zumbahlenas ," Linear Circuit design handbook,"2nd Edition ,Elsevier Publication, pp821-895, 2008.
[89] A.A.Fomani, J.C.W.Ng, A.Shorten," An integrated segmented gate driver with adjustable driving capability," in *Proc. IEEE Energy Conversion Congress and Exposition*, 2010, pp. 2430-2433.
[90] Hamilton Confortin Sartori, Hélio Leães Hey, José Renes Pinheiro, "An optimum design of PFC Boost Converters," *IEEE Transactions on Power Electronics*, vol.13, pp. 1-8, Sept 2009.
[91] M.H.Rashid, "Power Electronics handbook-Devices, circuits and applications" 2nd Edition, Academic press, 2007.
[92] N.Coruh, S.Urgun, T.Erfidan, "Design and implementation of flyback converter," in *Proc. IEEE Industrial Electronics and Applications*, 2010, pp. 1189 - 1193.
[93] Jian Sun, D.M.Mitchell, M.F.Greuel, P.T.Krein, R.M.Bass, "Averaged modeling of PWM converters operating in discontinuous Conduction mode," *IEEE Transactions on Power Electronics*,vol. 16, pp. 482-492,Jul 2001.
[94] Liang Cheng ,Ye Yunyue, Zhuo Zheng, "Design of Improved Single Phase Flyback Switching Power for PMSM Drive System," in *Proc. IEEE International conference on Artificial Intelligence, Management Science and Electronic Commerce*, 2011, pp.3898-3901.
[95] B.M.Hasaneen, A.A.E. Mohammed, "Design and simulation of DC-DC boost converter," in *Proc. IEEE Power System Conference, 2008,* pp. 335 – 340.
[96] M. El-Zanaty, M. Orabi, M.Z. El-Sadek, "Review of synchronous buck converter design optimization," in *Proc. IEEE Power System Conference, 2008,* pp. 588 – 592.
[97] T.R. Salvatierra, M.K. Kazimierczuk, "Inductor design for PWM buck converter operated as dynamic supply or amplitude modulator for RF transmitters," in *Proc. International Midwest Symposium on Circuits and Systems*,2013, pp.37 – 40.